A THERMODYNAMIC, SPECTROSCOPIC, AND MECHANICAL CHARACTERIZATION OF THE WOOD-POLYPROPYLENE INTERPHASE

By

DAVID PAUL HARPER

A dissertation submitted in partial fulfillment of
the requirement for the degree of

DOCTOR OF PHILOSOPHY

WASHINGTON STATE UNIVERSITY
Department of Civil and Environmental Engineering

December 2003

To the Faculty of Washington State University:

Them members of the Committee appointed to examine the dissertation of DAVID PAUL HARPER find it satisfactory and recommend that it be accepted.

_____
Chair

_____

_____

_____

ACKNOWLEDGEMENT

I would like to start by thanking my advisor, Mike Wolcott. Mike let me forge my own path and solve my own problems. I possessed more freedom and at the same instant, more responsibility than most graduate students. I am very grateful for the opportunities afforded me. I would like to thank my committee: Marie-Pierre Laborie, Frank Loge, and Kelvin Lynn for their time and comments in preparing this dissertation. I would also like to extend a special thanks to Tim Rials. He provided much insight, advice, and friendship over the many years that I was in graduate school. All of the above proved to be valuable mentors in the pursuit of my doctoral degree.

I would like to thank the Office of Naval Research whose funding provided financial support for my research. In addition, I would like to thank Honeywell Corporation for providing many of the materials used. Scott Hacker of Honeywell was especially helpful and provided many useful comments.

The staff of the Wood Materials and Engineering Laboratory has been very helpful throughout my years in Pullman. I would like to thank Janet Duncan, Judy Edmister, Bob Duncan, Scott Lewis, and our esteemed director Don Bender for their help and support. I would like to extend a special thank you to Pat Smith. Thank you for always looking out for the little guy, dotting the i's and crossing the t's. I want to acknowledge Tony Nilson and Marty Lentz for all of their help. You may be gone, but you are not forgotten. In addition, I would like to give the staff at the Electron Microscopy Center a special thank you for always trying to help. Probably the people that influenced me the most over the years are the many graduate students and post docs with whom I have worked: Karl Englund, Brian Tucker, Vikram Yadama, Kristin Meyers, Alejandro Bozo, Jahanghir Chowdhury, Anke Shirp, and Tiequi Li. Thank you guys.

The most important part of my life is my family. I would never have been able to accomplish any of my goals without the support of my wife, Jessica, and my children, Wyatt, Sam, and Ruth. I love you with all of my heart. I will never be able to express all

of my gratitude. You had faith in me and what I was doing even when I had lost it. Thank you for all of you help and sacrifice. I would also like to thank my parents. They were always there when I needed them. I hope someday I could provide as much help and support for my children. I love you and thank you.

A THERMODYNAMIC, SPECTROSCOPIC, AND MECHANICAL CHARACTERIZATION OF THE WOOD-POLYPROPYLENE INTERPHASE

Abstract

By David Paul Harper, Ph.D.
Washington State University
December 2003

Chair: Michael P. Wolcott

Extruded composites composed of wood and semicrystalline polyolefin thermoplastics are gaining acceptance for use in structural, exterior applications. Wood and polyolefins are inherently incompatible making the use of a coupling agent necessary for improved stiffness and strength. However, the improvements to properties are negated by the addition of processing lubricants used in extrusion. The mechanisms for degrading the properties of the composite are largely unknown. The goal of this research is characterize the mechanisms that lead to improvements in properties in wood-polypropylene (PP) composites with the use of a coupling agent, maleic anhydride polypropylene (MAPP), and the degradation of properties with the incorporation of lubricants, a polyester (OP), zinc stearate (ZnSt), and ethylene bisstearamide (EBS). A combination of experimental techniques was used to probe the impact crystal and amorphous polymer morphology has on the mechanical response of the system. The use

of dynamic mechanical spectroscopy allowed for the determination molecular interaction at the wood-PP interface and between polymer molecules in the bulk. The analysis revealed that MAPP improved the stiffness of the composite by several different mechanisms. MAPP improves crystal nucleation off the wood surface and created a large interphase that likely increases bending stiffness. In addition, there is improved interaction between matrix and filler leading to decreased mechanical damping. These effects are negated with the incorporation of ZnSt because of a reaction with the MAPP's polar groups. This leads to poor packing and nucleation of PP molecules at the wood surface leading to a decrease in strength and stiffness.

Table of Contents

List of Figures

List of Tables

Chapter 1 Project Introduction

1.1 Introduction

A new class of structural materials has emerged in the past decade based on a composite of thermoplastic and wood (WPC). The materials take advantage of the low density of wood, low cost, resistance to ultra-violet radiation, and ability to be recycled. The thermoplastic component in the WPC provides improved resistance to moisture and biological attack over traditional wood composites by encapsulating the wood. However, the thermoplastic matrix does not chemically interact with the wood leading to poor stress transfer and pathways for moisture uptake (Johnson and Nearn 1972). The search for the ability to adhere the wood and thermoplastics has led to much research in the area of coupling agents (Lu et al. 2000). Much of this research still has left questions of how load is transferred from the matrix to the fiber, and if this interface governs the mechanical response of the material. Many possible mechanisms exist for improved performance ranging from enhanced wood distribution to covalent bonding the wood fibers and matrix.

A WPC is composed of between 40 - 65% wood, 25 - 60% polyolefin homopolymer, 0 - 5% coupling agent, and up to 3% processing additives. An extrusion process is the most common means of manufacturing structural WPC's. A die on the end of the extruder forms the profile of the product. Processing additives or lubricants serve two important functions: to reduce the friction between the die and melt and to reduce melt viscosity. These two additive functions help achieve the melt properties needed to extrude a smooth

profile for a given die. Additives, however, have a detrimental impact on the performance of wood-polyethylene composites (Wolcott et al. 2001). This issue has been adequately addressed in the literature. Further, there has been little attention given to the interaction between additives and other material constituents.

The low cost and processing temperatures below that of wood degradation makes polyolefins the most common thermoplastics used in WPC. In particular, high-density polyethylene and isotactic polypropylene (PP) are used in structural applications because of their stiffness and toughness. The semi-crystalline nature of these polymers leads to the development of a three-phase morphology in the WPC because the surface of the wood acts as a nucleating surface for the melt. In PP for example, impinging nuclei have led to curious interfacial morphology with the formation of a transcrystalline layer (TCL) (Fig. 1.1) around the fiber. Growth in the resulting crystal structures occurs perpendicular to the fiber surface forming a three dimensional interphase. The boundary between two phases forms a surface termed the interface. There is little understanding of the mechanism causing the formation of the TCL, and little is known of the effect of the TCL morphology on mechanical properties of the composite. Research by Gray (1974), Wang and Hwang (1996), and Lee (2002) has shown that fiber topography, chemical composition of the surface and surface energy dictates the nucleating ability of a surface. Yin et al. (1999) has suggested that the blending of an iPP homopolymer with a copolymer-coupling agent, maleic anhydride polypropylene (MAPP), changes the morphology of the TCL interphase. To date, it is greatly debated over the influence that the TCL will have on the properties of a thermoplastic composite. A few studies have

attempted to determine the influence of the transcrystallinity on the adhesive interaction between fiber and matrix (Felix and Gateholm 1994, Wang and Hwang 1994, Gati and Wagner 1997). The influence between fiber type and matrix type makes global conclusions on the effect of the TCL difficult to form. The nature of the wood-plastic interface, therefore, appears to be very specific to fiber type and the polymer matrix.

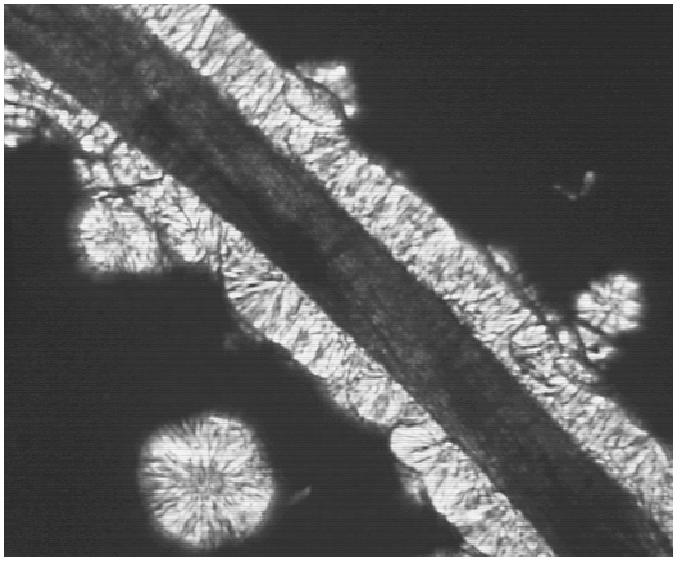

Figure 1.1: Transcrystalline growth on the surface of a wood slice embedded in a 5% MAPP and 95% PP blend.

1.2 Background

1.2.1 Polymer Crystallization

Linear polymers such as polyethylene and polypropylene crystallize folding long chains in on it to form a crystal lamella. The folds of the lamella form the thin dimension of a polymer crystal. This fold length must reach a minimum thickness, l, before a crystal nucleus can form. The nucleation of a semi-crystalline polymer occurs at a temperature below the melt (T_c) when it becomes thermodynamically more favorable to form a crystal. The difference between the equilibrium melts temperature (T_m°) and T_c is termed

the degree of supercooling (i.e. $\Delta T = T_m^{\circ} - T_c$). As supercooling increases, l decreases and accordingly the observed melt of the crystal following relationships derived by Hoffman et al. (1976):

$$\Delta G_{crystal} = 4xl\sigma + 2x^2\sigma_e - x^2 l\Delta h_f(\Delta T)/T^{o}_{m,} \qquad \textbf{Equation 1.1}$$

$$T_m = T_m^{\circ}\left[1 - \frac{2\sigma_e}{\Delta h_f l}\right] \qquad \textbf{Equation 1.2}$$

where $\Delta G_{\text{crystal}}$ is the free energy of fusion for the crystal, x is the large dimension, σ is the lateral free surface energy, σ_e is the fold surface free energy, and Δh_f is the heat of fusion independent of temperature near the melt. The thickness required for nucleus is reduced by the presence of an active foreign substrate. This effectively reduces $\Delta G_{\text{crystal}}$.

The hypothesis for characterization of polymer crystallization is that: if polymers are miscible in the melt then crystal growth should slow at higher concentration of copolymer or lubricant as seen in PEO/PMMA systems (Alfonso and Russell 1986). All materials tend to crystallize in the pure form. Therefore, the kinetics of crystallization is dependent on the amount of dilution of the crystallizable material (Flory 1949). The change in the mixture of the components between the semicrystalline amorphous components can lead to changes in morphology such as a roughening of the spherulitic structure (Keith and Padden 1963, 1964). Nucleation and growth are separate phenomena that are influenced by the same processing parameters. Many polar materials are effective nucleating agents. MAPP has proven to be an effective nucleating agent for PP in two separate studies (Yin et al. 1999, Seo et al. 2000). Yin et al. (1999) showed that MAPP was an effective nucleating agent for the bulk polymer and also increased the

nucleating ability of the fiber. Greater nucleation in the bulk will lead to smaller spherulite sizes and a reduced TCL from impingement. Thus, nucleation and growth need to be considered separately as they both impact morphology.

1.2.2 Polymer Interaction

The thermodynamic meaning of miscible is defined as a single phase down to the molecular level, where the value for the free energy of mixing is negative $\Delta G_m = \Delta H_m - T\Delta S$ (Utracki 1989). Here, $\Delta G_m < 0$ only if in a binary polymer the Flory-Huggins interaction parameter, χ_{12}, is also negative. Utracki defined the composition of χ_{12} as: dispersion forces, free volume, and other specific interactions. Specific interactions occur on different levels and in different phase states of the material. As a result, a large number of scientific techniques that range from visualization, mechanical, spectroscopic, to diffraction has been developed to evaluate materials.

A widely studied example is a blend of poly(methyl methacrylate) (PMMA) and poly(ethylene oxide) (PEO) (Alfonso and Russell 1986, Ito et al. 1987, Russell et al. 1988, Zawada et al. 1992, Parizel et al. 1997). These blends are miscible in the melt state and exhibit some miscibility at the molecular level in the solid state. The use of a combination of ^{1}H and ^{13}C nuclear magnetic resonance (NMR) methods determined that there are three phases of PEO in PEO/PMMA blends: a crystalline phase, a constrained amorphous phase around the lamella, and an amorphous fraction that is miscible with PMMA (Parizel et al. 1997). This model of PEO/PMMA blends is in agreement with the lattice model for semicrystalline/amorphous polymer blends of Kumar and Yoon (1989)

that predicts the existence of an interphase of the semicrystalline polymer that is restrained aound the crystals. The polymer tends to disorder asymptotically once a threshold is reached. This study found that the entropic constraints at the crystal leads to almost complete phase separation with $\chi_{12} \approx 0$, but conceded that the composition of the amorphous phase may depend highly on crystallization conditions and polymer concentrations.

The constraint of the amorphous regions around crystals has been observed by investigating the broadening of segmental relaxation (Ngai and Roland 1993). Amorphous polymers observe an asymmetric shift in their relaxation spectrum, *E(t)*, that can be described by the coupling model (Ngai et al. 1991). The coupling model describes the temperature dependence of an ensemble of regions in a polymer that need to rearrange in order to relax. This model provides a long-range view of molecular interactions, where the movement of the ensembles are restricted by the configuration of surrounding groups. A degree of cooperativity between groups is required for the polymer to relax without configuration changes in the ensemble. A high degree of cooperativity is characterized as a divergence from Arrhenius (exponential) behavior around the glass transition. This description of cooperative movement is analogous to that of the restricted amorphous fraction around crystals within a semicrystalline polymer. This is termed the rigid amorphous phase. In systems were the χ_{12} can be zero in the solid phase, longer-range interactions can be present between the immiscible phases. However, the rigid amorphous phase display a broadening in the relaxation about T_g that often follows an Arrhenius behavior. This divergence from cooperativity can be

described by the concept of fragility. This model is based upon a relationship developed by Angell to describe the resistance of glassy substances to thermal degradation (strong) and those that deviate from Arrhenius law (weak) (Böhmer et al. 1993). Strong glass formers exhibit very high intermolecular interactions that commonly do not result from weak secondary forces. Strong glasses typically follow Arrhenius behaviour.

The study of the crystallization of semicrystalline polymers can yield information about the miscibility of polymers in the melt state. It is true that most materials crystallize in the pure form and those impurities or additives are expelled during this process. However, as observed by Nishi and Wang (1975) there is a melting point depression and, under dynamic conditions, crystallization temperature depression in crystalline amorphous polymer pairs that are miscible in the melt state. For blends that are miscible in the melt, the melting point of the blend should be depressed in relationship to the temperature of crystallization (Hoffman and Weeks 1962). A plot of the T_m vs. T_c gives an estimation of the equilibrium melting point can be that can be made by extrapolation. The melting points of polymers isothermally crystallized at different temperatures are extended to intersect a line where $T_m^o = T_c^o$ (Hoffman et al. 1976). The point of this intersection is considered T_m^o. This melting point is systematically depressed with increasing amounts of miscible polymers (Nishi and Wang 1975). The nonlinearity of plot gives an indication of the inclusion of defects into the crystal structure for the blends (Utracki 1989). The miscibility of two polymers required for melting point depression as observed by Scott (1949):

$$\chi_{12} = \frac{1}{2}\left[\frac{1}{\sqrt{m_1}} + \frac{1}{\sqrt{m_2}}\right]^2, \qquad \textbf{Equation 1.3}$$

where m is the degree of polymerization, 1 and 2 represent the amorphous and crystalline polymers respectively. The entropy contribution for two long chain polymers is negligible but becomes significant as m_1 approaches 1, which is the case of a solvent-polymer system (Scott 1949).

1.2.3 Semicrystalline Polymer-fiber Interfaces

Many filled semi-crystalline polymer systems are actually three phase systems. An interphase results around the filler where the morphology of the matrix material is broken-up. The interphase can be the result of coupling or toughening agents used to affect the bulk mechanical properties. Gao and Tsou (1999) recently outlined three factors that effect the mechanical performance of a filled polymer (1) strength and modulus of the filler, (2) chemical stability and strength of the matrix, and (3) the adhesion between the polymer matrix and the filler. The latter point highlights the importance for the transfer of stresses across the interphase. The damping characteristic of the composite under dynamic load is an effective tool for characterizing the morphology of the interphase (Nielsen and Landel 1994). Boluk and Schreiber (1986) observed differences in the damping characteristics of a polymer and filler without specific interactions (i.e. Acid-Base). The attributed differences were related to an effective immobilized layer around the filler that increased the perceived filler volume fraction according to the model proposed by Nielson (Nielson and Landel 1994):

$$\tan\delta_c = \tan\delta_p(1-\varphi_f), \qquad \textbf{Equation 1.4}$$

where δ is the phase angle between the real and imaginary components of the dynamic mechanical response for the composite (c) and polymer (p) respectively. φ_f is the volume fraction of the filler in the composite. Interaction around between the filler and the matrix could, perceivably, affect the damping and increase φ_f. Lipatov (1979) described in general that strong interaction and surface adsorption would slow crystallization, the absence of interaction should not impact crystallization, and moderate interaction would use the surface for nucleation. Thus, given a high volume fraction of an inactive surface, the crystallization of the polymer would be interrupted and would possess a highly amorphous fraction. This would perceivably reduce the elastic and dynamic modulus of the composite by reducing the modulus of the polymer phase. For an incompatible semicrystalline interface, Wool (1995) stated that longer crystallization times should produce stronger interfaces by allowing for more entanglement. However, the properties could very well depend on the volumetric contraction and densities of the spherulitic structures that are formed at the interface. The increase in packing density around many polymer fillers often leads to a drop in the T_g of many composites (Lipatov 1979). It is expected that strong nucleating filler would have a higher T_g than that of an inactive surface that would interrupt the crystallization process.

1.2.4 Transcrystalline Morphology

The interface between the wood and the plastic matrix lies between what Lipatov (1979) saw as moderate and no interaction. The presence of wood in polypropylene acts as a nucleating surface. The addition of lubricant systems and copolymers will likely change the morphologies of the resulting interphase. There is considerable debate on the benefits

TCL has on the mechanical performance of a composite (Folkes and Hardwick 1987, Felix and Gatenholm 1994, Wang and Hwang 1994, Gati and Wagner 1997). The uses of 100 percent MAPP copolymer or MAPP melt blended with PP caused a much higher nucleation density on the fiber surface (Yin et al. 1999). The presence of the TCL leads to improved adhesion in cellulose and PP composites and the interfacial shear strength increases with thickness (Gatenholm et al. 1996). Folkes reported that the TCL without the presence of MAPP is stiffer and stronger in shear than the bulk polymer (Folkes and Hardwick 1987). However, the relative increase in mechanical properties of the TCL does not explain the improved stress transfer. The increase in adhesion is not observed in all fiber types. The TCL around Kevlar fibers embedded in a poly(caprolactone) matrix did not effect the adhesive strength when subjected to single fiber pullout test (Gati and Wagner 1997).

The development of the TCL is further complicated when considering different fiber types and the addition of MAPP. Gray (1974) found that highly purified cellulose (bleached softwood craft) had a higher nucleating ability than other wood fiber types in PP. The ability to nucleate growth was noted too similar to other polymers such as teflon, nylon, and PET in a semi-crystalline polymer matrix. Yin et al. (1999) documented that little nucleation occurs on the surface of whole wood fibers with the use of pure PP. However, the nucleating ability of the fiber is enhanced with a matrix blended with MAPP. The nucleating ability of the bleached and unbleached kraft pulp fiber was increased when damaged (Lee 2002). The damage may have exposed reactive sites that caused nucleation in pure PP. Undamaged portions of the fibers did not induce

nucleation. A TCL was observed with the addition of five percent MAPP. Further, the size of the spherulites in the bulk decreased dramatically with the presence of MAPP and to the smallest size at 100 percent MAPP.

The development of the TCL and the morphology of the layer may have a dramatic impact on the mechanical properties of the composite. There is some debate regarding the influence that the TCL will have on the whole composite. Folkes and Hardwick (1987) reported increased modulus and shear strength of the TCL in polypropylene reinforced with PET over bulk properties. However, Quillin et al. (1993) argues that the bulk performance of the composite may decrease at high fiber volume fractions because of gaps between spherulites. The TCL produces an almost continuous network of gaps compared to a more random dispersion of gaps in composites without a TCL. The continuous gaps could provide a weak plane for shear failures and fiber pullout. This may lead to a more brittle failure around a stiff TCL.

Felix and Gatenholm (1994) used a single fiber fragmentation test and noted improved stress transfer between the fiber and matrix with an increase in TCL thickness. Felix and Gatenholm believe that the long crystallization times improve mechanical interlock between the matrix and fibers. Long crystallization times at low degrees of supercooling allow for improved adsorption of the polymer onto the surface. For polytetrafluoroethylene (PTFE) fibers embedded in a PP matrix the presence of transcrystallinity does not promote adhesion (Wang and Hwang 1996). In addition, the thickness of the TCL does not have a significant effect on the adhesive fracture energy.

The residual compressive stresses that result for cooling from the crystallization temperature, T_c, do increase the friction during the fiber pullout process in PTFE/PP composites.

1.3 Objectives

A great deal of research over the past decade has demonstrated the efficacy of the use of coupling agents in a WPC. However, it remains that little is still known on the mechanisms for improved mechanical properties when coupling agents are used. The addition of additives further complicates the mechanisms for understanding stress transfer in a WPC. The possibility of additive-coupling agent, wood-additive, and homopolymer-additive interactions is now introduced. The goal of this research is to determine how the addition of copolymer coupling agents and additive systems impact the morphology, chemistry, and mechanical properties of the wood-plastic interphase. The interphase is of interest in this study because of the vast differences that have been observed in the wood-plastic literature and the potential for its alteration by additives and coupling agents. Further, the interphase is the region where stress transfer will take place between the bulk plastic and wood. The specific objectives of this research are:

1. Determine the influence of material constituents on crystallization and the development of morphology in wood-polypropylene composites,
2. Evaluate the spatial distribution of material constituents in the composite and determine chemical interaction among them,
3. Delineate the influence of selected commercial lubricants and coupling agents on the formation of the composite morphology and wood-polymer interphase,

4. Assess the mechanical behavior of the interphase and the bulk polymer.

1.3.1 Rationale and Significance

To date, little information is available on the specific mechanisms that control stress transfer between the wood and plastic in a WPC. The addition of coupling agents has shown improvement performance over formulations containing neat resin and wood (Clemons et al. 1992, Mishra and Naik 1998, Lai et al. 2003). The mechanisms for property improvement have not been definitively attributed to any one phenomenon. Much research has focused on identifying covalent or secondary interactions between coupling agents and the wood but with no positive results (Kazayawoko et al. 1997a, Kazayawoko et al. 1997b, Kazayawoko et al. 1998, Son et al. 2000). Recent research has shown that there may be an interaction between either the wood or coupling agents with the lubricants contributing to a decrease in bulk mechanical properties (Wolcott et al. 2001). In order to process a composite, processing lubricants are a necessity to be able to extrude a stable profile. The WPC literature is lacking on the subject of coupling agents and additive interaction. Many additives used are polar in nature and can compete with coupling agents at the wood interface. Further, the addition of polar components will impact the nucleation of the crystals and thus, morphology. The influence of bulk mechanical properties by many parameters including particle dispersion and size, void distribution and volume, and thermal histories make conclusions about individual mechanisms hard to form.

An investigation into each of the possible mechanisms that could govern the mechanical

performance of the composite is warranted. These mechanisms include: morphology development, specific and long-range interactions, and chemical bonding. These mechanisms may not be limited to the wood-plastic interface, but may occur in the bulk plastic or at the amorphous-crystalline interface. This study will investigate on the effects of the interaction of the material constituents and the change in chemistry, morphology, and stress transfer that they impart on the composite. Spectroscopic, optical, thermal, and mechanical techniques will be utilized to follow the interactions. The scale of the interaction also needs consideration since these interactions can manifest on different orders of magnitude. This study proposes limiting mechanical testing to the microscopic scale or on the order where mechanical interactions occur. The large member testing would complicate the study by adding variables that are processing specific. This research would provide a fundamental basis for selecting material constituents that could apply to many processing techniques.

At the heart of a composite is the structure. All of the material constituents come together under a given set of processing conditions that determines the material morphology and thus the performance. Thermal and microscopic techniques characterize structure and monitor its development. The development of this structure is modeled and then related to thermodynamic principles. Still another factor that needs consideration is the chemical interactions that occur. If materials are similar in structure, they may incorporate into the matrix but serve as defects that cause crystal instabilities. However, materials usually crystallize pure pushing impurities and non-crystallizable material to the growth front. Molecular weight and chemical functionality also governs the

migration of materials in the melt. The proposed research will reveal the mechanisms forming the structure and mechanical behavior of the wood and PP composite materials. Links will form between chemical and physical structure to the response of the material under dynamic loading. Ultimately, the configuration and interaction of the polymers in the system will govern the composite properties as revealed thermal analysis. This will reveal the impact that additives have on mechanical performance of the composite on a large scale.

1.4 References

Alfonso GC, Russell TP, Kinetics of crystallization in semicrystalline/amorphous polymer mixtures, Macromolecules 19 (1986), 1143-1152.

Böhmer R, Ngai KL, Angell CA, Plazek DJ, Nonexponential relaxations in strong and fragile glass fromers, Journal of Chemical Physics 99 (1993), 4201-4209.

Boluk MY, Schreiber HP, Interfacial interactions and the properties of filled polymers: i. Dynamic-mechanical responses, Polymer Composites, 7 (1986), 295-301.

Clemons C, Young RA, Rowell RM, Moisture sorption properties of composite boards from esterified aspen fiber, Wood and Fiber Science 24 (1992), no. 3, 353-363.

Felix JM, Gatenholm P, Effect of transcrystalline morphology on interfacial adhesion in cellulose/polypropylene composites, Journal of Materials Science 29 (1994), 3043-3049.

Flory PJ, Thermodynamics of crystallization in high polymers. iv. a theory of cystalline states and fusion in polymers, copolymers, and their mixtures with diluents, The Journal of Chemical Physics 17 (1949), 223.

Folkes MJ, Hardwick ST, Direct study of the structure and properties of transcrystalline layers, Journal of Materials Science Letters 6 (1987), 656-658.

Gao Z, Tsou AH, Mechanical properties of polymers containing fillers, Journal of Polymer Science: Part B: Polymer Physics 37 (1999), 155-172.

Gatenholm P, Hedenberg P, Karlsson J, Felix J, Modification of morphology and properties of polypropylene using engineered biofibers, ANTEC, 1996, pp. 2302-2304.

Gati A, Wagner HD, Stress transfer efficiency in semicrystalline-based composites comprising transcrystalline interlayers, Macromolecules 30 (1997), 3933-3935.

Gray DG, Polypropylene transcrystallization at the surface of cellulose fibers, Journal of Polymer Pcience: Polymer Letters 12 (1974), 509-515.

Hoffman JD, Davis GT, Lauritzen JI, The rate of crystallization of linear polymers with chain folding, Treatise on Solid State Chemistry, vol. 3: Crystalline and Noncrystalline Solids, ch. 7, pp. 497-614, Plenum Press, New York, 1976.

Hoffman JD, Weeks JJ, Rate of spherulitic crystallization with chain folds in polychlorotrifluoroethylene, Journal of Chemical Physics 37 (1963), 1723-1741.

Ito H, Russell TP, Wingnall GD, Interactions in mixtures of poly(ethylene oxide) and poly(methyl methacrylate), Macromolecules 20 (1987), no. 2213-2220.

Johnson JA, Nearn WT, Theory and design of wood and fiber composite materials, ch. 15. Reinforcement of polymeric systems with Douglas-fir bark fibers, pp. 371-400, Syracuse University Press, 1972.

Kazayawoko M, Balantinecz JJ, Woodhams RT, Diffuse reflectance Fourier transform infrared spectra of wood fibers treated with maleated polypropylenes, Journal of Applied Polymer Science 66 (1997), 1163-1173.

Kazayawoko M, Balatinecz JJ, Woodhams RT, Law S, Effect of ester linkages on the mechanical properties of wood fiber-polypropylene composites, Journal of Reinforced Plastics and Composites 16 (1997), 1383-1406.

Kazayawoko M, Balatinecz JJ, Woodhams RT, Sodhi RNS, X-ray photoelectron spectroscopy of lignocellusic materials treated with maleated polypropylenes, Journal of Wood Chemistry and Technology 18 (1998), no. 1, 1-26.

Keith HD, Padden FJ, A phenomenological theory of spherulitic crystallization, Journal of Applied Physics 34 (1963), 2409-2421.

Keith HD, Padden FJ, Spherulitic crystllization from the melt. i. fractionation and impurity segregation and their influence on crystalline morphology, Journal of Applied Physics 35 (1964), 1270-1285.

Kumar SK, Yoon DY, Lattice model for interphases n binary semicrystalline/amorphous polymer blends, Macromolecules 22 (1989), 4098-4101.

Lai SM, Yeh FC, Wang Y, Chan HC, Shen HF, Comparative study of maleated polyolefins as compatibilizers for polyethylene/wood flour composites, Journal of Applied Polymer Science 87 (2003), 487-496.

Lee SY, Transcrystallization behavior and interfacial strength of a semicrystalline polymer combined with thermomechanical pulp (TMP) fiber, Masters Thesis, University of Idaho, Moscow, Idaho, 2002.

Lipatov SY, Physical chemistry of filled polymers, Rubber and Plastics Research Association of Great Britain, 1979

Lu JZ, Wu Q, McNabb HS, Chemical coupling in wood fiber and polymer composites: a review of coupling agents and treatments, Wood and Fiber Science 32 (2000), 88-104.

Mishra S, Naik JB, Absorption of water at ambient temperature and steam in wood-polymer composites prepared from agrowaste and polystyrene, Journal of Applied Polymer Science 68 (1998), 681-686.

Ngai KL, Rendell RW, Plazek DJ, Couplings between the cooperatively rearranging regions of the Adam-Gibbs theory of relaxations in glass-forming liquids, Journal of Chemical Physics 94 (1991), 3018-3029.

Ngai KL, Roland CM, Intermolecular cooperativity and the temperature dependence of segmental relaxation in semicrystalline polymers, Macromolecules 26 (1993), 2688-2690.

Nielsen LE, Landel RF, Mechanical Properties of Polymers and Composites, second ed., Marcel Dekker, New York, 1994.

Nishi T, Wang TT, Melting point depression and kinetic effects of cooling on crystallization in poly(vinylidene fluoride)-poly(methyl methacrylate), Macromolecules 8 (1975), 909-915.

Parizel N, Lauprêtre F, Monnerie L, N.M.R and D.S.C. investigations of the miscibility of poly(methyl/methacrylate)/poly(ethylene oxide) blends, Polymer 15 (1997), 3719-3725.

Quillen DT, Caulfield DF, Koutsky JA, Crystallinity in the polypropylene/cellulose system. i. nucleation and crystalline morphology, Journal of Applied Polymer Science 50 (1993), 1187-1194.

Russell TP, Ito H, Wingnall GD, Neutron and x-ray scattering studies on semicrystalline polymer blends, Macromolecules 21 (1988), no. 1703-1709.

Scott RL, The thermodynamics of high polymer solutions. v. phase equilibria in the ternary system: polymer 1-polymer 2-solvent, Journal of Chemical Physics 17 (1949), 279-284.

Seo Y, Kim J, Kim KU, Kim YC, Study of the crystallization behaviors of polypropylene

and maleic anhydride grafted polypropylene, Polymer 41 (2000), 2639-2646.

Son S, Lee Y, Im S, Transcrystalline morphology and mechanical properties in polypropylene composites containing cellulose treated with sodium hydroxide and cellulase, Journal of Materials Science 35 (2000), 5767-5778.

Utracki LA, Polymer Alloys and Blends: Thermodynamics and Rheology, Hanser Publishers, Munich, 1989.

Wang C, Hwang LM, Transcrystallization of PTFE fiber/PP composites I. Crystallization kinetics and morphology, Journal of Polymer Science: Part B: Polymer Physics 34 (1996), 47-56.

Wang C, Hwang LM, Transcrystallization of ptfe fiber/pp composites i. Crystallization kinetics and morphology, Journal of Polymer Science: Part B: Polymer Physics 34 (1996), 47-56.

Wolcott MP, Chowdhury M, Harper DP, Li T, Heath R, Rials TG, Coupling agent/lubricant interactions in commercial woodfiber-plastic composite formulations, 6th International Conference on Woodfiber-Plastic Composites, Forest Products Society, May 2001, pp. 197-204.

Wool RP, Polymer interfaces: Structure and strengths, Hanser/Gardner Publications, Inc., Cincinnati, 1995.

Yin S, Rials TG, Wolcott MP, Crystallization behavior of polypropylene and its effect on woodfiber composite properties, The Fifth International Conference on Woodfiber-plastic Composites, 1999, pp. 139-146.

Zawada JA, Ylitalo CM, Fuller GG, Colby RH, Long TE, Component relaxation dynamics in a miscible polymer blend: poly(ethylene oxide)/poly(methyl methacrylate), Macromolecules 25 (1992), 2896-2902.

Chapter 2 Interaction between Coupling Agent and Lubricants in Wood-polypropylene Composites

2.1 Abstract

Commercially available additives and a copolymer system were investigated for their impact on composite morphology and crystallization kinetics. This research focuses on the influence of the coupling agent and lubricants on the crystallization of polypropylene in the bulk and interphase regions and the subsequent spatial distribution of the additives. Differential scanning calorimetry and polarized light microscopy were used to determine kinetic parameters for the crystallization process of the polypropylene in the bulk composite melt and at the wood-polypropylene interface. No differences were found in the kinetics of the crystal formation nucleated on the wood surface and in the bulk polymer by polarized microscopy. Using microbeam Fourier transform infrared spectroscopy, the spatial distribution of lubricants and coupling agents were delineated. Lubricants that tended to interfere with wood-polypropylene coupling dispersed throughout the transcrystalline region around the fiber. In contrast, lubricants with lower degree of interference appeared to be phase separated in the amorphous regions between the crystals. These findings are consistent with calorimetric results that show differences in the quality of the crystals formed by the neat polypropylene.

2.2 Introduction

To satisfy the need for a naturally durable wood-based construction material, a new class of structural composites has emerged that combine thermoplastics and natural fibers such as wood. The new composite takes advantage of wood's low density, low cost, UV resistance, and machining properties, while the thermoplastic component facilitates flow during melt processes and acts as a barrier layer to retard moisture intrusion and biological attack. However, the thermoplastic matrix and wood do not generally interact, leading to poor stress transfer at the interface (Johnson and Nearn 1972) and pathways for moisture uptake and biological attack (Pendleton et al. 2002). This lack of interaction has led many researchers to investigate ways to couple the two phases (Lu et al. 2000). The most common example is the use of maleic anhydride polypropylene (MAPP) as a coupling agent. MAPP copolymer displays efficacy as a coupling agent at low concentrations when dry blended with the wood and isotactic polypropylene (PP) (Krzysik et al. 1990). Dry blending provides a processing cost advantage over other coupling methods that rely on the pretreatment of the wood (Lu et al. 2000).

Regardless of formulation, the introduction of cellulose fiber into a PP melt leads to a change in the morphology of the crystallizing polymer (Gray 1974). The cellulose fiber provides a surface upon which crystals may nucleate. With sufficiently high nucleation density, the embryonic crystals may impinge on one another and grow radially from the fiber surface. The resulting interphase morphology is termed the transcrystalline layer (TCL) and is commonly found in semicrystalline thermoplastic composites with many different synthetic and natural fiber types (Ishida and Bussi 1991a, Wolcott et al. 2001,

Felix and Gatenholm 1994, Gati and Wagner 1997, Heppenstall-Butler et al. 1996) (Figure 2.1). There is considerable debate of the mechanism causing the formation of the TCL and its influence on the mechanical properties of the composite. Research by Gray (1974), as well as Wang and Hwang (1996), has shown that fiber topography, chemical composition of the surface, and surface energy all influence the nucleating ability of the surface. Different surface treatments have been applied to cellulose fibers to alter their nucleating ability (Quillen et al. 1994, Wang and Harrison 1994). For the system studied here, Yin et al. (1999) noted a change in the interphase morphology when blending the PP matrix with MAPP. The addition of MAPP increased the nucleating ability of the fiber over neat PP. However, for polyamide and poly-tetrafluoroethylene fibers, an increase in surface roughness increased the nucleating ability of the PP melt on the fiber surface (Lin and Du 1999). The consistency between the studies appears to be that increased adsorption of the surface increases the nucleating ability. This can be achieved by adding coupling agents to the fiber in the melt or by increasing the surface roughness. Still, the development of the composite interphase appears to be very specific to fiber type and the polymer matrix.

2.3 Objectives

For thermoplastic wood composites, the selection of processing aids and parameters influence material morphology, which impacts mechanical properties. The goal of this research is to determine how lubricants and coupling agents influence the morphology of the wood-polypropylene interphase. Specific objectives of this research are to:

1. Determine the influence of material constituents on crystallization and the development of morphology in the wood-polypropylene composite.
2. Evaluate the spatial distribution of material constituents in the composite and determine chemical interactions among them.
3. Delineate the influence of selected commercial lubricants and coupling agents on the formation of the composite interphase.

2.4 Materials and Methods

Formulations studied in this research consisted of various blends of isotactic polypropylene homopolymer (Solvay HB 9200), maleated polypropylene copolymer (Honeywell A-C 950P), and lubricants. The two commercial lubricant systems studied included a 2-1 blend of zinc stearate (ZnSt) (Ferro DLG-20B) and EBS (GE Specialty Chemicals N,N´-ethylene-bisstearamide) waxes and a polyester-based wax (Honeywell OP-100). Polymer blends consisted of homopolymer, either 0 or 5 percent MAPP copolymer, and either 0 or 3 percent lubricant system. All materials were added to the formulation on a mass basis as a percentage of the total formulation. For differential scanning calorimetry (DSC), these polymer formulations were compounded with 30 total mass percent maple flour (American Woodfibers 4010). For polarized light microscopy (POM), the polymer blends were cast into 0.2 mm thick films.

Isothermal DSC was performed at four temperatures below the melt (132.5, 135, 137.5, 140ºC). The blends were ramped to 200°C and held for 30 min, to erase crystallization history prior to obtaining isothermal conditions. Subsequently, the melts were cooled at

20°C/min to the isothermal crystallization temperature and held. Upon completion of crystallization, the specimens were quenched to room temperature and heated at 20°C/min.

Radial growth of the spherulites and TCL was measured for the same polymer blends used in the DSC analysis at isothermal conditions between 126-140°C. A film of the polymer blend and a 0.8 μm microtomed slice of red maple (*Acer rubrum*) were placed between glass cover slips on a heating/cooling stage (Linkam FTIR). The heating stage was attached to a polarizing light microscope (POM) (Olympus BX51) at a magnification of 200×. As in the DSC experiments, the samples were heated to a temperature of 200°C, held for 30 min to erase the crystallization history, and cooled at 20°C/min to the isothermal crystallization temperature. Images were acquired at set intervals with a monochrome high-resolution digital camera (Diagnostics Instruments Spot Insight BW). The temperatures were calibrated with melt standards. Microbeam Fourier transform infrared (FTIR) spectroscopy was performed on the specimens following crystallization on the microscope heating stage. Chemical functional groups were imaged using a ThermoNicolet Continuum FTIR microscope equipped with a MCTA detector and ThermoNicolet Nexus 670 FTIR. The crystallized specimens were placed on a 2 μm thick KBr window. Spectral maps were collected from the specimens with a spatial resolution of 20 μm in transmission. Each spectrum was developed from an average of 110 scans.

2.5 Kinetics

The growth and nucleation of both the TCL and bulk crystals can be modeled using kinetics. Nucleation and growth are separate phenomena that are influenced by the same processing parameters. The nucleation of a semi-crystalline polymer occurs at a temperature below the melt (T_c) when it becomes thermodynamically more favorable to form a crystal. The difference between the equilibrium melt temperature (T^0_m) and T_c is termed the degree of supercooling (i.e. $\Delta T = T^0_m - T_c$). A foreign surface can influence the thickness of the lamella required for nucleation by reducing the surface free energy difference ($\Delta\sigma$). This is referred to as heterogeneous nucleation, which is not a random process. The rate of heterogeneous nucleation (*I)* can be determined by equation (Eq. 1) (Wang and Hwang 1996):

$$\ln I = \ln I_0 - \frac{U^*}{R(T_C - T_\infty)} - \frac{16\sigma\sigma_e\Delta\sigma T_m^{o\,2}}{k_B T_C(\Delta T\Delta h_f f)}, \qquad \textbf{Equation 2.1}$$

$$K_i = \frac{16\sigma\sigma_e\Delta\sigma T_m^{o\,2}}{k_B\Delta h_f^2}. \qquad \textbf{Equation 2.2}$$

The values for U^*, T_∞, and Δh_f can be obtained from the literature for PP (Clark and Hoffman 1984). The plot of ln I vs. $1/(T_c\Delta T^2)$ has the slope of the nucleation constant, K_i (Figure 2.2). However, the ability to reliably determine I becomes difficult with very high nucleation densities.

Ishida and Bussi (Ishida and Bussi 1991b) devised an alternative for counting individual nuclei along a fiber. The induction time (t_i) is linearly related to I through a constant (Figure 2.3) (Ishida and Bussi 1991b):

$$K_i = \frac{d \ln I(T_C)}{d(1/T_c \Delta T^2)} = \frac{d \ln 1/t_i(T_C)}{d(1/T_c \Delta T^2)}, \qquad \textbf{Equation 2.3}$$

The induction time is extrapolated from the plot of the spherulite radius versus time, where t_i would correspond to the infinitesimal radius. Since the crystal growth is measured on a single focal plane on the fiber, I is based upon the assumption that the nucleation density on the fiber circumference is the same as the nucleation along the length. The induction time gives reference to the time required to form and grow a nuclei of minimum thickness. Because the minimum thickness required to form nuclei increases with decreasing degrees of supercooling, the induction time increases with temperature.

The subsequent kinetic growth rate of the crystal, G, can be determined by:

$$\ln G = \ln G_0 - \frac{U^*}{R(T_C - T_\infty)} - \frac{K_g}{T_C \, \Delta T \, f}, \qquad \textbf{Equation 2.4}$$

where G_0 is a constant and K_g varies with crystallization regimes and is dependent upon the free energy parameter (Hoffman et al. 1976). Depending upon the regime behavior of the growth process, the free energy parameters of the surface and crystal will be determined through K_g. For example, regime II behavior yields,

$$K_g = \frac{2b_0 \, \sigma \sigma_e T_m^0}{k_B \, \Delta h_f}. \qquad \textbf{Equation 2.5}$$

In contrast, an overall description of crystallization, combining the effects of growth and nucleation, can be described using Avrami kinetics (Avrami 1939),

$$\ln[-\ln(-\chi(t))] = \ln k + n \ln[t], \qquad \textbf{Equation 2.6}$$

where χ ranges from 0 to 1. In order to characterize the growth behavior by thermal

techniques, certain geometry of the crystallites and athermal nucleation must be assumed (Supaphol and Spruiell 2000). Then, solving for G and substituting into Equation 2.4 a relationship between the growth rate and crystallization time can be achieved. Secondary nucleation is ignored in this approach to growth kinetics. For spherical crystallites with athermal nucleation, *k* can be defined as:

$$k = \frac{4}{3}\pi G^3 N \,. \qquad \textbf{Equation 2.7}$$

The spherical geometry simplifies relating Avrami kinetics to Lauritzen-Hoffman growth rate theory (Hoffman et al. 1976) by assuming an Avrami exponent of *n = 3*. Therefore, a relationship exists between the time at a specified degree of crystallization (t_χ) and G (Figure 2.4):

$$t_\chi^{-1} = A_1 G_0 \exp\left(-\frac{U^*}{R(T_C - T_\infty)} - \frac{K_g}{T_C(\Delta T)f}\right). \qquad \textbf{Equation 2.8}$$

The surface free energy difference can be obtained from the relationship between K_g and K_i. From this, the advantage (*A*) that the fiber gives to nucleation can be calculated (Ishida and Bussi 1991b),

$$A = \frac{\Delta\sigma'}{\Delta\sigma}, \qquad \textbf{Equation 2.9}$$

where the $\Delta\sigma'$ the change in surface energy for the bulk crystals and $\Delta\sigma$ represents the same for the fiber. The $\Delta\sigma$ for each of the two phases can be computed as:

$$\Delta\sigma = \frac{K_i}{K_g}\frac{b_o \Delta h_f}{8 T_m^o} \,. \qquad \textbf{Equation 2.10}$$

2.6 Results and Discussion

2.6.1 Crystallization Kinetics

Two approaches to determining kinetic parameters were outlined in the previous section. Specifically, the Lauritzen-Hoffman approach separates the nucleation and growth phenomena in crystallization, whereas these processes are combined in the Avrami approach. The measures in the Avrami kinetics should be impacted if there is a change from either the nucleation or growth component since no distinction can be made between the heats generated from either process in the DSC. In a polymer system where foreign surfaces are being introduced, a reasonable hypothesis would be that nucleation would be impacted. This would influence the shape parameter. A more rigorous approach to kinetics can be under taken by observing the individual growth and nucleation of bulk spherulites and the TCL under POM.

Based upon the assumptions of athermal nucleation and spherulitic growth, the K_g ranged from -3.44 to $-4.07 \cdot 10^5$ K^2 for all polymer blends with and without wood as obtained from the DSC growth kinetics (Table 2.1). The addition of wood as a nucleating surface appears to have some impact on the growth kinetics and is dependent on the additive. The addition of OP had the most dramatic impact on growth by increasing K_g and then a large decrease when wood was added over the homopolymer. The addition of MAPP increased K_g in the bulk polymer. The change in K_g for the Avrami analysis may be the result of more than growth. The phenomena of nucleation and growth are separate but influenced by the same processing parameters (i.e. temperature). Therefore, it is difficult

to separate if the observed differences are from nucleation, growth, or a secondary crystallization step.

A previous study of thermoplastic-cellulose composites by Quillen et al. has shown that the presence of a TCL changes the *n* exponent in the Avrami analysis (Quillen et al. 1994). In that study, the change in *n* was linked to the change in shape of the crystallites brought about by changes in nucleation densities with the inclusion of wood. An empirical correlation has been made to *n* and the shape of the crystallites formed under certain conditions (Wunderlick 1981). An analysis of variance (ANOVA) was performed to determine the significance of the variation in *n* for each constituent (Table 2.2). The ANOVA used a general linear model procedure in SAS® software with a balanced block design, and the probability of committing a type I error was set at 0.05. This analysis does not take into account statistical interactions between material constituents, but instead treats each component as an independent factor. Wood was the only constituent that imparted a statistically significant change in the analysis by decreasing *n* from 2.20 to 1.98. For the heterogeneous nucleation case, the shape lies between a diffusion controlled sphere ($n = 3.0$) and a truncated sphere ($n = 1.5$) (Table 2.1). The addition of wood tends to push the crystallites more towards a truncated shape. This shift is likely to result from the increased nucleation on the wood surface and not from a change in the crystal growth. The increased nucleation density causes the impinging nuclei to truncate from complete spherulitic structures. On the wood surface, this impingement permits growth to occur in only the radial direction from the wood surface.

To validate the findings of the Avrami analysis, POM crystallization experiments were conducted to investigate the individual nucleation and growth phenomena in primary crystallization. When Lauritzen-Hoffman growth kinetics is applied in the case of POM, the computed K_g values indicate little difference between the growth of the TCL and bulk (Table 2.2). The growth results from POM are consistent with other studies that found no change in growth kinetics from the TCL to the bulk (Wang and Hwang 1996, Ishida and Bussi 1991b). Further, the growth of the different blends appears to follow the same kinetic processes. Once the crystals nucleate, the growth of the PP proceeds mostly unencumbered, at the same rate regardless of the constituents present. Therefore, co-crystallization of the copolymer or lubricant components with the homopolymer is unlikely.

From the Avrami and Laurizten-Hoffman treatments different values for K_g were obtained. A possible explanation for this difference comes from the assumptions made when evaluating the growth kinetics from the DSC data. The simplification of the Avrami kinetics to the Lauritzen-Hoffman approach assumes that $n = 3$ for a spherical shaped crystallite, which the DSC results showed was violated in all cases (i.e. $n < 3$). The actual shape has a more truncated geometry leading to restricted growth in some of the directions. Further, nucleation is not completely athermal with a significant amount occurring after the onset of crystallization. The Avrami analysis ignored the effects of secondary nucleation that may occur and is likely significant in the late stages of the crystallization process when the lubricants and copolymer crystallize. The amount of heat generated during this secondary nucleation step is unclear. However, it is clear that

the Avrami analysis can be used as a means of detecting the presence of an active nucleating surface in a polymer blend. Quantifiable growth kinetic parameters are unlikely attainable from the Avrami analysis in its present form. Modification to the analysis is needed to account for the effects of geometry and secondary nucleation.

Since $K_i/K_g \propto \Delta\sigma$ and little difference existed for K_g among the various blends, comparisons between the nucleating ability of the polymer melts can be made independent of the determination of $\Delta\sigma$. Larger values of $\Delta\sigma$ and K_i correspond to a decreased nucleating ability of the polymer. The nucleation in the bulk was enhanced by the addition of copolymer coupling agents. This finding is signified by the decreased $\Delta\sigma'$ values of the blends compared to that of the neat PP (Table 2.3). The blends containing ZnSt resulted in the largest impact on the bulk nucleation and likely contained the largest amount of polar components. In its commercial form, ZnSt contains a large amount of ash content (6-13%) that is dominated by ZnO_2. Many of these polar low molecular weight components are likely to collect at the wood surface, which results in the decreased $\Delta\sigma$ over neat PP. The addition of MAPP increases the nucleating ability of both the bulk and TCL compared to that of the homopolymer. However, the large decrease in $\Delta\sigma'$ results in a somewhat reduced advantage for fiber nucleation. When MAPP is added to the blends containing either lubricant system, the $\Delta\sigma'$ remains relatively unchanged. In contrast, the MAPP appears to significantly improve the nucleating ability of the interface as evidenced by the reduced $\Delta\sigma$. This result is consistent with that previously obtained by Yin et al. (1999) where the nucleation on the fiber surface improved with MAPP addition.

The intensity of the TCL is dependent upon the nucleating ability of the fiber surface. However, the eventual volume of the TCL is influenced by the relative preference for crystallization at the interface and bulk because the interfacial crystals will continue to grow until impeded by those in the bulk. This dependence is characterized by the advantage (A) that the fiber affords the nucleation process on the fiber surface over the bulk. For instance, when $A = 0$ the fiber surface is inactive for nucleation purposes, whereas $0 < A < 1$ is considered a moderately active surface, and $A > 1$ relates to an active surface (Ishida and Bussi 1991b). The wood surface only affords a nucleation advantage over the bulk with neat PP, since A is only greater than 1 for this case (Table 2.3). The addition of either lubricant decreases the nucleation advantage of the fiber, however, this reduction is most severe with ZnSt containing blends. Combining the MAPP to the lubricated blends increases fiber advantage approximately 30% over the same formulation without MAPP, however in all cases, they remain lower than either the neat PP or the un-lubricated MAPP blends. It is interesting to note that when adding MAPP to the blends, the most substantial influence occurs with the interface rather than the bulk. This is contrasted with the lubricants that simultaneously increase the nucleating ability of the bulk while decreasing that on the fiber.

2.6.2 Thermal Analysis

The melt calorimetry of isothermally crystallized blends of PP blends, reveal an endothermic event with a lower temperature shoulder between 160 and 165°C and a distinct exothermic peak centered at a formulation dependent temperature (Figure 2.5).

The difference in temperature between the lower ($T_{m,1}$) and higher temperature melt ($T_{m,2}$) is consistently 5 to 6ºC. The dual melting behavior likely represents only the melt of the PP homopolymer because the OP 100, ZnSt, and MAPP all exhibit melts well below 160°C; at 108, 121, and 149, respectively. Melt endotherms with two events have been observed with other polyolefins (Supaphol and Spruiell 2000, Schmidtke et al. 1997, Zhao et al. 2001, Zhou et al. 2000, Liu and Petermann 2001, Liu et al. 2001). The reasons associated with similar double melting behavior have been given as: (1) melt re-crystallization during slow heating ramps, (2) secondary nucleation of crystals in "impure" polymeric materials, and (3) a refinement or annealing of the lamella within crystals. For the data presented here, an attempt to minimize the effect melt re-crystallization and lamella thickening was made by using a sufficiently high heating rate (e.g. 20º C/min), but these two phenomena may still contribute to the melt.. Different degrees of perfection could give rise to the double melt behavior from varying degrees of tacticity and imperfections along the PP backbone. However, the addition of wood appears to change the melt behavior of the system in blends containing ZnSt/EBS. In these blends, the endothermic peak is shifted to the lower temperature, $T_{m,1}$ (Figure 2.6). It is likely that a less thermally stable crystal structure is formed with ZnSt/EBS blends in the presence of wood.

To confirm this hypothesis, the melt of crystals in the bulk and TCL regions were observed using POM (Figure 2.7). The TCL crystals were found to melt at temperatures about 5ºC lower than those in the bulk. These findings are consistent with the DSC data that found a 5-6ºC difference between T_{m1} and T_{m2}. Matsuoka et al. (1968) noted that the

TCL of polyethylene formed in contact with CuO_2 melts before the bulk. Ishida and Bussi (1991b) hypothesized that in crystals formed from a highly energetically favored process, the nuclei may not reach their equilibrium shape before impinging and ceasing growth. If Ishida and Bussi's hypothesis were correct one would believe the melt of the PP would shift to the lower endotherm with the addition of wood, however this is not the case. The impact of ZnSt/EBS as a nucleating agent coupled with the thermal instabilities of the interphase region likely both contribute. Further, a study of branched polyethylene by Fakarov *et al.*(2000) has linked thermal instabilities to reduced mechanical properties. However, the inherent instability of TCL crystals would contradict others that have recently hypothesized improved tensile properties in the fiber direction of aramide-reinforced polypropylene resulting from the formation of a TCL (Assouline et al. 1989). In the case of thermoplastic-wood composites, it is unclear whether the TCL is contributing to a reduction in strength or if it is improving interactions between the material constituents.

2.6.3 Spectroscopy

Spectra of the individual components reveal key absorbance peaks, which are distinct to that constituent. The spectra of MAPP reveal an absorbance at 1788 cm^{-1} where an anhydride peak is expected. This absorbance is close to the aliphatic ester at 1745 cm^{-1} that is present in the OP100 lubricant and in the wood. Note that stearate has a carboxylic acid salt absorbance at 1552 cm^{-1}, which stands out nicely between aromatic C=C ring breathing in wood lignin at 1500 and 1596 cm^{-1}. However, the wood has such

strong absorbencies in the range from 1745 cm^{-1} and below, that other material absorbance peaks can often be masked.

The FTIR spectra of MAPP reveals a peak around 1788 cm^{-1} wavenumbers, corresponding well with the expected split anhydride peak at 1775 cm^{-1} (Figure 2.8). The combination of MAPP with the ZnSt/EBS lubricant reveals a shift to the hydrolyzed form of the copolymer at 1712 cm^{-1}. In addition, there is an apparent increase in the carboxylic acid-salt absorption at 1552 cm^{-1}. The stearate appears to form a bond with the anhydride, while the zinc may combine with the remaining carboxyl group to form an acid salt. The consumption of the MAPP polar groups from this reaction may inhibit bonding with the wood surface and therefore, reduce or negate coupling effects. Previous researchers have proposed that MAPP may interact with wood by forming an ester bond with the reaction of the anhydride with a hydroxyl group or through simple hydrogen bonding between a hydroxyl and carboxyl groups (Takase and Shiraishi 1989). Previous spectroscopy of wood-plastic composites coupled with MAPP copolymers without lubricants have failed to conclusively reveal a covalent ester linkage to the whole wood component (Kazaywoko et al. 1997 and Kazayawoko et al. 1998). As in the past research, the large ester absorptions present in the wood at 1745 cm^{-1} prevent the quantitative assessment of covalent bonds in this research. The mechanical evidence for the improvement in the performance of the wood-plastic composites strongly suggests some interaction is taking place (Wolcott et al. 2001). However, it is still not clear whether the improvement is from improved adhesion, better dispersion of the wood in the composite, or changes in crystal morphology.

FTIR microscopy was used to construct data plots to image the functional groups associated with specific material components. This technique facilitates imaging the spatial distribution of the particular chemical functionality and its associated constituent. Chemical imaging has revealed that during the crystallization process, soluble components that do not co-crystallizing with the PP are pushed to the growth front and are not incorporated in the crystal lamella. This material then collects in the margins and either undergoes a secondary crystallization step or remains amorphous in the interstitial regions. The ZnSt, OP 100, and MAPP are all semicrystalline in their pure forms. Still, the PP makes up the majority of the TCL and spherulites in the bulk polymer as observed by tracking the 2950 cm^{-1} with the absence of other functionality (Figure 2.9). The ZnSt appears to be excluded from the same regions of the PP crystals and collects mostly in the margins between the spherulitic structures (Figure 2.9). MAPP has also been excluded from the TCL and pushed away from the wood during the crystallization process. As observed previously, the 1712 cm^{-1} absorption is stronger in the composite containing ZnSt and MAPP than that of the 1788 cm^{-1}. The MAPP by itself is semicrystalline, however, it is not evident that, if combined with ZnSt under these conditions, a crystalline structure is formed. The natural variability of the wood leads to differences in the absorptions at 1745 cm^{-1} and below. Therefore, quantitative assessment of wood-MAPP or wood-stearate interaction was difficult to assess.

The OP 100 ester-based lubricant was pushed out of the crystal structure much like that of the MAPP and ZnSt. (Figure 2.10). The polyester material collects in the amorphous

regions between the spherulites and at the edge of the TCL. The interaction of the OP 100 lubricant and the wood is masked by the strong ester absorption in the wood. Because of the variable nature of the wood component, no quantitative comparison could be made. Further, interactions with the MAPP seem plausible by observing the sharp drop in K_i for the interphase, but no evidence was observed in the spectroscopy of the blends. The absorption at 1788 cm^{-1} was still present in the blends containing both OP 100 and MAPP.

2.7 Conclusions

The presence of wood in polypropylene blends has a definitive effect on the crystallization and morphology of the resulting material. Crystal growth kinetics revealed that neither the wood nor additives had an influence on the growth rate of the polypropylene crystals. However, the wood provided substantial surface area for nucleation, resulting in observed differences. The increased nucleation density on the wood surface changed the shape of the spherulites from a spherical to a truncated form, leading to a change in the Avrami exponent. The spherulites nucleating on the wood surface impinge on one another as they grow radially from the wood surface and truncate their spherulitic structure to form the observed TCL.

The inclusion of MAPP in the PP matrix, leads to increased nucleation on the surface of the wood and in the bulk. However, the significant increase in nucleating ability of the bulk lead to a net decrease in the nucleating advantage of the fiber over that of the neat PP. FTIR spectroscopy of the interphase did not confirm covalent bonding of the wood

with the MAPP because spectra of the two components overlapped. Any MAPP present at the wood-plastic interface was masked by the strong infrared absorption of the wood. However, the MAPP was observed to collect at the edge of the TCL. It is still unclear if improvements in material strength with the addition of maleic anhydride copolymers are the result of improved wood-plastic interaction, better dispersion of the wood component, or changes in the thermoplastic morphology.

The ZnSt/EBS system led to a decrease in thermal stability and perfection of the crystallized polymer. This destabilization was increased in the presence of wood. All blends containing the ZnSt/EBS lubricant system displayed significant decrease in nucleating advantage of the wood surface. The more pronounced shift in the melt observed in the DSC is likely that of the weakly formed TCL layer that was observed to melt before the bulk crystallites.

Evidence exists that ZnSt chemically interacts with MAPP. This interaction may impair any potential for bonding between the MAPP and wood. The ester-based OP 100 combined with MAPP had an increased the fiber nucleating advantage over the MAPP/ZnSt/EBS system and did not display a radical decrease in thermal stability. MAPP, ZnSt, and OP 100 were found in the highest concentrations at the edges of the TCL and spherulites, concentrated in the amorphous regions of the matrix.

Resent research has shown that the amorphous regions in fiber-reinforced PP composites play a major role in their mechanical performance (Assouline et al. 2001). It is possible

that the collection of the low molecular weight material in these amorphous regions will have a detrimental impact on mechanical properties. The mechanical implications of the TCL remain unclear and still very much debated in the literature [8,9,29]. Further investigation into the mechanical properties of the TCL and its adhesive action with the wood surface is needed.

2.8 List of Symbols

T_c crystallization temperature

T_m^o equilibrium melt temperature

ΔT degree of supercooling

$\Delta\sigma$ interfacial surface free energy difference (TCL)

$\Delta\sigma'$ interfacial surface free energy difference (bulk)

I rate of heterogeneous nucleation

I_o a constant

U^* activation energy

R ideal gas constant

T_∞ temperature at where all crystallization ceases

k_B Bolzmann's constant

Δh_f heat of fusion of the polymer

f correction factor ($2\ T_c /(T_c - T_\infty)$

σ lateral surface free energy

σ_e fold surface free energy

t_i induction time

K_i nucleation constant

G growth rate

G_o a constant

K_g nucleation exponent

b_o layer thickness for the growth plane

χ relative crystallinity

k Avrami crystallization constant

n Avrami exponent

N number of nucleation sites

t_χ time at a specified χ

A_1 arbitrary proportionality constant

A advantage for fiber nucleation

2.9 References

Assouline E, Grigull E, Marom G, Wachtel E, Wagner HD, Morphology of α-transcrystalline isotactic polypropylene under tensile stress studied with synchrotron microbeam X-ray diffraction, J Polym Sci Part B: Polym Phys 2001;39:2016-2021.

Avrami M, Kinetics of phase change: I general theory, J Chem Phys 1939;7:1103.

Cark EJ, Hoffman JD, Regime III crystallization in polypropylene, Macromol 1984;17(4):878-885.

Felix JM, Gatenholm P, Effect of transcrystalline morphology on interfacial adhesion in cellulose/polypropylene composites, J Mat Sci 1994;29:3043-3049.

Gati A, Wagner HD, Stress transfer efficiency in semicrystalline based composites comprising transcrystalline interlayers, Macrom 1997;30:3933-3935.

Gray DG, Polypropylene transcrystallization at the surface of cellulose fibers, Journal of Polymer Science: Polymer Letters 1974;12:509-515.

Heppenstall-Butler D, Bannister DJ, Young RJ, Astudy of transcrystalline polypropylene/single-aramid-fibre pull-out behavior using Raman spectroscopy, Comp A 1996;27:833-838.

Hoffman JD, Davis GT, Lauritzen JL, The rate of crystallization of linear polymers with chain folding, In: Hannay NB editor. Treatise on Solid State Chemistry, vol. 3: Crystalline and Noncrystalline Solids, ch. 7. New York: Plenum Press, New York, 1976, p. 497-614.

Ishida H, Bussi P, Induction time approach to surface induced crystallization in polyethylene poly(-caprolactone) melt, J Mat Sci 1991a:26;6373-6382.

Ishida I, Bussi P, Surface-induced crystallization in ultrahigh-modulus polyethylene fiber reinforced polythylene composites, Macromol 1991b;24:3569-3577.

Johnson JA, Nearn WT, Theory and design of wood and fiber composite materials, ch. 15. Reinforcement of polymeric systems with Douglas-fir bark fibers, Syracuse University Press, 1972. p. 371-400.

Kazayawoko M, Balantinecz JJ, Woodhams RT, Diffuse reflectance fourier transform infrared spectra of wood fibers treated with maleated polypropylenes, J Appl Polym Sci 1997;66:1163-1173.

Kazayawoko M, Balatinecz JJ, Woodhams RT, Sodhi RNS, X-ray photoelectron spectroscopy of lignocellusic materials treated with maleated polypropylenes, J Wood Chem Tech 1998:18(1):1-26.

Krzysik AM, Youngquist JA, Myers GE, Chahyadi IS, Kolosick PC,Wood-polymer bonding in extruded and nonwoven web composites panels, in Wood Adhesives 1990 Symp. of USDA Forest Service. Madison, WI, 1990. p.183-189.

Lin CW, Du YC, Effect of surface topographies of PTFE and polyimide as characterized by atomic force microscopy on the heterogeneous nucleation of isotactic polypropylene, Mat Chem Phys 1999;58:268-275.

Liu T, Petermann J, He C, Liu Z, Chung TS, Transmission electron microscopy observations on lamellar melting of cold-crystallized isotactic polystyrene, Macromol 2001;34:4305-4307.

Liu T, Petermann J, Multiple melting behavior in isothermally cold-crystallized isotactic polystyrene, Polym 2001;42:6453-6461.

Lu JZ, Wu Q, McNabb HS, Chemical coupling in wood fiber and polymer composites: a

review of couploing agents and treatments, Wood Fiber Sci 2000;32:88-104.

Matsuoka S, Daane JH, Bair HE, Kwei TK, A further study of the properties of transcrystalline regions in polyethylene, J Polym Sci Polym Lett Ed 1968;6:87.
28. Fakirov S, Krumova M, Rueda DR, Microhardness model studies on branched polyethylene, Polym 2000;41:3047-3056.

Pendleton DE., Hoffard TA, Adcock T, Woodward B, and Wolcott MP, Durability of an Extruded Hdpe/Wood Composite. Frst Prod J 2002;52(6):21-27.

Quillen DT, Caulfield DF, Koutsky JA, Crystallinity in the polypropylene/cellulose system. II. crystallization kinetics, J Appl Polym Sci 1994;52:605-615.

Schmidtke J, Stobl G,Thurn-Albrecht T, A four-state scheme for treating polymer crystallization and melting suggested by calorimetric and small angle x-ray scattering experiments on syndiotactic polypropylene, Macromol 1997;30:5804-5821.

Supaphol P, Spruiell JE, Thermal properties and isothermal crystallization of syndiotactic polypropylenes: differential scanning calorimetry and overall crystallization kinetics, Journal of Applied Polymer Science 75 (2000), 44-59.

Takase S, shiraishi N, Studies on composites from wood and polypropylene II., J Appl Polym Sci, 1989;37:645-659.

Wang C, Hwang LM, Transcrystallization of ptfe fiber/pp composites I. crystallization kinetics and morphology, J of Pol Sci: Part B: Polym Phys 1996;34:47-56.

Wang G, Harrison LR, Study of the preferential crystallization of polypropylene on the surface of wood fibers, In:ANTEC, 1994. p. 1474-1475.

Wolcott MP, Chowdhury M, Harper D, Heath R, Rials TG, Coupling agent/lubricant interactions in commercial woodfiber-plastic composite formulations. In: Proceedings of the6th International Conference on Woodfiber-Plastic Composites, Maddison, May 2001. p.197-204.

Wunderlick B, The basis of thermal analysis. In: Turi E, editor. Thermal Characterization of Polymeric Materials: Academic Press, 1981. p.91-234.

Yin S, Rials TG, Wolcott MP, Crystallization behavior of polypropylene and its effect on woodfiber composite properties, In: Proceedings of the Fifth International Conference on Woodfiber-plastic Composites, 1999, p. 139-146.

Zhao Y, Vaughan AS, Sutton SJ, Swingler SG, On the crystallizatin, morphology, and physical properties of a clarified propylene/ethylene copolymer, Polymer 2001;42:6587-6597.

Zhou W, Cheng SZD, Putthanarat S, Eby RK, Reneker DH, Lotz B, Magonov S, Hsieh ET, Geerts RG, Plackal SJ, Hawley GR, Welch MB, Crystallization, melting and morphology of syndiotactic polypropylene fractions. 4. *in situ* lamellar single crystal growth and melting in different sectors, Macromol 2000;33:6861-6868.

Formulation	***No Wood***		***30% Wood filled***	
	K_g (10^5 K^2) +/- 0.03×10^5 K^2	*n*	K_g (10^5 K^2) +/- 0.03×10^5 K^2	*n*
PP	3.44	2.03	4.01	1.98
OP	4.07	2.11	3.59	2.05
ZnSt/EBS	3.47	2.30	3.73	1.77
MAPP	3.73	2.45	3.92	1.95
MAPP/OP	4.03	2.40	3.65	1.88
MAPP/ZnSt/EBS	3.95	2.35	3.77	1.95

Table 2.1: Comparison of the Avrami exponents (*n*) averaged over all temperatures for polymer blends with and without wood and the nucleation exponent (K_g). Their predicted shape lies somewhere between a diffusion controlled and truncated sphere for *n* = 1.5-3 [27].

Source	DF	Sum of Squares	Mean Square	F	Pr > F
Model	4	0.71735883	0.17933971	5.90	0.0007
Error	43	1.30718095	0.03039956		
Corrected Total	47	2.02453978			
	R-Square	Coeff Var	Root MSE	*n* Mean	
	0.354332	8.340943	0.174355	2.090347	
Source	DF	Sum of Squares	Mean Squares	F	Pr > F
Wood	1	0.61070756	0.61070756	20.09	0.0001
MA	1	0.00439196	0.00439196	0.14	0.7057
Lubricant	2	0.1022593	0.05112966	1.68	0.1980

Table 2.2: ANOVA table was calculated where the Avrami exponent, *n*, is the dependent value. The class variables are wood and MAPP at two levels of addition each and OP with three levels of addition. The total number of observations is 48. Wood has the only significant effect on *n* for this model when the probability of a Type I error was set for $\alpha = 0.05$.

Formulation	*Bulk*			*Interphase*			A
	K_i (10^6 K^3)	K_g (10^5 K^2)	$\Delta\sigma'$ (10^{-11} J/m^2)	K_i (10^6 K^3)	K_g (10^5 K^2)	$\Delta\sigma$ (10^{-11} J/m^2)	
PP	6.1	1.9	11.5	4.7	2.1	8.0	1.4
OP	3.3	1.9	6.2	6.8	2.4	10.1	0.61
ZnSt/EBS	2.1	2.3	3.3	6.5	2.2	10.6	0.31
MAPP	3.5	2.2	5.7	4.8	2.4	7.2	0.80
MAPP/OP	3.5	2.3	5.4	3.6	2.2	5.9	0.93
MAPP/ZnSt/ EBS	1.7	2.2	2.8	4.3	2.2	7.0	0.40

Table 2.3: Kinetic parameters determined from polarized light microscopy for nucleation and growth in the bulk and at the wood interface

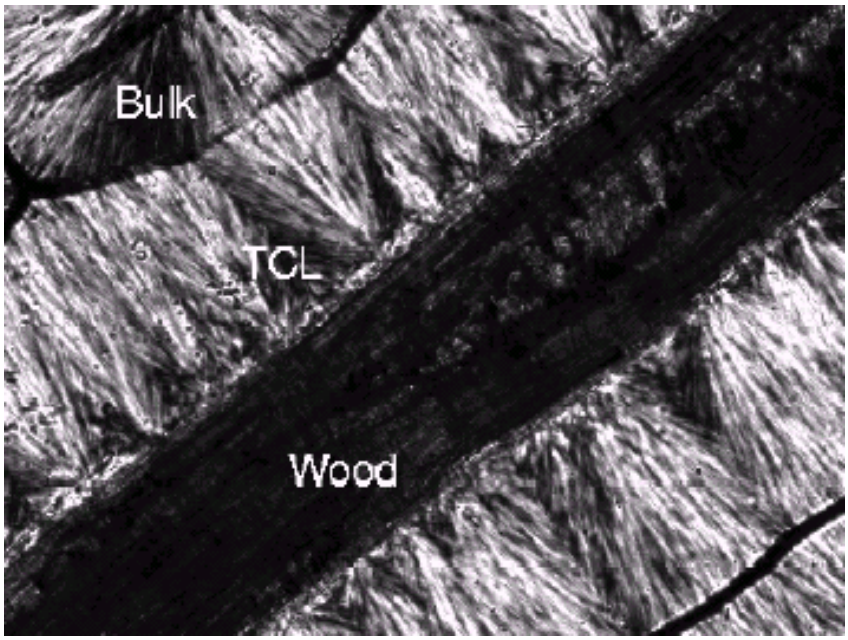

Figure 2.1: Wood and the transcrystalline layer (TCL) in a wood plastic composite.

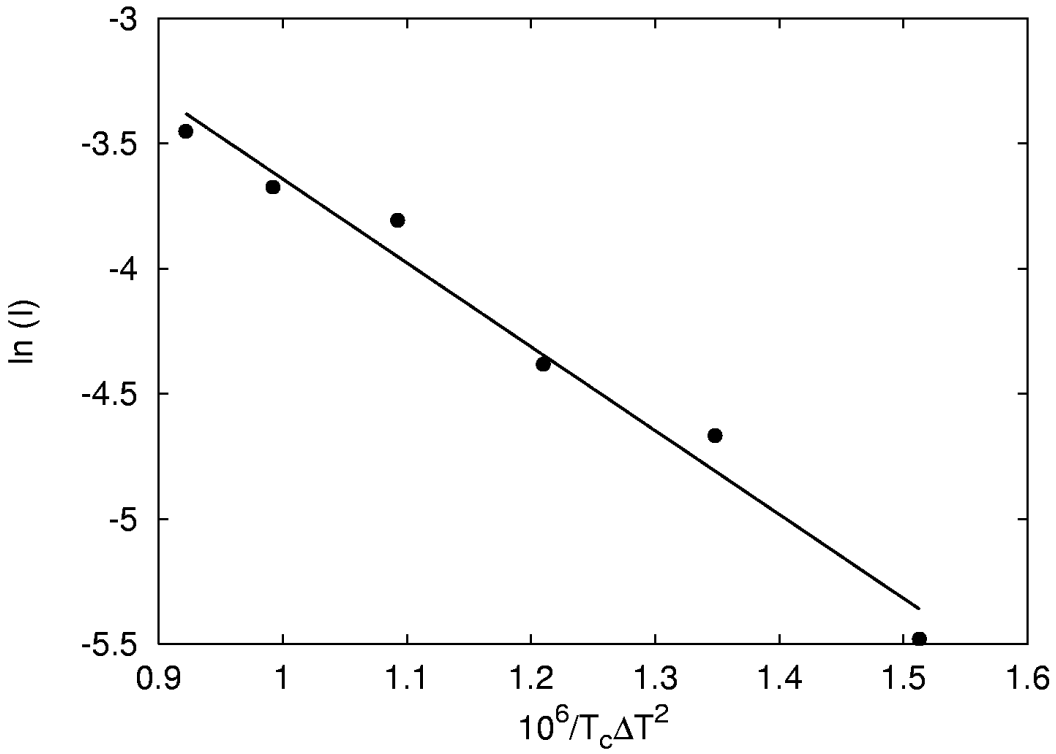

Figure 2.2: Nucleation plot where the slope of the line is K_i for 5% MAPP:95% PP for nuclei in the bulk.

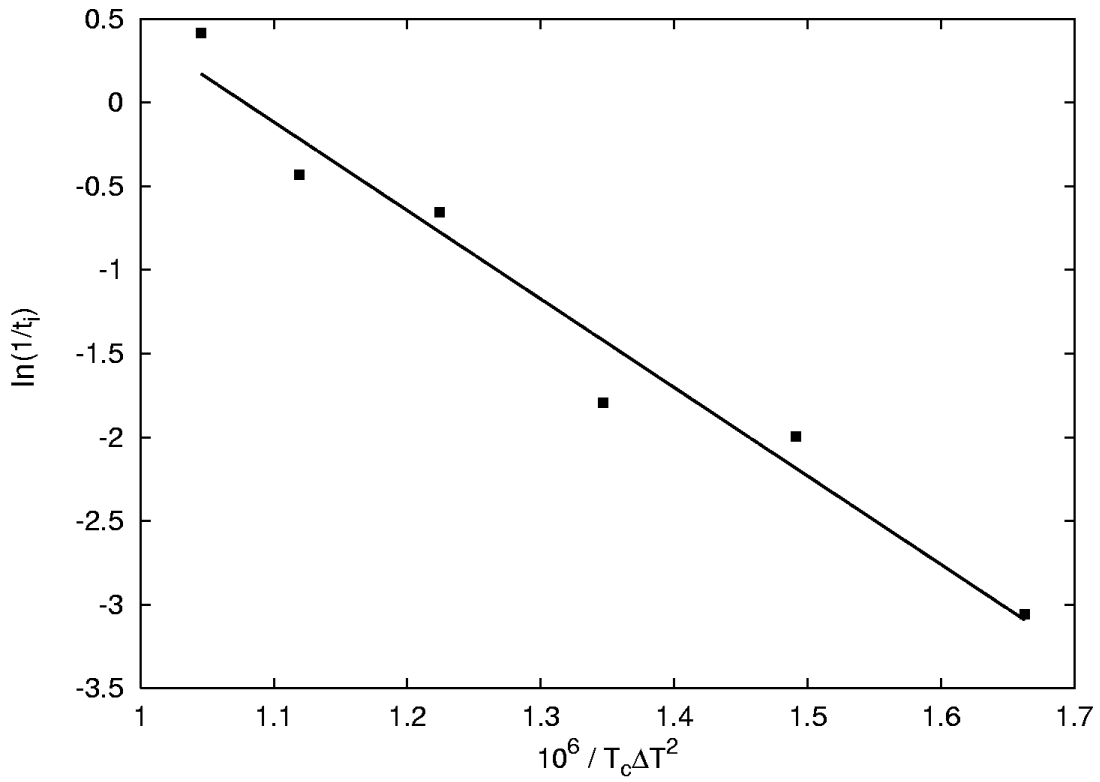

Figure 2.3: Induction time plot where the slope of the line is K_i for 5% MAPP:95% PP for nuclei formed on the wood surface.

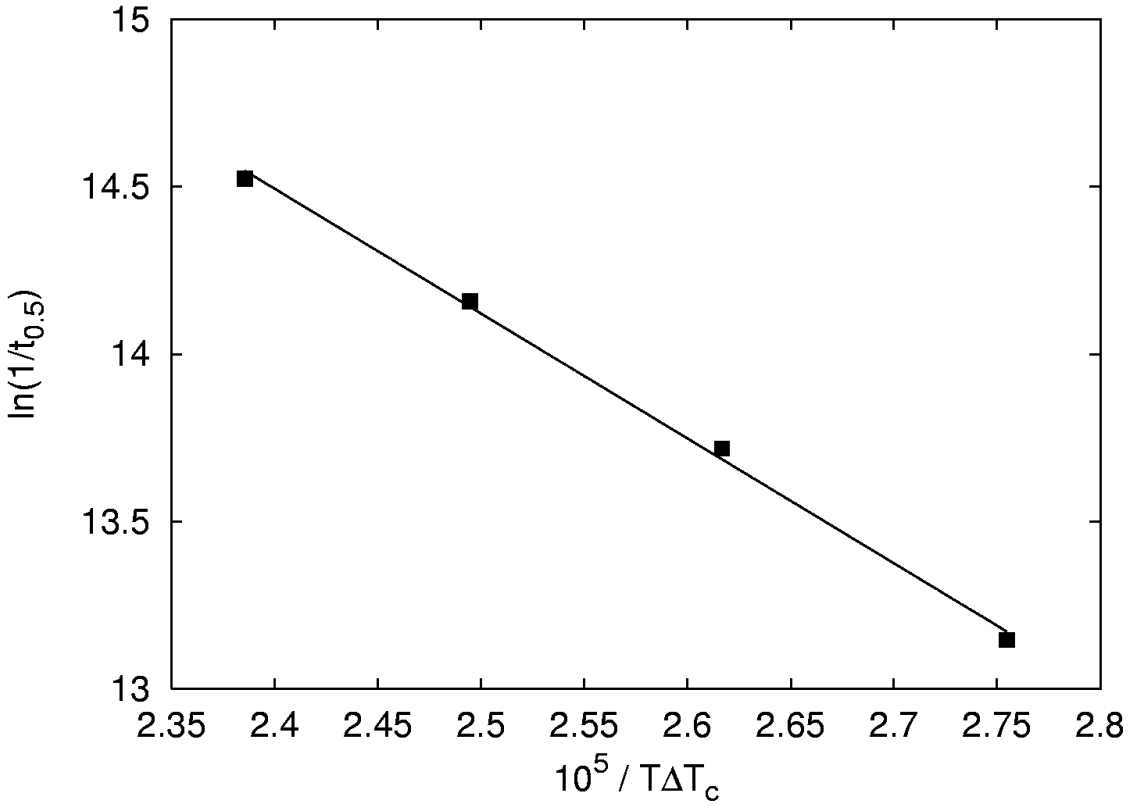

Figure 2.4: Avrami growth analysis for a polymer blend of 5% MAPP:95% PP.

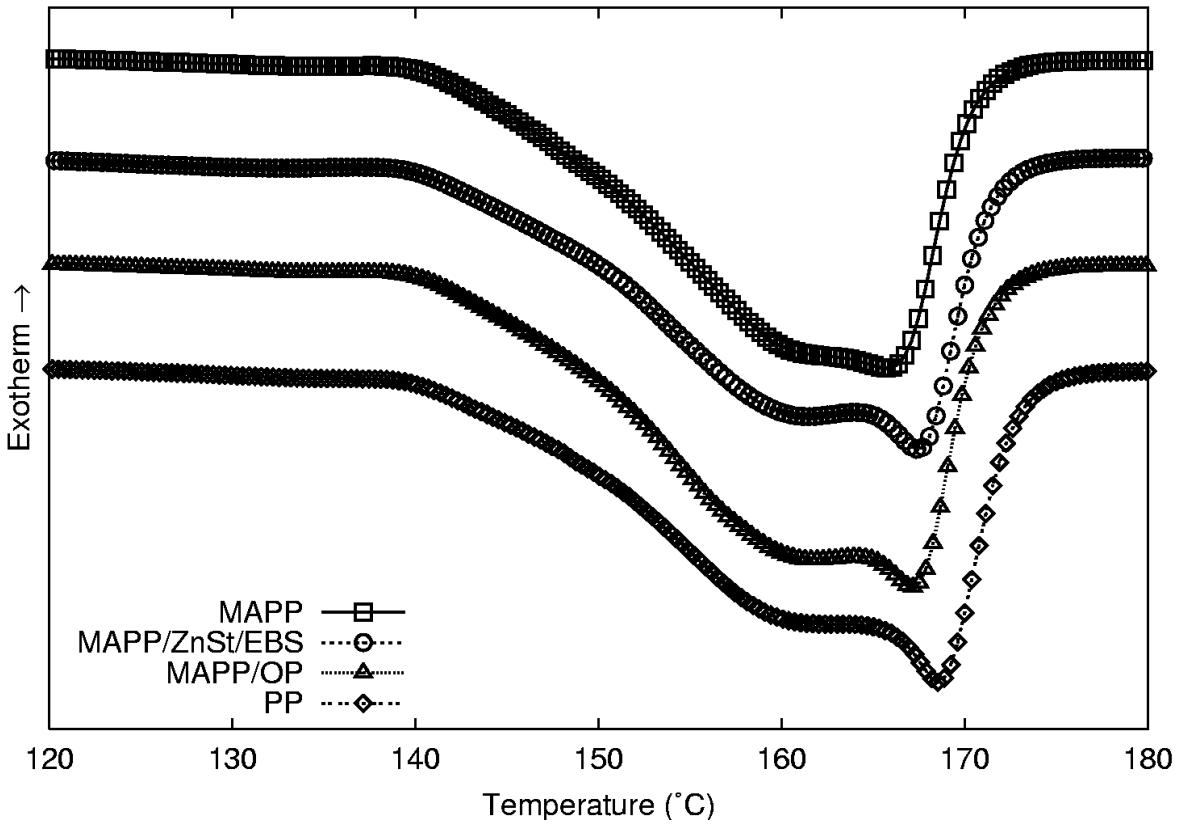

Figure 2.5: Comparison of the DSC melt behavior of polymer blends crystallized at 135ºC and containing 5% MAPP, 5% MAPP:3%ZnSt/EBS, 5%MAPP:2.7% OP 100, and 100% iPP.

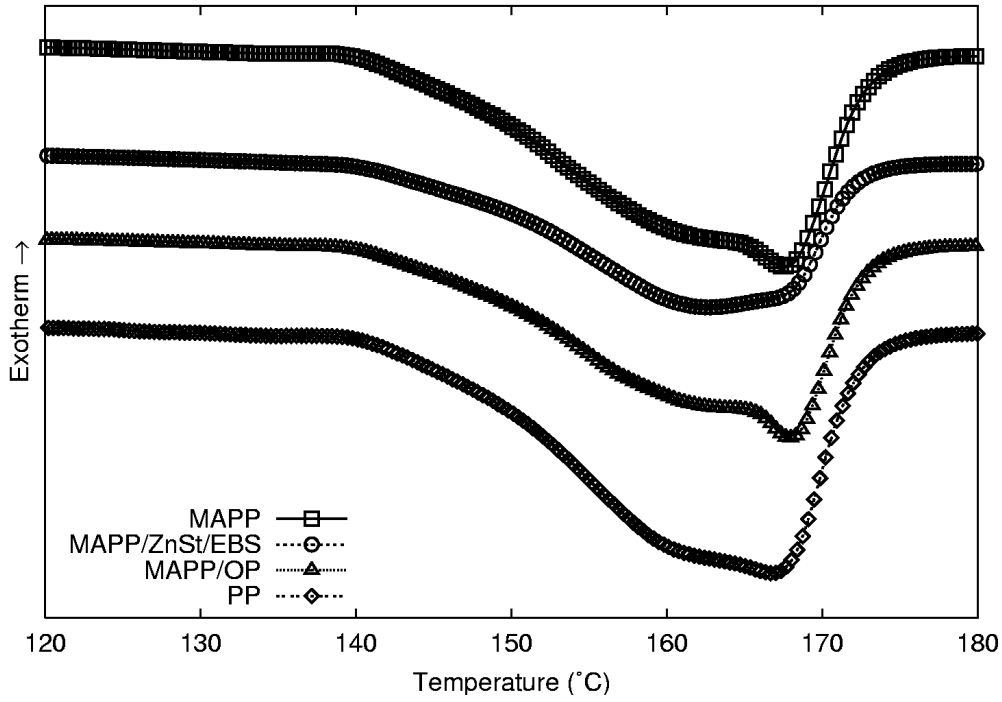

Figure 2.6: Comparison of the DSC melt behavior of polymer blends crystallized at 135ºC and containing 5% MAPP, 5% MAPP:3%ZnSt/EBS, 5%MAPP:2.7% OP 100, and 100% iPP. The polymer blends were compounded with 30% wood to 70% polymer.

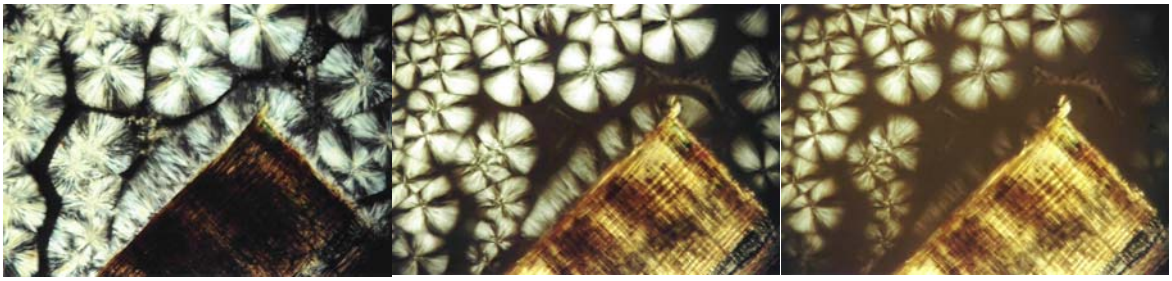

A B C

Figure 2.7: POM micrographs of a composite containing 3% ZnSt/EBS and 97% iPP ramped through the melt of the TCL A) 25ºC B) 162ºC C) 164ºC.

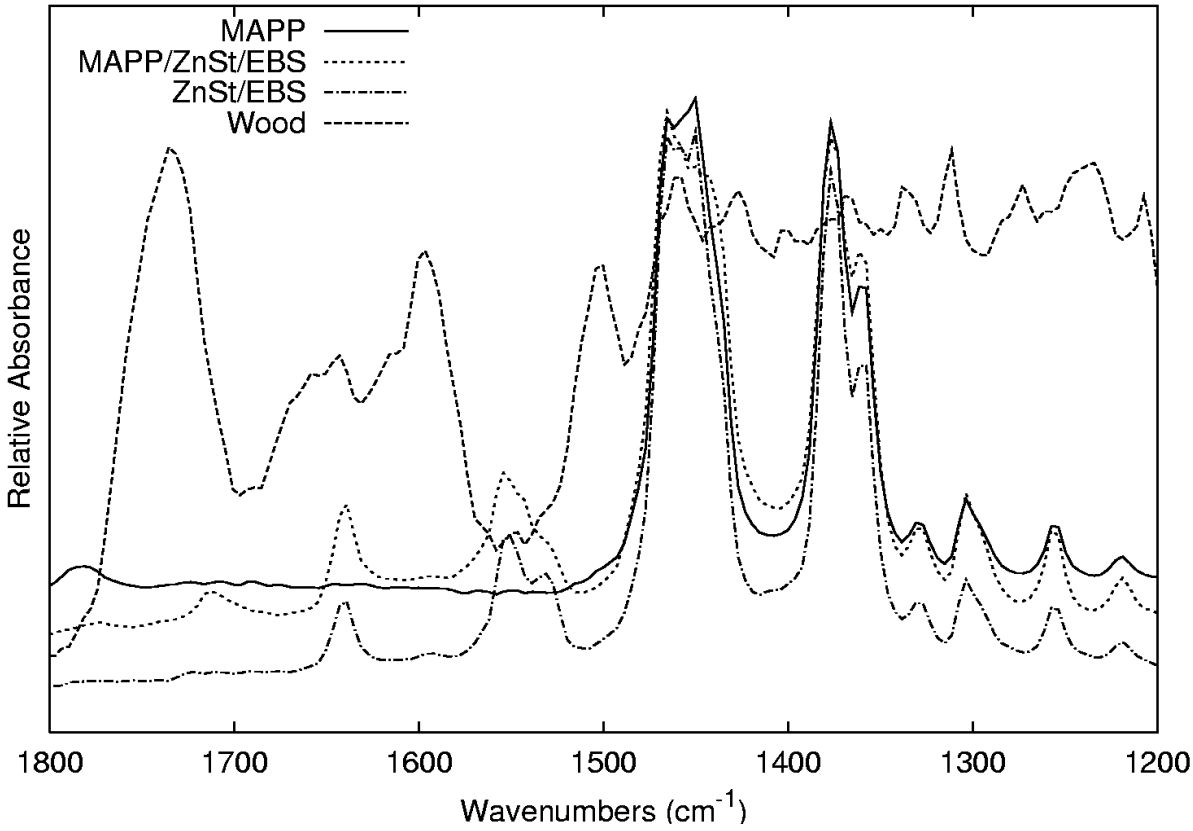

Figure 2.8: FTIR spectra taken from the edge of the TCL for blends with MAPP/ZnSt/EBS, ZnSt/EBS, and MAPP. The MAPP blend has absorption at 1788 cm^{-1} that is very weak in the MAPP/ZnSt/EBS blend. The MAPP/ZnSt/EBS blend displays an absorbance at 1712 cm^{-1} associated with hydrolysis of the MAPP.

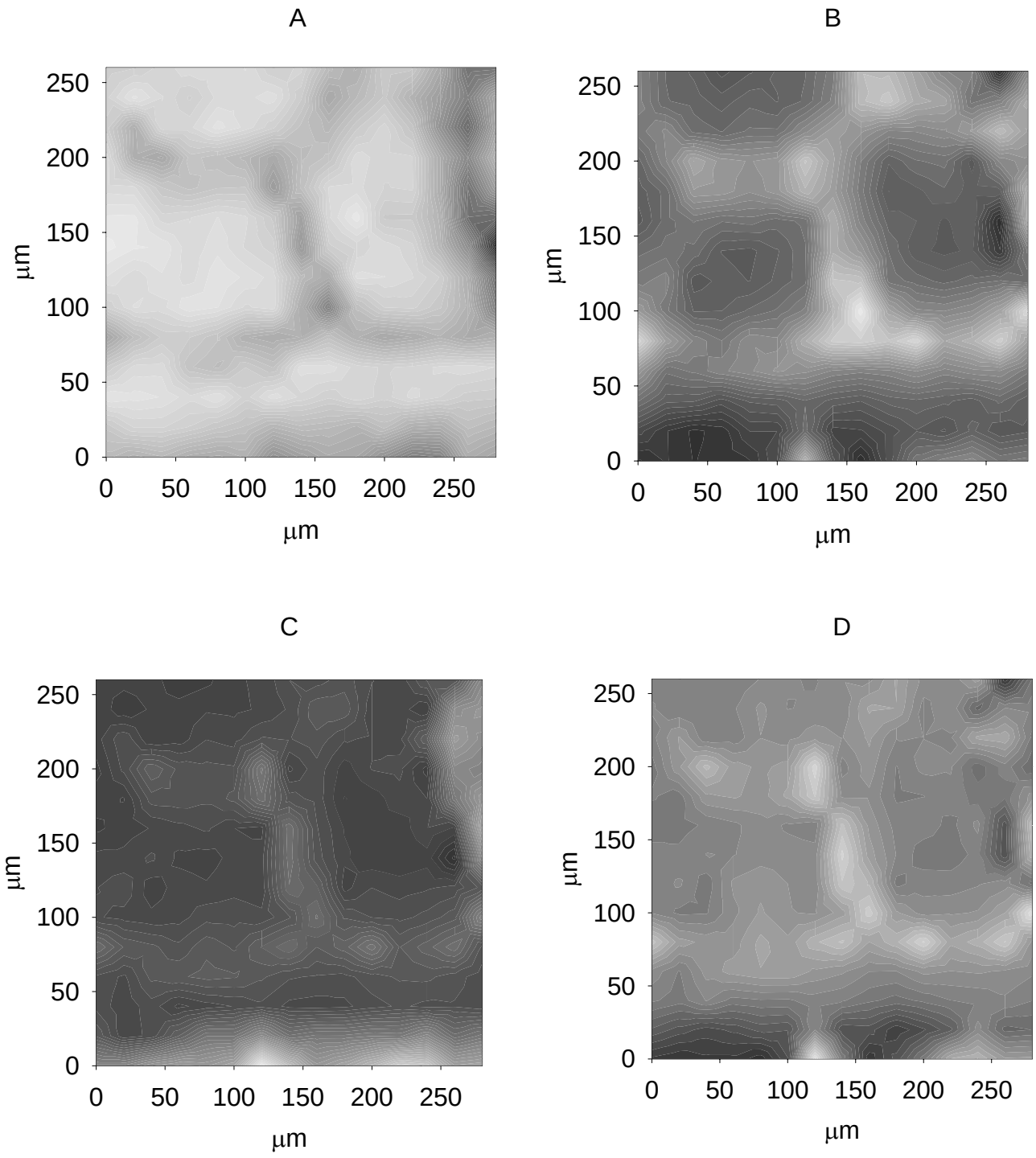

Figure 2.9: An FTIR contour map of a MAPP/ZnSt/EBS-wood composite system where the maps are of absorptions at A) 2950 cm^{-1} –CH stretching B) 1552 cm^{-1} acid-salt C) 1712 cm^{-1} acid and D) 1788 cm^{-1} anhydride. The wood is present at below 40 μm on the *y*-axis, most evident on plot C. The lighter shade of gray represents an increase in relative absorbance.

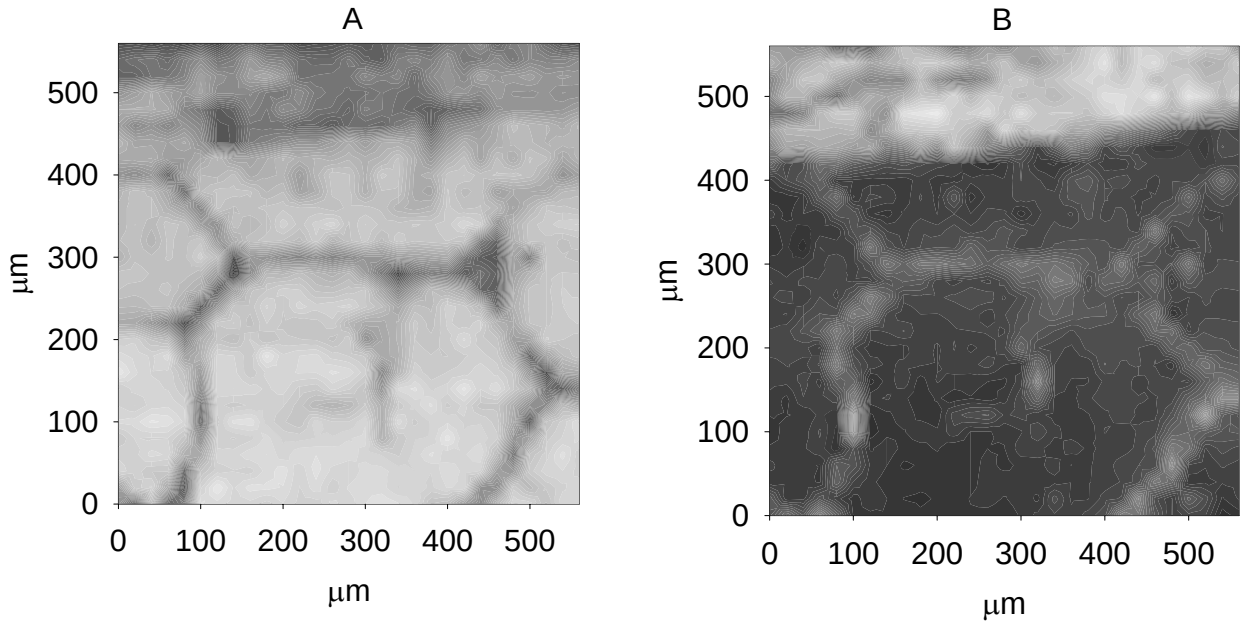

Figure 2.10: An FTIR contour map of an MAPP/OP 100-wood composite system where the gray scale is from dark to light (i.e. 0 to 1) in relative absorbance. The maps are of absorptions at A) 2950 cm^{-1} and B) 1745 cm^{-1} wavenumbers. The wood in the system is present above 450 μm on the *y*-axis.

Chapter 3 Chemical Imaging of Wood-Polypropylene Composites

3.1 Abstract

Recent investigations of wood plastic composites have revealed a detrimental effect of using lubricant systems in production. This includes nullifying part or all of the mechanical benefit of using a polar compatibilizer, maleic anhydride polypropylene (MAPP), in the composite formulation. Speculation exists whether the mechanism is lubricant interaction with the wood surface or with the bulk polymer that results in morphological and property changes in the composite. This research investigates the location of the material constituents and the impact on the chemistry of the interphase and wood-PP interface. To facilitate this investigation, lubricants labeled with deuterium were used in conjunction with Fourier transform infrared spectroscopy (FTIR). The deuterium labeling allowed for the separation of individual lubricants from all other constituents. The MAPP used in this study is not labeled. All of the deuterium labeled lubricants, used without MAPP, revealed their expulsion from the wood interface during crystallization. However, MAPP coupling agent was found to exist near the wood, but it is unclear if any covalent bonding occurred with the hydroxyl functionality on the wood surface occurred. The addition of zinc stearate lubricants appears to nullify the activity of the anhydride functionality near the wood surface as evidenced by a shift in the FTIR spectra to the hydrolyzed form of the coupling agent. Most of the additives collect at the edges of the spherulitic crystals in mostly amorphous regions of the material. The

consequence of this morphology may be a weak amorphous fraction compared to that of neat PP.

3.2 Introduction

The addition of processing lubricants has proven, in some cases, to be detrimental to the strength of wood-plastic composites (Wolcott et al. 2001). There are several possibilities for this result: (1) poor distribution of the wood component, (2) preferential migration of the lubricants to the wood-plastic interface, (3) a change in the morphology of the plastic phase, and (4) chemical reactions with the copolymer coupling agent. Two of these components, morphology and chemical reactions have shown to play an important role in wood-PP composites (Harper 2003). The morphology of a composite determines its performance. This is true for wood-plastic composites that possess a three-phase morphology whose development is dependent on processing conditions, coupling agents, and processing lubricants. Previous research has shown that different processing lubricants and copolymer coupling agents can impact the nucleating ability of wood in a polypropylene (PP) melt (Harper 2003). Increased nucleation can lead to an interphase around the wood that has higher modulus in the fiber direction (Assouline et al. 2001). Thus, the interphase increases reinforcement in addition to that provided by the wood. Further, high nucleation density of PP at the wood surface can expel lubricants and coupling agents from the wood surface. This could lead to expulsion of the coupling agent in some systems. In the case of polyethylene-wood composites, differences in the interphase and bulk morphology could present a mechanism for reduced bending strength with the addition of lubricants (Wolcott et al. 2001).

Chemical interactions may also play a role leading to the improvements in mechanical properties when a coupling agent is present. In the case of maleated polyolefins (e.g. maleated polypropylene (MAPP) (Fig. 3.1)), the potential of chemical reactions with the hydroxyl groups on the wood surface exists (Fig. 3.2). However, evidence of a covalent bond to date is found only when cellulose fibers are used with maleated polyolefin (Felix and Gatenholm 1991, Kazayawoko et al. 1997a, Kazayawoko et al. 1997b, Joly et al. 1996). FTIR investigations into the composite interfaces using whole wood or wood pulp fibers have revealed little conclusive information on the presence of a covalent bond between MAPP and wood chemical interaction at the wood-plastic interface (Kazayawoko et al. 1997a, Kazayawoko et al. 1997b, Son et al. 2000). The presence of lignin at the composite interface appears to make covalent bonding difficult when a maleic anhydride copolymer is used. Maleic anhydride alone has been shown to react with the hydroxyl groups in lignin (Kazayawoko et al. 1997a). However, steric hindrance effects can play a large role to impede the reactivity of maleic functionality on a MAPP copolymer when compared to that of MA alone. Even if a MA-OH reaction occurs, the aliphatic esters in lignin pose significant difficulties in quantifying ester formed at the wood interface when using FTIR.

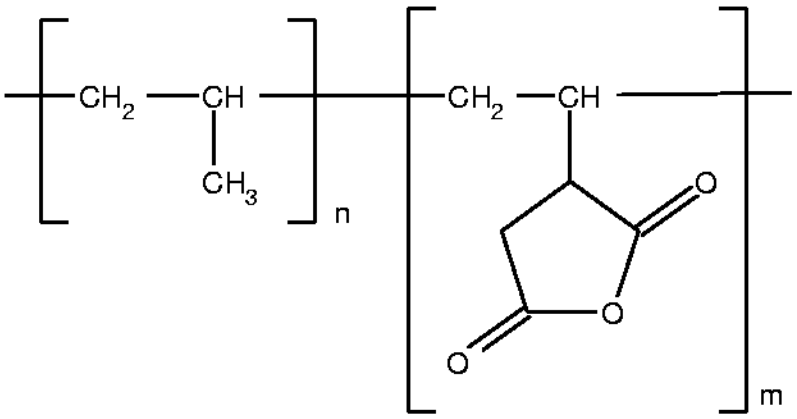

Figure 3.1: A proposed chemical structure of maleic anhydride polypropylene copolymer where the number repeating monomer units n and m are not know. Further, the frequency and termination of the copolymer chain is not known.

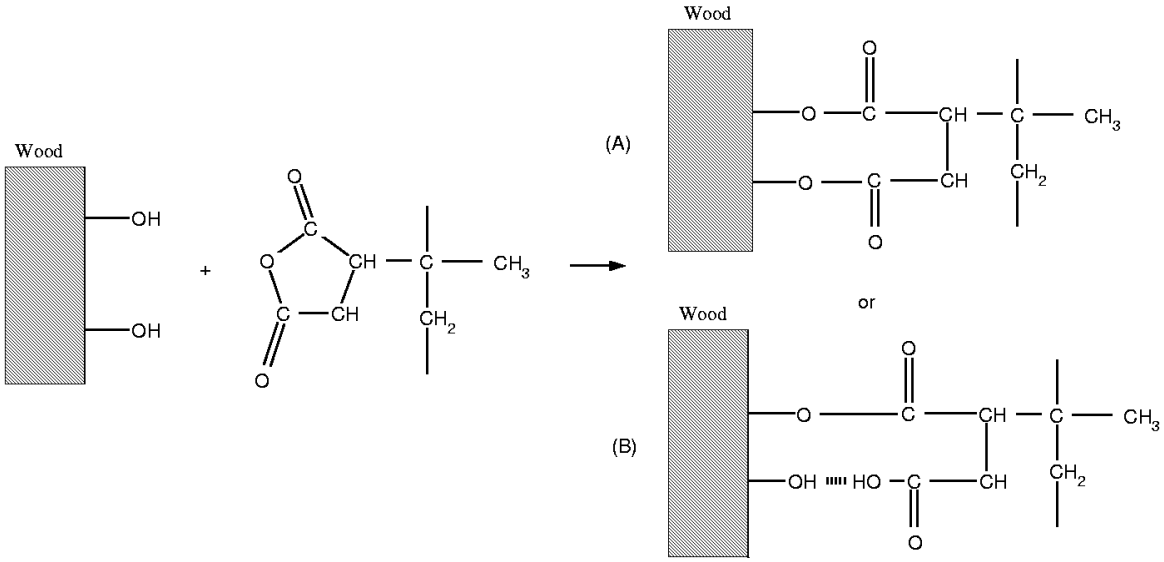

Figure 3.2: Potential reaction schemes for grafting MAPP to the wood surface as proposed by Bledzki et al. (1996).

Recent investigations into the development of crystal morphology in PP-wood composites show differences in the PP nucleating ability on the fiber surface when different lubricants are used (Harper 2003). Zinc-stearate (ZnSt) (Fig. 3.3) and ethylenebisstearamide (EBS) (Fig. 3.4) containing blends displayed decreases in thermal stability and the ability to nucleate on the wood surface. Previous research has also

shown that polyolefins containing these same two lubricants have negated the effects of coupling agents (Wolcott et al. 2001). The incorporation of zinc stearate as a lubricant in composites hydrolyzes the maleic anhydride group on the copolymer effectively negating any potential for covalent bonding or acid-base interaction (Harper 2003). .

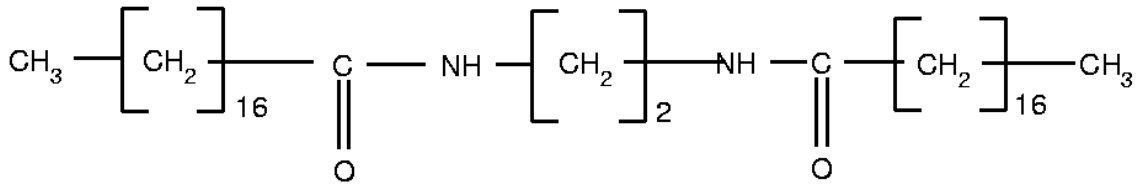

Figure 3.3: The chemical structure of ethylene bisstearamide (EBS).

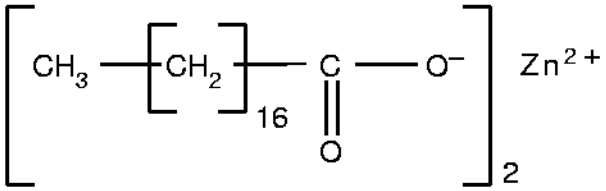

Figure 3.4: The chemical structure of zinc-stearate (ZnSt).

3.3 Objectives

The overall goal of this research is to determine if the lubricants used in extrusion interfere with the adhesion of coupling agents to wood. The lubricants have the potential to interact with the coupling agents and the wood making bond formation difficult. In many cases, the coupling agent is the highest cost component that is incorporated into the composite. Therefore, efficient coupling agent use is imperative to keep costs at a minimum and maximize the performance of the composite. The research focuses on the chemical functionality of the wood-PP interface and interphase. This will lend insight to

chemical bonding between material constituents. The specific objectives of this paper are to:

1. Identify the chemical functionality of materials at the wood-plastic interface,
2. Find the location of all material constituents in the composite,
3. Determine if chemical interactions exists between material constituents.

3.4 Methods and Materials

The deuterium-labeled Optipac 100 polyester lubricant (OP) (Honeywell), ZnSt, and EBS wax were obtained and prepared by Honeywell Corporation. The deuterium-labeled lubricants were used as received from Honeywell. Microbeam FTIR was performed using a Thermo Nicolet Continuμm Microscope. Background and transmission spectra were collected in transmission and a background was collected on the same window holding the specimen. For both the spectra and background, 128 scans were performed using Happ-Genzel apodization with a wavenumber resolution of eight. The aperture size varied depending on signal strength and thickness of the material. The same FTIR setup was used for subsequent spectral mappings discussed below.

Six polymer blends consisting of a nominal 3% lubricant were compounded in a 69-ml mixing head (Thermo Haake) with roller rotors at 180°C at 22 rpm for 8 min (Table 1). Five percent maleic anhydride polypropylene (MAPP) (Honeywell A-C 950P) that has a saponification number of 45 KOH/g and M_n = 8000, was used as a coupling agent in half of the polymer blends. The homopolymer used was a commercially available isotactic polypropylene (PP) (Solvay HB 9200) with M_n = 35000 with a melt-flow index of 4.0 g/10-min. The blends in film form were then placed individually on a microscope

heating/cooling stage (Linkam FTIR) attached to an Olympus BX51 microscope with a 40-μm thick microtomed slice of red maple (*Acer rubrum*) between two cover glasses. The wood-plastic laminates were then heated to 200ºC for 10 min under slight pressure to remove air bubbles and then cooled and held to the set temperatures of 128, 130, 132.5, 135, 137.5, and 140ºC to fully crystallize. Digital images with 1600 × 1200 pixels^2 density were acquired at set intervals during crystallization under polarized light with a high-resolution digital camera (Diagnostic Instruments Spot Insight). Following crystallization, the specimen was removed from the cover glasses and placed on a 2 mm thick KBr window. The specimen and window were then placed in FTIR microscope for spectral mapping. Maps were collected on a 20 μm × 20 μm square grid using the same size aperture. The range of spectra collection was from inside to the wood, through the interphase, and into the bulk matrix. Specimens were prepared as mentioned above on a microscope hot stage and mounted on aluminum stubs with a pressure sensitive carbon film. This procedure was followed for all collected spectra.

To detect the presence of Zn within the PP crystal structure, elemental dispersive X-ray diffraction (EDX) (KEVEX 3200) was conducted using a Hitatchi S-570 scanning electron microscope (SEM) at 15 kV with a working distance of 18 mm. The EDX has a 0.008 mm window and data was acquired for 60 s on each specimen. The specimens were then sputter coated with carbon before being placed in the SEM. Data was collected at the nucleus, halfway, and at the edge of the TCL and bulk spherulites. Further, care was taken to ensure that spectra were collected at the interface of the wood and the plastic material.

Blend	%PP	%MAPP	%OP	%ZnSt	%EBS
PP/DOP	97.3	0	2.7*	0	0
PP/MA/DOP	92.3	5	2.7*	0	0
PP/DZnSt/EBS	97	0	0	2*	1
PP/MA/DZnSt/EBS	92	5	0	2*	1
PP/ZnSt/DEBS	97	0	0	2	1*
PP/MA/ZnSt/DEBS	92	5	0	2	1*

Table 3.1: Polymer blends formulations compounded for FTIR investigation of the wood-plastic interface presented in mass percentages. The "*" and the D in the blend name represents the deuterium labeled component in the formulation.

3.5 Results and Discussion

3.5.1 Characterization of the deuterium labeled lubricants

Fully deuterated lubricants were individually substituted in formulations to assist in separating the spectral peaks of the lubricants in an FTIR map from those of the PP and wood (Fig. 3.4). The deuterium labels should shift the C-H stretching in agreement with the Teller-Redlich product rule for isotope substitution (Bower and Maddams 1989).

$$\left[\frac{v_1'}{v_1}\right]\left[\frac{v_2'}{v_2}\right]\cdots\left[\frac{v_n'}{v_n}\right] = \sqrt{\left[\frac{m_1}{m_1'}\right]\left[\frac{m_2}{m_2'}\right]\cdots\left[\frac{M'}{M}\right] f\left(I, I'\right)}, \qquad \textbf{Equation 3.3.1}$$

Where the quantities v_1, v_2, …v_n, are the frequencies of the n normal vibrations of the given symmetry species, the quantities m_1, m_2, …, are the masses of an individual member of each of the symmetry-related atoms in the molecule, M is the total mass of the molecule, t is the number of given translations of the given symmetry species, and $f(I', I)$ is the product of the ratios of the moments of inertia about each of the primary axis (I'_i/I_i where *benefit* is x, y, and z). By considering fully deuterated polyethylene as a model, a

value calculated of 0.707 is obtained for B_{3u} vibration and 0.756 for a B_{1g} vibration. Thus, assuming a wavenumber of 2950cm^{-1} for the original molecule a value of 2086cm^{-1} is obtained for C-D stretching.

The spectra for deuterated and hydrogenated versions of the lubricants display C-D stretching as a split peak of wavenumbers 2193cm^{-1} and 2100 cm^{-1}. These peaks are characteristicly similar for all the deuterated lubricants (Figures 3.6-8). The spectra of ZnSt and EBS show an absence of C-H stretching relating to nearly full deuterium substitution for H. The OP still has a presence of some C-H stretching, but it is not clear if it is in the main chain because of the proprietary nature of the lubricant.

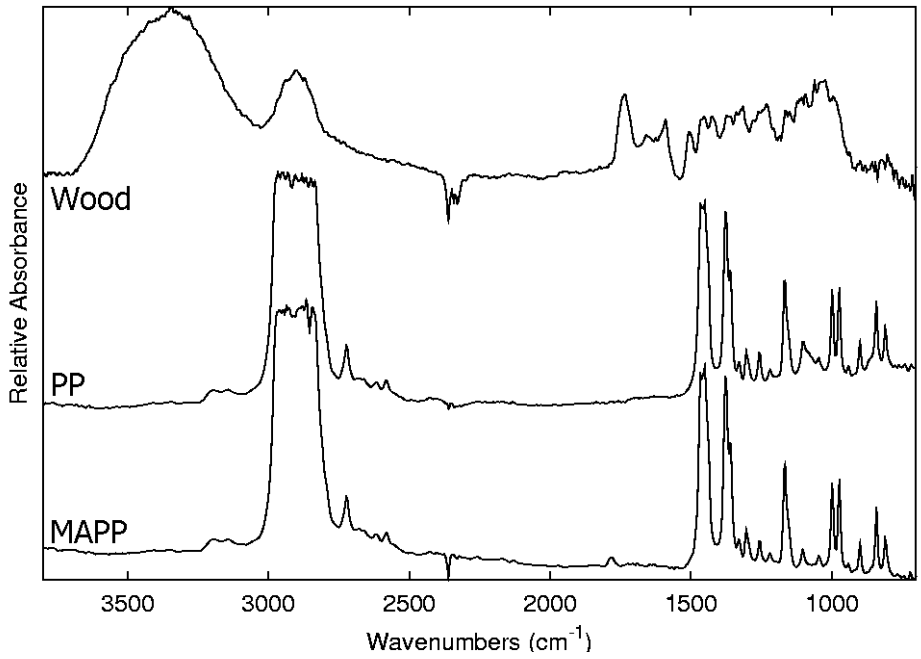

Figure 3.5: FTIR spectra recorded for wood, PP, and MAPP. A weak absorbance for the anhydride group at 1788 cm^{-1} shows in the MAPP spectrum and can be masked by the strong ester absorption in wood at 1745 cm^{-1}

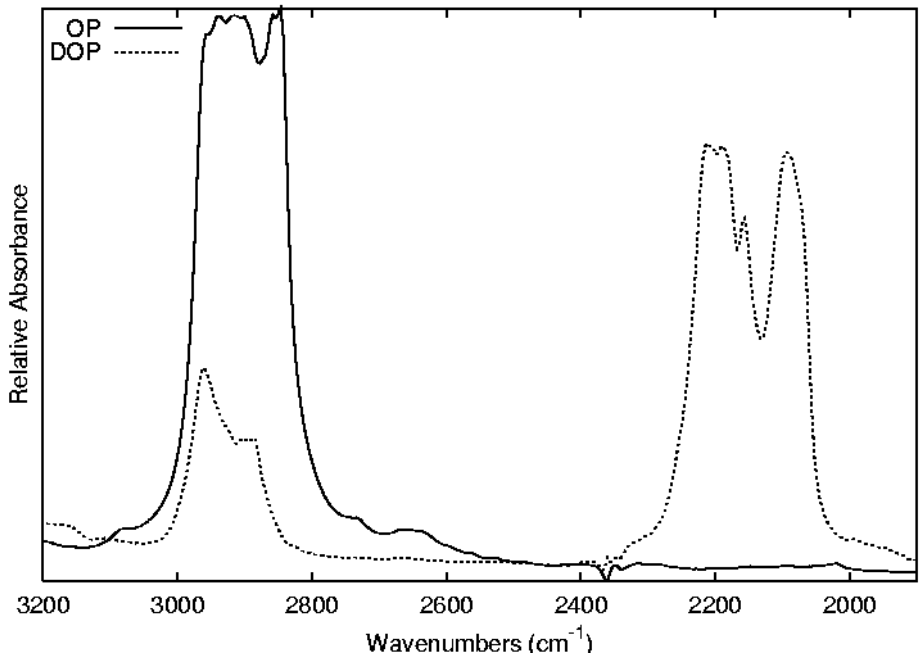

Figure 3.6: A comparison of the C-H to C-D peaks for labeled and unlabeled ester-stearate lubricant, OP.

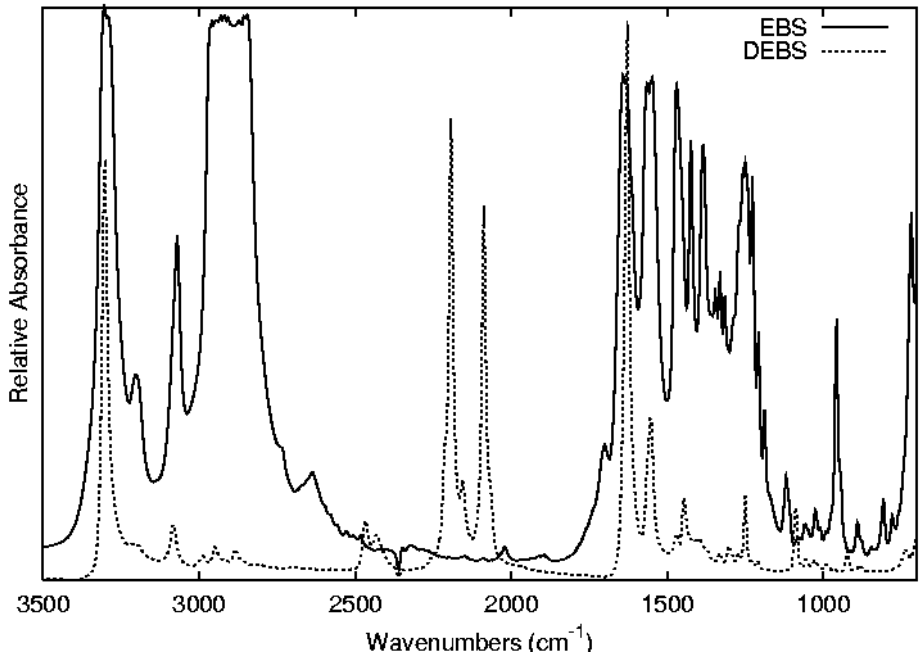

Figure 3.7: A comparison of the FTIR spectra of a hydrogenated and fully deutererated samples of EBS.

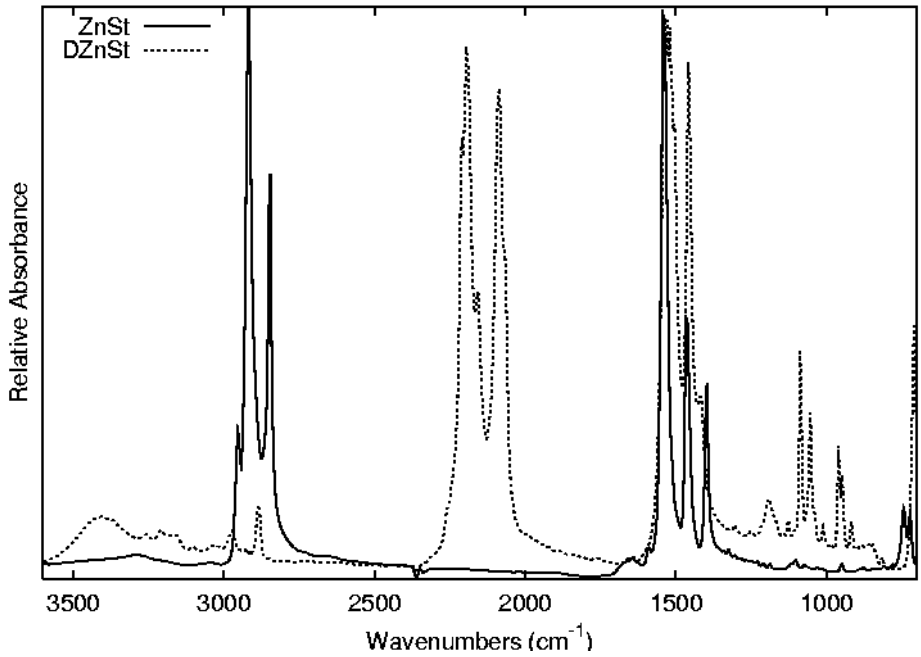

Figure 3.8: A comparison of the FTIR spectra of hydrogenated and fully deutererated ZnSt .

3.5.2 Location of DOP

A map was generated for of the C-D stretching for a composite of DOP and wood by plotting the ratio between 2193 cm^{-1} and 2950 cm^{-1} (Figure 3.9). The lighter colors reveal the location where the OP is in highest concentrations. The DOP collects in the highest concentrations in the margins between the spherulites. The light spots present in the wood reveal a thickness difference in the wood where the overall transmission through the specimen was reduced. Most importantly in this analysis, the OP appears to be mostly excluded from the wood-PP interface. There does, however, exist an amount of OP still at the interface (Figure 3.10). This may contribute to a previous observation of reduced nucleation on the wood surface (Harper 2003).

The inclusion of MAPP reveals most of the lower density regions at the edges of the interphase and spherulites similar to without MAPP (Figure 3.11). There appears to be no miscibility between the PP and the OP in the crystalline phase. In general, the structure polyesters do not permit miscibility in PP. However, it may lower the mechanical properties of the amorphous regions by collecting at the edges of crystallites. Adding an immiscible polymer to a blend is often detrimental to strength (Utracki 1989).

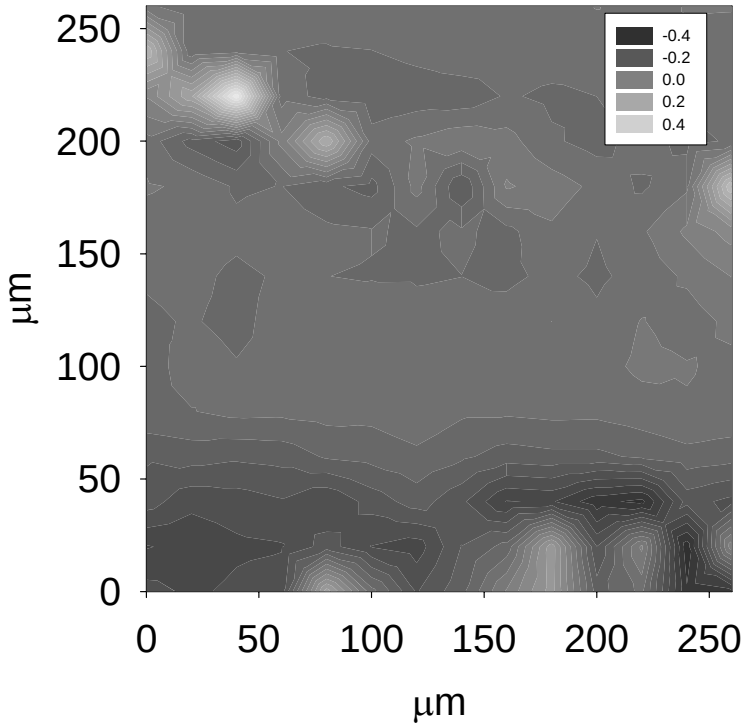

(A)

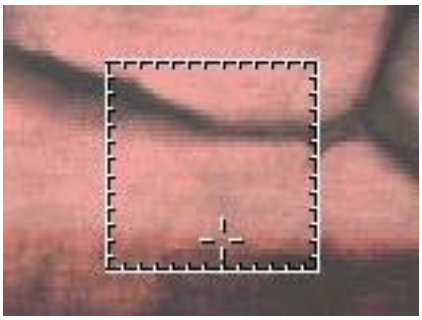

(B)

Figure 3.9: A map of the 2193 cm^{-1} absorption of C-D stretching in the deuterium labeled component (OP) normalized with the 2950 cm^{-1} absorption for C-H stretching in a PP/DOP blend (A). The wood interface is present between 40-60 µm as seen in the microscope image (B) where each tic represents 20 µm.

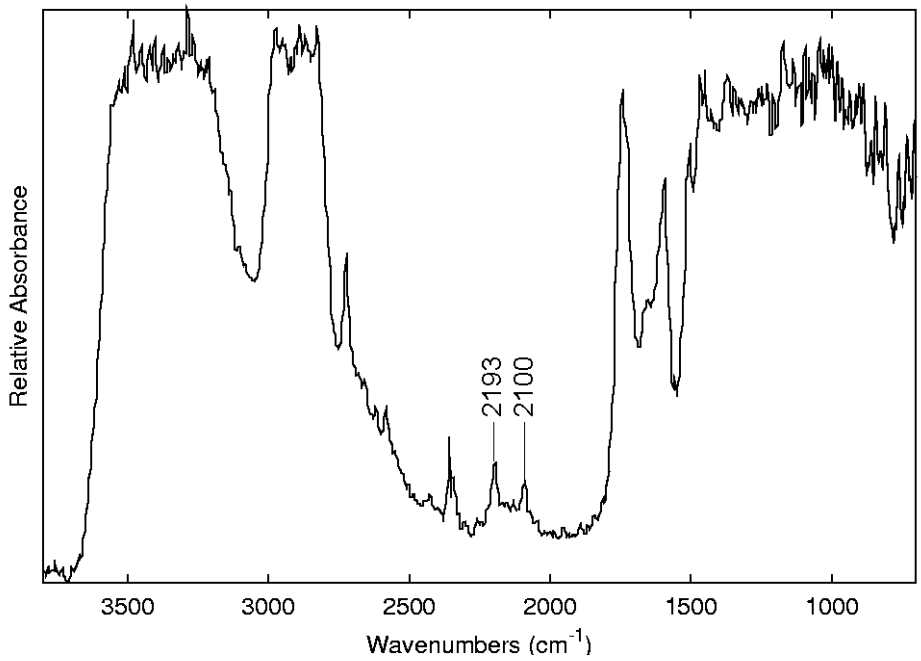

Figure 3.10: FTIR spectra taken at the interface of a PP/DOP blend and wood.

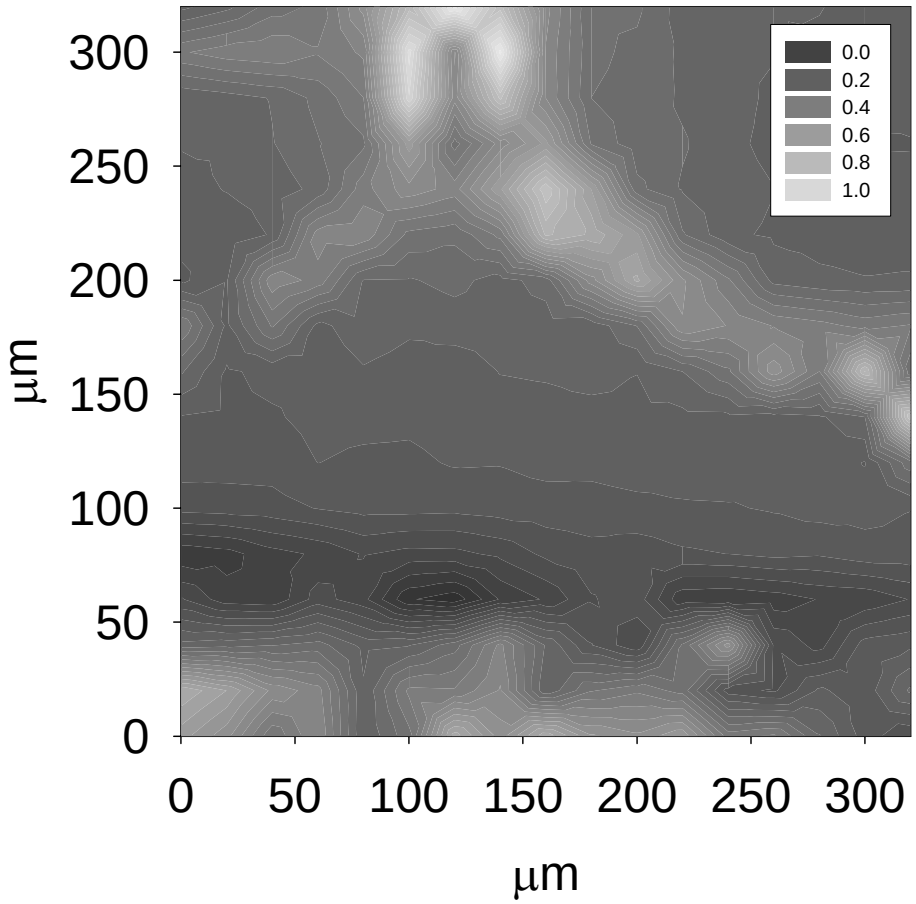

(A)

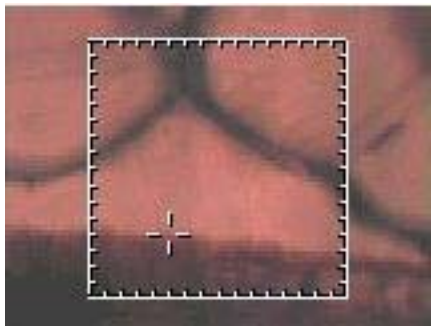

(B)

Figure 3.11: A map of the 2193 cm^{-1} absorption of C-D stretching in the deuterium labeled component (OP) normalized with the 2950 cm^{-1} absorption for C-H stretching in a PP/MAPP/DOP blend (A). The wood interface is present between 60-80 μm as seen in the microscope image (B) where each tic represents 20 μm.

3.5.3 Location of DEBS

DEBS is tracked in the same manner as DOP by normalization of the C-D 2193 cm^{-1} with 2950 cm^{-1} in a contour map (Figure 3.12). Much like the OP, the highest intensities are at the edges of cystallites. The DEBS is added at lower levels than the OP to be consistent with levels used during composite manufacture. Much like DOP, DEBS remains in a small amount at the wood interface (Figure 3.13). EBS may play a role in limiting nucleation of PP at the wood interface, but it is more likely that the combination of ZnSt/EBS as a lubricant behaves as a nucleating agent (Harper 2003). The ZnSt/EBS presents surfaces that are more favorable for nucleation in the bulk than wood.

The normalized 2193 cm^{-1} wavenumber occurs in highest concentrations outside of the interphase in a blend incorporating DEBS and MAPP (Figure 3.14). This again demonstrates that the majority of the lubricants are collecting at the crystal growth front and being pushed away from the wood surface. However, the lubricants in general decrease the nucleation on the fiber surface. Some lubricant is likely trapped between impinging crystallites in their embryonic state. Thus, a small amount of the lubricant is retained at the interface and in the interphase.

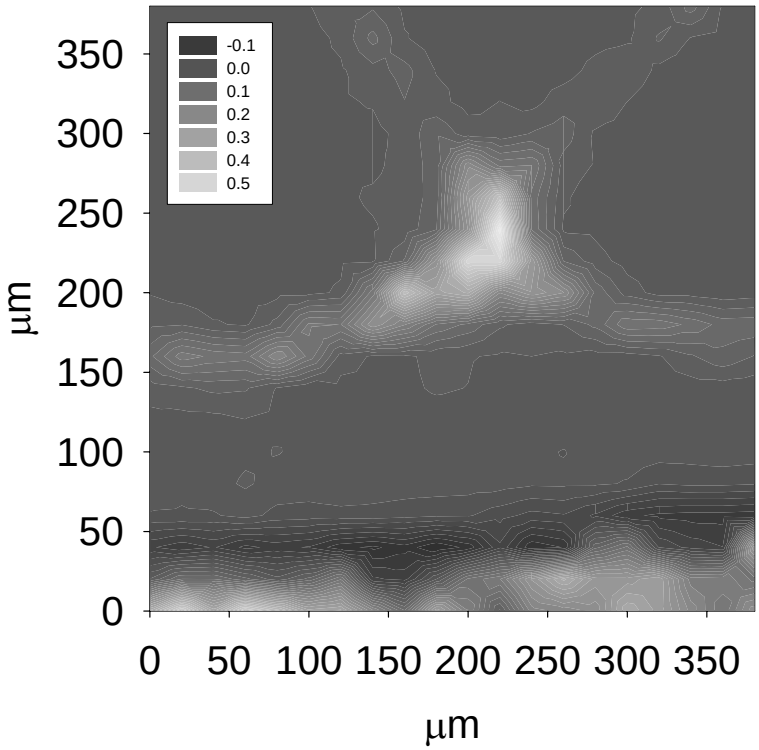

(A)

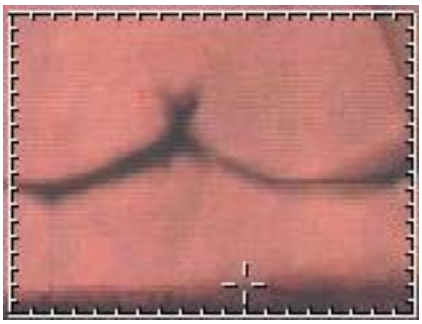

(B)

Figure 3.12: A map of the 2193 cm^{-1} absorption of C-D stretching in the deuterium labeled component (EBS) normalized with the 2950 cm^{-1} absorption for C-H stretching in a PP/ZnSt/DEBS blend (A). The wood interface is present between 20-50 μm as seen in the microscope image (B) where each tic represents 20 μm.

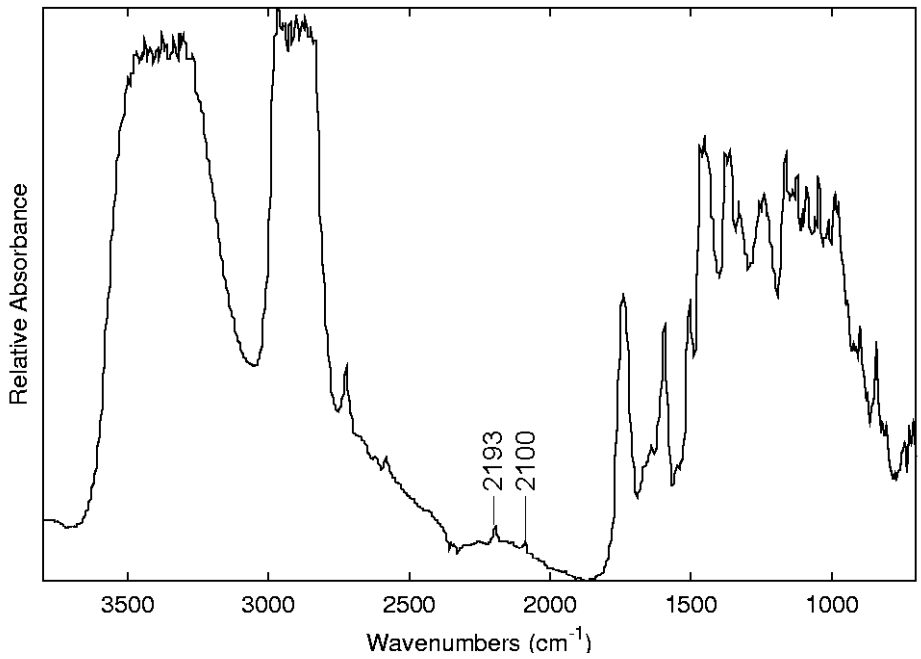

Figure 3.13: An FTIR spectra taken at the interface of a PP/ZnSt/DEBS blend and wood.

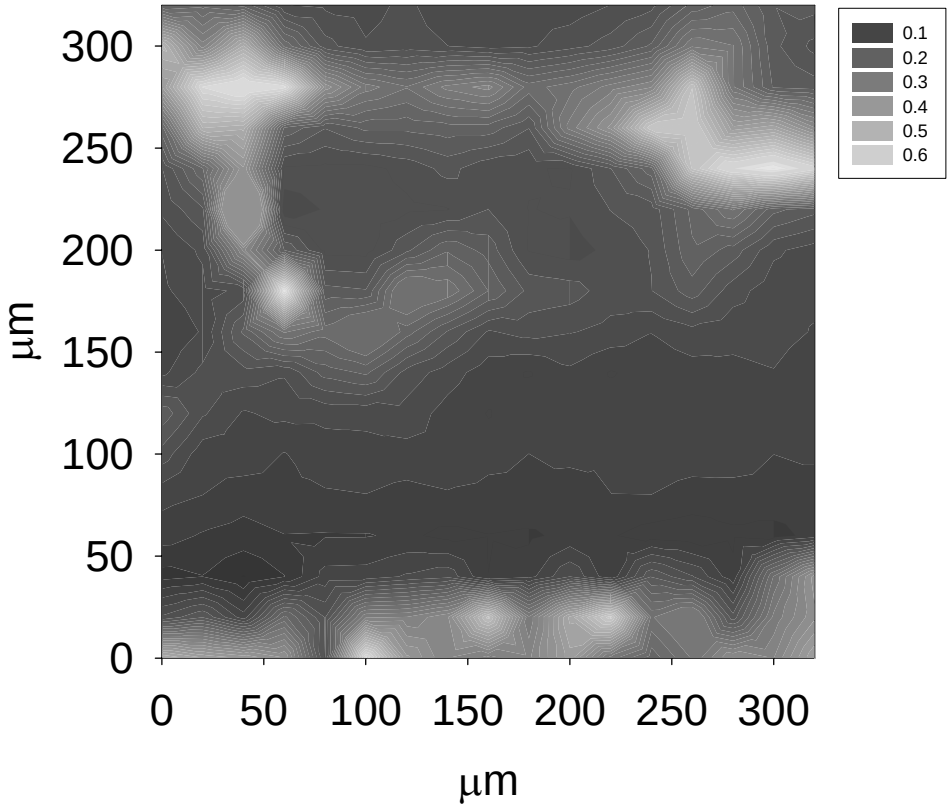

(A)

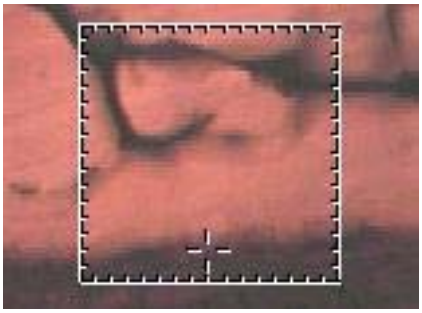

(B)

Figure 3.14: A map of the 2193 cm^{-1} absorption of C-D stretching in the deuterium labeled component (EBS) normalized with the 2950 cm^{-1} absorption for C-H stretching in a PP/MAPP/ZnSt/DEBS blend (A). The wood interface is present between 40-80 µm as seen in the microscope image (B) where each tic represents 20 µm.

3.5.4 Location of zinc stearate

The C-D stretching in the PP/DZnSt blends, like the other lubricants, exists largely at the edges of spherulites and the interphase (Figure 3.15). There still exist some amount of DZnSt at the wood interface (Figure 3.16). What is not apparent in any of these analyses is if there is any secondary bond formation between the wood and the lubricants. The FTIR spectra of the lubricants are mostly unchanged from their original form in PP blends. This further leaves in question how much the small lubricant presence at the interface impacts mechanical properties.

Blends containing MAPP and DZnSt once again displayed the greatest amount of C-D stretching at the boundary of the interphase and spherulites (Figure 3.17). Unlike the other lubricants, it was demonstrated that there is hydrolysis of the anhydride when ZnSt is incorporated into the blend (Harper 2003). There is a change from the anhydride at 1788 cm^{-1} to a 1712 cm^{-1} absorption characteristic of either a ketone or carboxylic acid (Figure 3.18). The slight broadening in the spectra between 2500-3000 cm^{-1} comes from O-H stretch vibrations of a carboxylic acid dimer. These vibrations are characteristically lower in the acid than an alcohol. The strong hydrogen bonds present in the carboxylic acid make it much less reactive than the anhydride form. Therefore, the efficacy for wood adhesion is greatly reduced with the incorporation of ZnSt.

ZnSt is unique in this study because it is the only lubricant containing a metal. EDX was therefore available as a tool for identifying the location of elemental Zn. ZnSt has a considerable ash content (11%) that is composed of mainly ZnO. The ZnO itself may

play an important and as yet unidentified role in the composite. EDX analysis is, therefore, useful in that it can detect the location of elemental Zn where FTIR is limited to mostly organic materials. Much like the FTIR results, EDS revealed the only presence of Zn to be at the edges of the spherulites and the TCL for blends without MAPP (Figure 3.19). The inclusion of MAPP, however, gives rise to K_a diffraction of Zn that is slightly above baseline at the wood interface and between the nucleus and spherulite edge (Figure 3.20). The copolymer is now acting as a carrier to incorporate the stearate into the spherulitic structure. This is further indication of the interaction between the MAPP and ZnSt. The incorporation of stearate will likely have a destabilizing effect on the crystal structure that will lead to decreased mechanical properties. A large Ca band is present on the wood surface and is likely associated with the wood ash content. No Ca containing substances were added to the composite with the possible exception of wood.

3.5.5 Location of MAPP

An uncertain feature of using MAPP in wood-PP composites is its mechanisms for improving properties. There has been much supposition of the existence of the formation of an ester bond discussed previously. Deuterium labeling of the anhydride group on the copolymer was determined to be insufficient to produce a strong enough signal to detect a possible chemical reaction by using FTIR. A mapping of the anhydride absorption at 1788 cm^{-1} was normalized with the C-H stretching peak at 2950 cm^{-1} (Figure 3.21). The C-H stretching is primarily from PP, the main blend component. There does appear some increase in intensity at the edges of spherulites, but the MAPP appears to be well

dispersed throughout the matrix. The high intensities around the wood are from the very strong neiboring 1745 cm^{-1} absorbance of wood lignin.

Previous research has revealed that there exists the possibility of co-crystallization of MAPP with PP when MA is present at low concentrations on the backbone (Duvall et al. 1994). The mechanical strength of a PP-MAPP matrix was improved when a low MA content was used. FTIR maps display some degree of separation of the copolymer at the edges of the TCL and spherulites. This behavior was much less pronounced than that observed with the lubricants. It is necessary to note that some of the differences might be from the differences in material concentration used in this research.

A waterfall plot of a PP/MAPP blend extends from the edge of the interphase into the wood (Figure 3.22). The anhydride absorbance is present throughout the interphase and into the wood. The anhydride shows a slight shoulder on the 1745 cm^{-1} ester absorbance. However, there is the possibility of diffraction and overlap of the aperture that would contribute to the shoulders presence. A reaction between the wood hydroxyl groups and MAPP would also produce an absorbance of 1745 cm^{-1}. There are aliphatic esters in wood lignin in unknown concentrations, making the prospective of subtracting out the amount of ester created from a possible MA-OH reaction improbable. The 1788 cm^{-1} peak is present in high enough concentrations to produce a shoulder that appears on the 1745 cm^{-1} peak (Figure 3.22). This line profile reveals that MA is present throughout the interphase and at the interface. The maps of the FTIR spectrum do not reveal that the

wood hydrolyzes the MA, but does not discount that some interaction is taking place in the melt state.

.

The incorporation of ZnSt into the blend does not remove the copolymer from the interface and the interphase (Figure 3.23). The presence of the active anhydride group is diminished to almost nonexistent. Much like the formulations not containing lubricants, there is no indication of the formation of ester bonds with the wood. Further, the likelihood of an ester formation from a carboxylic acid is much less than that of the anhydride. The formation of hydrogen bonds with the wood surface is also unlikely. The two acid groups are more likely to form a dimer with other acid molecules than with the wood cellulose that will be less accessible. The hydrolyzing MAPP will result in a lack of an adhesion mechanism between the matrix and wood. In addition, the hydrogen bonding between molecules could lead to poor crystallization or packing density of the amorphous fraction of the copolymer. The mechanical consequences of the hydrolysis of the MAPP may lead to a weak interface and diminished composite properties.

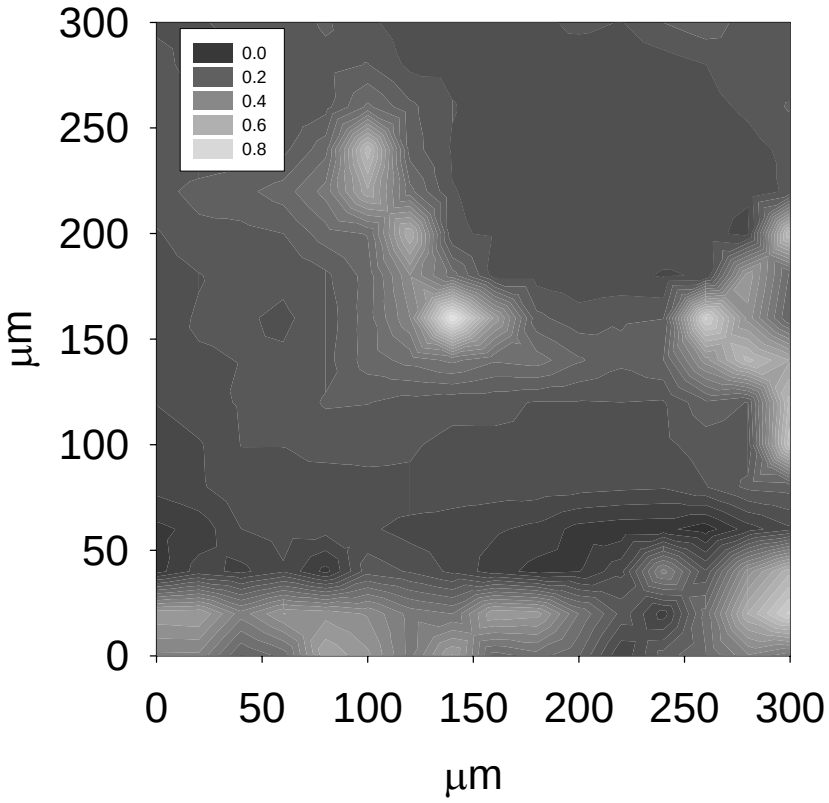

(A)

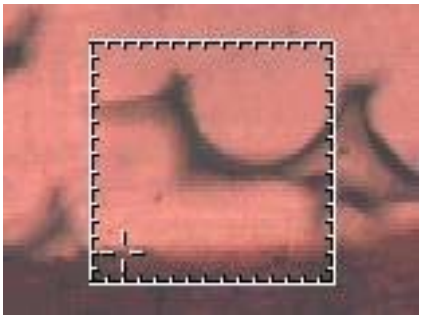

(B)

Figure 3.15: A map of the 2193 cm^{-1} absorption of C-D stretching in the deuterium labeled component (ZnSt) normalized with the 2950 cm^{-1} absorption for C-H stretching in a PP /DZnSt/EBS blend (A). The wood interface is present between 40-50 μm as seen in the microscope image (B) where each tic represents 20 μm.

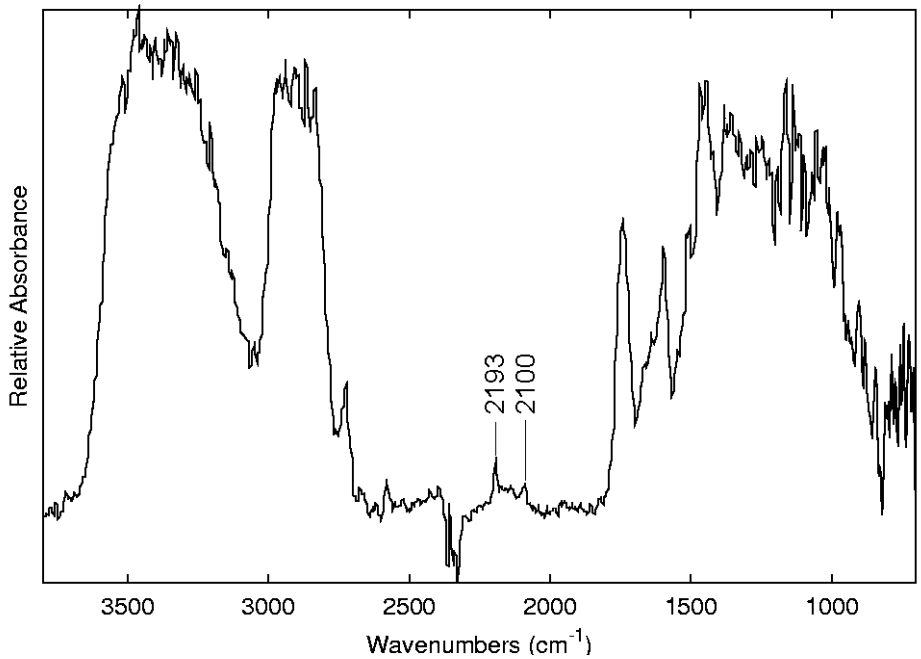

Figure 3.16: An FTIR spectra taken at the interface of a PP/DZnSt/EBS blend and wood.

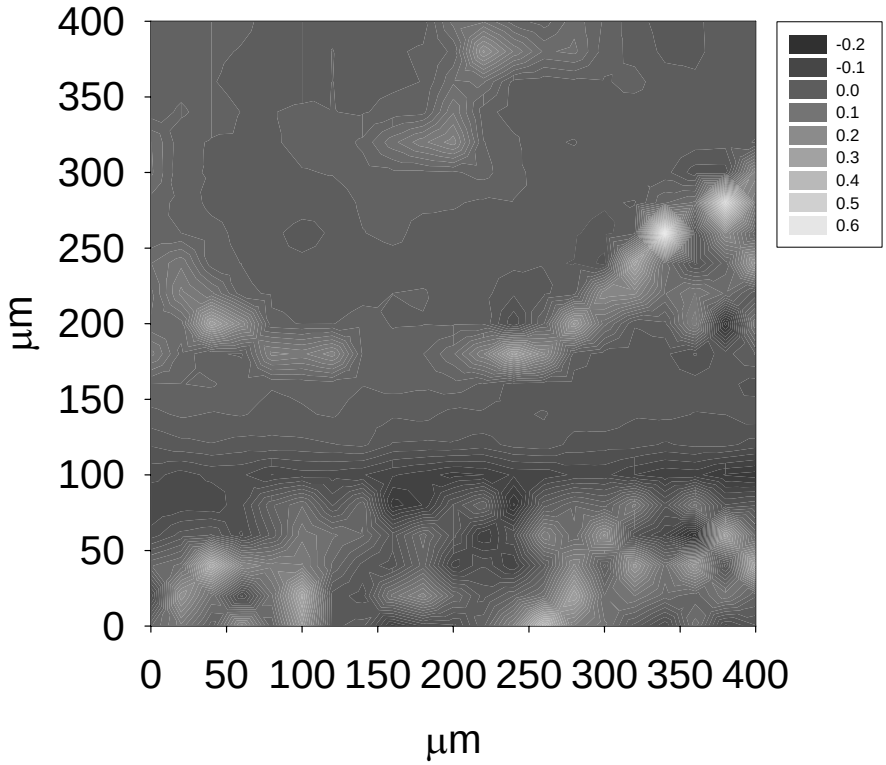

(A)

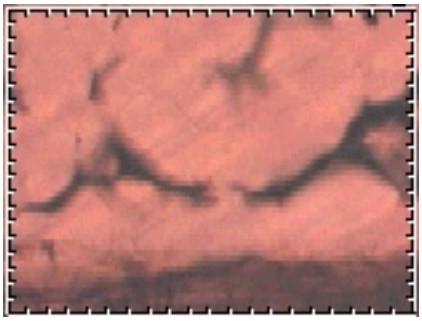

(B)

Figure 3.17: A map of the 2193 cm^{-1} absorption of C-D stretching in the deuterium labeled component (ZnSt) normalized with the 2950 cm^{-1} absorption for C-H stretching in a PP/MAPP/DZnSt/EBS blend (A). The wood interface is present between 80-100 μm as seen in the microscope image (B) where each tic represents 20 μm.

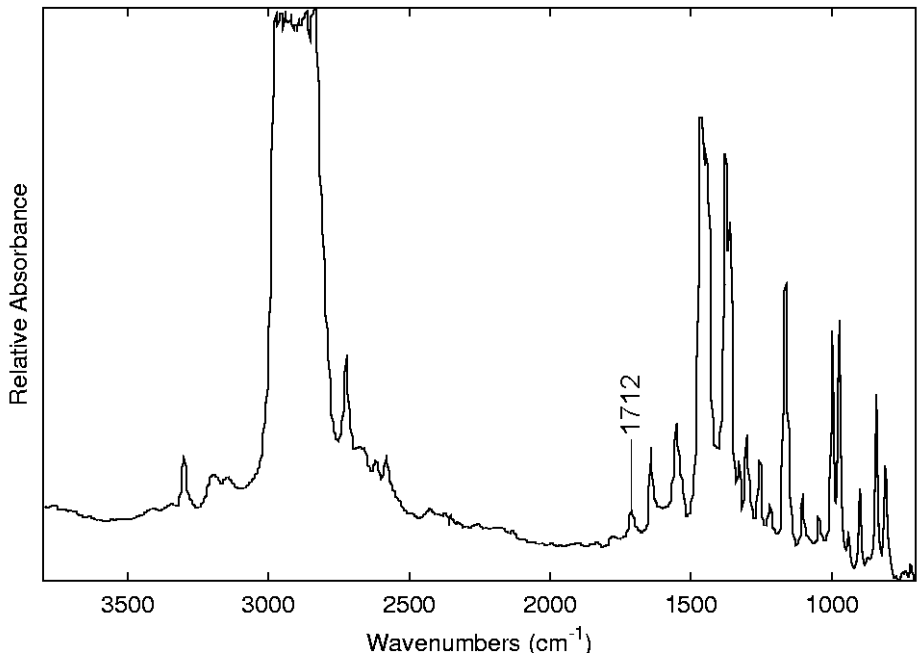

Figure 3.18: An FTIR spectra taken in the bulk matrix of a PP/MAPP/ZnSt/EBS blend. The 1712 cm^{-1} peak represents the formation of a carboxylic acid along with a broad O-H stretching band between 2500-3000 cm^{-1}.

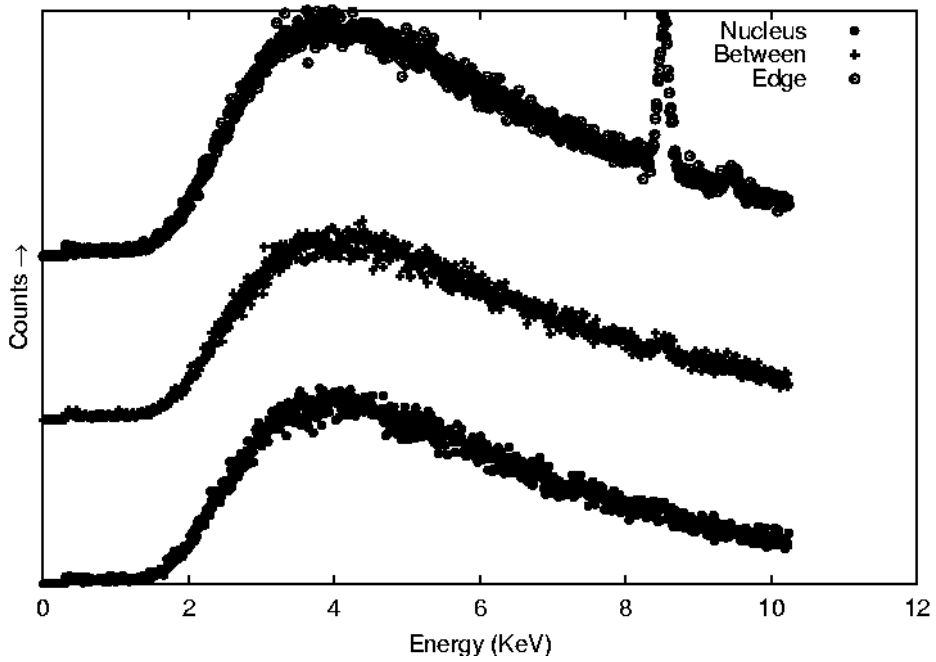

Figure 3.19: This is a plot of EDX diffraction of a spherulite of a PP/ZnSt/EBS blend where a peak at 8.63 keV is indicative of the Zn K_α diffraction and a smaller peak at 9.57 keV indicates the weaker K_β peak. The approximate area sampled was 31 μm × 35 μm at each location.

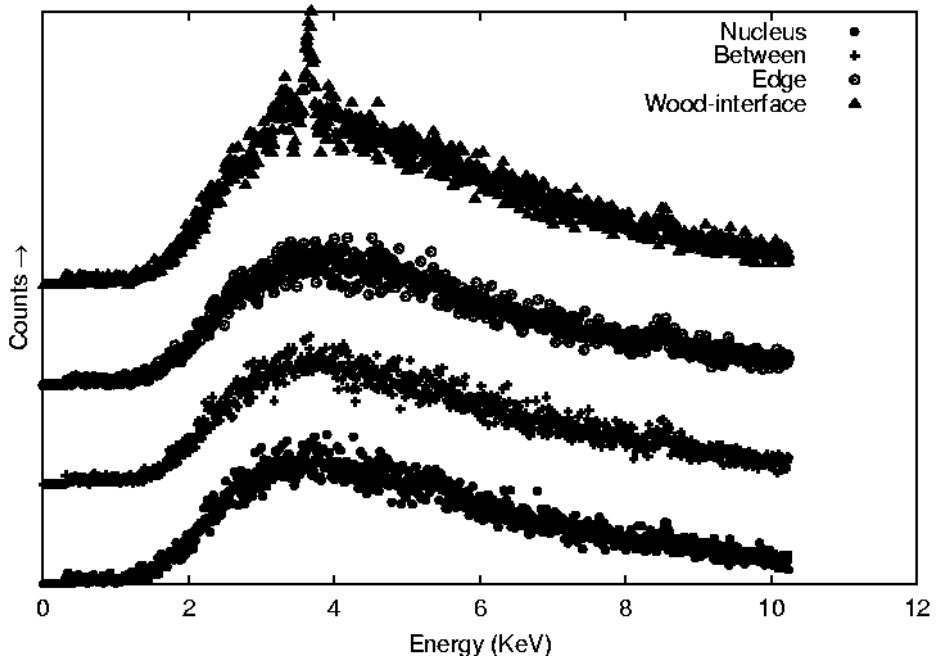

Figure 3.20: EDX analysis of a spherulite of a PP/MAPP/ZnSt/EBS blend was the Zn more dispersed in the middle to the edge of the spherulite over a 31 μm × 35 μm area. A peak at 8.63 keV is indicative of the Zn K_α diffraction and a peak at 3.69 keV indicates a K_α diffraction of Ca.

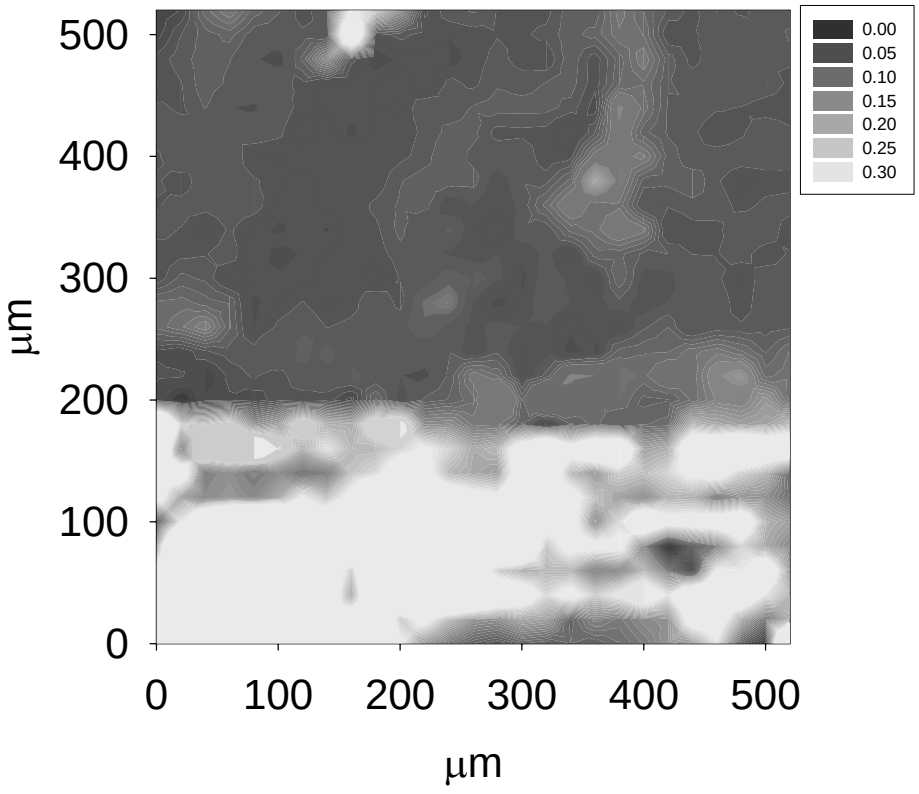

(A)

(B)

Figure 3.21: A map shows the 1788 cm^{-1} absorption where the anhydride was normalized with the 2950 cm^{-1} absorption for C-H stretching in a PP/MAPP blend (A). The wood interface is present between 200-220 µm as seen in the microscope image (B) where each tic represents 20 µm. The image of part of the wood in the FTIR map is not present in image B.

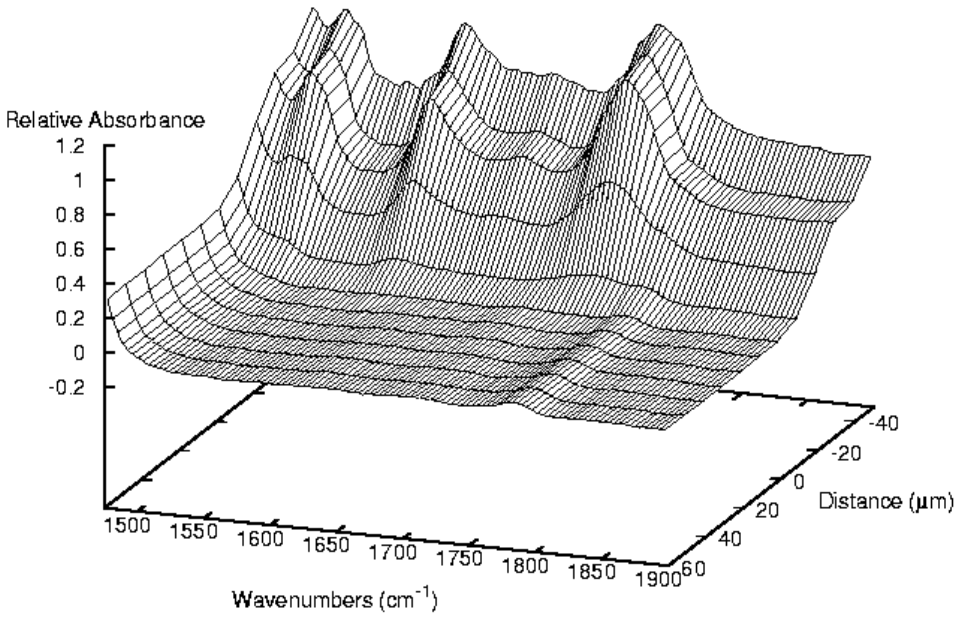

Figure 3.22: The spectra of a MAPP/PP blend is mapped where distance 0 is the wood-plastic interface and the positive values extend into the interphase. The aperture used during collection was 20 µm x 20 µm with step size of 10 µm. Therefore, there is some overlap and a transition region present at the interface.

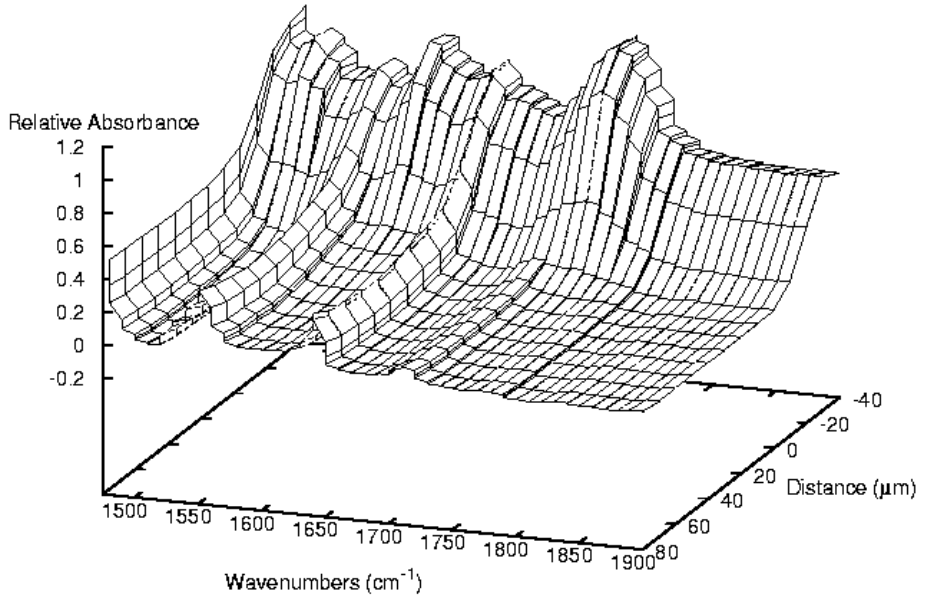

Figure 3.23: The spectra of a MAPP/ZnSt/PP blend is mapped where distance 0 is the wood-plastic interface and the positive values extend into the interphase. The aperture used during collection was 20 μm x 20 μm with step size of 10 μm.

3.6 Conclusions

The lubricants investigated collect in the greatest concentrations at the edges of the interphase and spherulites. The impurities collect at the growth front as crystallites are formed. As a consequence, a small amount of the lubricants actually appears to be trapped by impinging nuclei at the wood-matrix interface. There was no spectroscopic evidence presented suggesting that the lubricants interacted chemically with the wood. However, there is a chemical interaction between the ZnSt and MAPP. The MAPP is hydrolyzed when ZnSt is added to the blend. This effectively negates the ability for forming a chemical link between the wood and the matrix. Further, the ability to hydrogen bond with the wood hydroxyls may not be as favorable as other hydrolyzed

copolymers. This leaves the composite without an effective mechanism for adhesion to the wood surface.

There does appear to be some MA present at the interface of the wood and the plastic. It remains difficult to determine if there exists a covalent ester link between the MAPP copolymer and the wood. The aliphatic esters present within wood lignin prohibit the quantitative extraction of any ester absorbencies that may be present. This is largely the consequence of the inherent variability in wood. In addition, the transmitted IR energy through the wood is greatly reduced from that of the matrix material. A subtraction method would not prove quantitative enough to be justified. The lack of an ester link does not discount the possibility of secondary interactions, such as hydrogen bonding. The MAPP is in close proximity to wood making such interactions feasible. However, no proof of their existence was presented in this work.

3.7 References

Assouline E, Grigull S, Marom G, Wachtel E, Wagner HD, Morphology of transcrystalline isotactic polypropylene under tensile stress studied with synchrotron microbeam x-ray diffraction, Journal of Polymer Science: Part B: Polymer Physics 39 (2001),2016-2021.

Bledzki AK, Reihmane S, and Gassan, Properties and modification methods for vegetable fibers for natural fiber composites, Journal of Applied Polymer Science, 59 (1996), no. 8, 1329-1336.

Bower DI, Maddams WF, The vibrational spectroscopy of polymers, Cambridge University Press, Cambridge, 1989.

Felix J, Gatenholm P, The nature of adhesion in composites of modified cellulose fibers and polypropylene, Journal of Applied Polymer Science, 42 (1991) 609-620.

Harper DP, A Thermodynamic, Spectroscopic, and Mechanical Characterization of the Wood-Polypropylene Interphase, Ch 2., Doctoral Dissertation, Washington State University, Pullman, WA, 2003.

Joly D, Gauthier R, Escoubes M, Partial masking of cellulose fiber hydrophilicity for composites. Water sorption by chemical modified fibers, Journal of Applied Polymer Science, 61 (1996), 57-69.

Kazayawoko M, Balantinecz JJ, Woodhams RT, Diffuse reflectance Fourier transform infrared spectra of wood fibers treated with maleated polypropylenes, Journal of Applied Polymer Science 66 (1997), 1163-1173.

Kazayawoko M, Balatinecz JJ, Woodhams RT, Law S, Effect of ester linkages on the mechanical properties of wood fiber-polypropylene composites, Journal of Reinforced Plastics and Composites 16 (1997), 1383-1406.

Lipatov YS, Physical chemistry of filled polymers, Rubber and Plastics Research Association of Great Britain, 1979.

Son S, Lee Y, Im S, Transcrystalline morphology and mechanical properties in polypropylene composites containing cellulose treated with sodium hydroxide and cellulase, Journal of Materials Science 35 (2000), 5767-5778.

Utracki LA, Polymer Blends and Alloys: Thermodynamics and Rheology, Hanser Publishers, Munich, 1989.

Wolcott MP, Chowdhury M, Harper DP, Li T, Heath R, Rials TG, Coupling agent/lubricant interactions in commercial woodfiber-plastic composite formulations, 6th International Conference on Woodfiber-Plastic Composites, Forest Products Society, May 2001, pp. 197-204.

Chapter 4 Lubricant, Copolymer, and Homopolymer Interactions and their Impact of Mechanical Properties

4.1 Abstract

Differential scanning calorimetry (DSC) and dynamic mechanical analysis (DMA) were used to identify the mechanisms that lead to differences in the behavior of various formulations of PP use in wood-thermoplastic composites. Three lubricants, ethylene bisstearamide (EBS), zinc stearate (ZnSt), and a polyester based lubricant (OP), and a coupling agent, maleated polypropylene copolymer (MAPP), were used. Avrami kinetic analysis revealed that ZnSt and EBS act as nucleating agents in the melt leading to more truncated spherulitic shapes. However, the use of OP MAPP created spherulitic crystallites characteristic of heterogeneous nucleation. Dynamic mechanical analysis revealed increased stiffness with the inclusion of MAPP. The increase in stiffness was interpreted as an increase in intermolecular coupling as revealed by an increase in fragility over neat PP. Further, the incorporation of ZnSt in a blend with MAPP hydrolyzes the anhydride groups, reducing the intermolecular coupling.

4.2 Introduction

The addition of a copolymer-coupling agent (maleic anhydride polypropylene, MAPP) to wood-polypropylene composite changes the composite properties and morphogy. The addition of MAPP to a Wood-PP composite improves the bending strength and stiffness (Harper 2003c). However, the addition of certain lubricants into the composite negates the mechanical property gains achieved by MAPP addition. Previously, it has been

shown that the interaction of the MAPP with zinc stearate lubricant (ZnSt) produces different crystal morphology of the composite than with the addition of just MAPP (Harper 2003a). MAPP appears to carry the lubricant into the crystallite structure of the interphase and the bulk polymer and is at the same time subjected to hydrolysis. This reduces MAPP's efficacy as a coupling agent. This interaction is linked to a decrease in composite properties that has been observed elsewhere (Wolcott et al. 2001). The interaction of the lubricants, the homopolymer, and the copolymer become critical to the understanding of the coupling agent role in the composite. The combination of lubricants within a composite has complicated the understanding of their roles. The combination of lubricants in the ZnSt/EBS system acts as a nucleating agent, but the influence of the individual lubricants is not clear.

The thermodynamic meaning of miscible is defined as a single phase down to the molecular level, where the value for the free energy of mixing is negative $\Delta G_m = \Delta H_m - T\Delta S$. Here, $\Delta G_m < 0$ for miscible systems. Specific interactions occur on different levels and in different phase states of the material. As a result, a large number of scientific techniques that range from visualization, mechanical, spectroscopic, to diffraction has been developed to evaluate materials. Analogously, different techniques can be used to look at miscibility in different material phases.

Miscibility between two glassy polymers display an assymetric broadening of the glass transition towards lowerer frequencies (Roland and Ngai 1992). A relationship developed by Angell can be used to describe the temperature dependence of the

relaxation process (Böhmer et al. 1993). Strong glass formers exhibit very high intermolecular interactions that commonly display a broad distribution of relaxation times that obey Arrhenius behavior. Weak glass formers on the other hand display small molecular inteaction and their temperature dependence deviates from Arrhenius. Angel developed the concept of a normalized Arrhenius plot termed fragility and uses T_g for scaling (Bohmer et al. 1993):

$$m = \left. \frac{d \log\langle \tau \rangle}{d\left(T^*/T\right)} \right|_{T=T^*}, \qquad \text{Equation 4.1}$$

where m is the fragility and τ is the relaxation time. The higher values of m is corresponder to weaker the glasses. For a miscible system, a corresponding reducion in the m value would be expected.

A widely studied example is a blend of poly(methyl methacrylate) (PMMA) and poly(ethylene oxide) (PEO) (Alfonso and Russell 1986, Ito et al. 1987, Zawada et al. 1992, Parizel et al. 1997). These blends are miscible in the melt state and exhibit some miscibility at the molecular level in the solid state. The use of a combination of ^{1}H and ^{13}C NMR methods determined that there are three phases of PEO in PEO/PMMA blends: a crystalline phase, a constrained amorphous phase around the lamella, and an amorphous fraction that is miscible with PMMA (Parizel et al. 1997). This model of PEO/PMMA blends is in agreement with the lattice model for semicrystalline/amorphous polymer blends of Kumar and Yoon (1989) that predicts the existence of an interphase of pure crystalline polymer that behaves though it was amorphous. This study found that the entropic constraints at the crystal leads to almost complete phase separation, but

conceded that the composition of the amorphous phase may depend more on crystallization conditions and polymer concentrations.

The study of the crystallization of semicrystalline polymers can yield information about the miscibility of polymers in the melt state. It is true that most materials crystallize in the pure form and those impurities or additives are expelled during this process. However, as observed by Nishi and Wang (1975) there is a melting point depression when polymers are miscible in the crystalline phase and, under dynamic conditions, crystallization temperature depression in polymer pairs that are miscible in the melt state. For blends that are miscible in the melt, the melting point of the blend should be depressed in relationship the temperature of crystallization (Hoffman and Weeks 1962). A plot of the T_m vs. T_c can provide an estimation of the equilibrium melting point. For the estimate, the data is extrapolated to intercept a line where $T_m^o = T_c^o$ (Hoffman et al. 1976). The intercept is T_m^o for the polymer. Melting point depression from miscibility is based upon the assumption that, entropy constraints will be negligible for high molecular weights (Scott 1949). As is the case with many low molecular weight lubricant systems, the entropy of mixing cannot be considered negligible. If there is miscibility between polymer systems, there should be a reduction in the crystallization rate of the polymer. The specific interaction of the miscible system are likely to inhibit the mobility of the system needed for crystallization. Thus, there should be a reduction in the growth rate and a possible change in nucleation mechanisms. Both of these phenomenon can be explained through crystallization kinetics.

4.3 Crystallization Kinetics

Isothermal kinetics of a semicrystalline polymer is evaluated by thermal techniques assuming a relative degree of crystallinity ($\chi(t)$) measured from the heat evolved ($H(t)$) during crystallization (Equation 4.2):

$$\chi(t) = \frac{\int_0^t (dH/dt)dt}{\int_0^\infty (dH/dt)dt}. \qquad \text{Equation 4.2}$$

Relative crystallinity fits the Avrami (1939) kinetics for low degrees of crystallinity. Impinging crystallites and diffusion mechanisms cause the deviation from the model. Thus, the model is fit to $\chi < 0.5$,

$$\ln[-\ln(-\chi(t))] = \ln k + n \ln[t], \qquad \text{Equation 4.3}$$

where χ ranges from 0 to 1, n is the Avrami exponent, and k is the crystallization rate constant. Alternatively, the kinetic parameters may be obtained by assuming a first order mechanism where:

$$k_n = \ln[2]/t_{1/2}^n. \qquad \text{Equation 4.4}$$

The Avrami exponent has a relationship with the mechanism of nucleation and the geometry of the crystallizing polymer. A low n value indicates an athermal nucleation mechanism where a high value is more sporadic in nature. Because of the nature of the evaluation method, k_n contains both the nucleation and growth characteristics of the crystallizing polymers. These characteristics cannot be separated without making assumptions based upon the nucleating behavior of the polymer. However, by assuming instantaneous nucleation for heterogeneously nucleated polymers the growth rate

parameters can be calculated for the blends. By following Lauritzen-Hoffman growth rate theory:

$$\ln G = \ln G_0 - \frac{U^*}{R(T_C - T_\infty)} - \frac{K_g}{T_C \, \Delta T \, f}, \qquad \text{Equation 4.5}$$

where G_0 is a constant, K_g varies with crystallization regimes and is dependent upon the free energy parameter, and T_c is the crystallization temperature (Hoffman et al. 1976). The degree of supercooling ΔT is the difference between the isothermal crystallization temperature and the equilibrium melting point ($T_m°$). $T_m°$ is determined using a Hoffman-Weeks (1962) analysis to extrapolate melting points determined by DSC to that where $T_c = T_m$ (Figure 4.1). The temperature at which all crystallization ceases (T_∞) is also predicted from calorimetry data where $T_g - 20\text{K} = T_\infty$ is used as an estimate. Depending upon the regime behavior of the growth process, the free energy parameters of the surface and crystal will be determined through K_g. For example, regime II behavior, which applies to the degree of supercooling used in this study, yields,

$$K_g = \frac{2b_0 \, \sigma \, \sigma_e T_m^0}{k_B \, \Delta h_f}. \qquad \text{Equation 4.6}$$

Then, solving for G and substituting into Equation 4.5 a relationship between the growth rate and crystallization time can achieved. Secondary nucleation is ignored in this approach to growth kinetics. For instantaneous nucleation, spherical crystallite geometry, k can be defined as:

$$k = \frac{4}{3} \pi G^3 N. \qquad \text{Equation 4.7}$$

The spherical geometry simplifies relating Avrami kinetics to Lauritzen-Hoffman growth rate theory (Hoffman et al. 1976) by assuming an Avrami exponent of $n = 3$. This

simplification is adequate for low χ before impingement occurs and when there is no homogeneous nucleation present. Therefore, a relationship exists between the time at a specified degree of crystallization (t_χ) (e.g. $\chi = 0.5$) and G:

$$t_\chi^{-1} = A_1 G_0 \exp\left(-\frac{U^*}{R(T_C - T_\infty)} - \frac{K_g}{T_C(\Delta T)f}\right). \qquad \text{Equation 4.8}$$

Where A_1 is an arbitrary proportionality constant.

4.4 Objectives

Lubricant systems are added to aid in the production of extruded polymers. However, often their addition changes the properties of the polymer. Specifically, the morphology is greatly impacted when considering the application of lubricated polymer blends in composites. The resulting morphology is greatly impacted. It, however, remains a question whether it is the change in the morphology of the polymer-filler interface or the morphology of the bulk polymer that causes changes in mechanical properties. The morphology and mechanical performance of the lubricant-polymer blends need to be considered separately in order to discern the individual impact. Specifically the objectives are:

1. Evaluate the impact of binary combinations of lubricant or copolymer coupling agent on the crystallization of PP.
2. Characterize the impact of the lubricants and copolymer on the mechanical behavior of the polymer.
3. Determine if the mechanical performance depends on specific or long-range interactions or morphology.

4.5 Methods and Materials

The materials used consisted of an isotactic polypropylene (PP) homopolymer (Solvay HB 9200, M_n = 35000 g/mol) and maleic anhydride polypropylene copolymer (MAPP) (Honeywell A-C 950P, M_n = 8000 g/mol, SAP = 45 KOH/g), and three lubricants used in extrusion. The lubricants are zinc stearate (ZnSt) (Ferro), ethylene bisstearamide (GE Specialty Chemicals), and a polyester based lubricant (OP) (Honeywell Optipac 100). The lubricant and polymer blends were compounded in a Thermo Haaka mixing head at 180°C at 120 rpm with Braburn rollers for 8 min. The formulations were compounded for DSC and DMA analysis respectively as explained in Table 4.1 and 4.2. Additionally for DMA, the same basic binary blends were used as used for DSC, but with a range between 0-4% for the lubricants and 0-15% for MAPP. The selection for the blend ratios is based on previous research (Wolcott et al. 2001) where these specific formulations demonstrated variation in properties.

Blend	%PP	%MAPP	%OP	%ZnSt	%EBS
PP	100	-	-	-	-
PP/OP	97.3	-	2.7	-	-
PP/ZnSt	98	-	-	2	-
PP/EBS	99	-	-	-	1
PP/MAPP	98, 95	2, 5	-	-	-

Table 4.1: Binary blends compounded for DSC analysis.

Blend	%PP	%MAPP	%OP	%ZnSt	%EBS
PP/ OP*	99.5, 99, 98.5, 98, 97.3	0	0.5, 1, 1.5, 2, 2.7	0	0
PP/MA/OP	97.3	5	2.7	-	-
PP/ZnSt/EBS	97	-	-	2	1
PP/MA/ZnSt/EBS	92	5	-	2	1

Table 4.2: Blends compounded for DMA analysis including combinations and binary (*) blends of the copolymers and lubricants. At least two specimens were tested for each blend.

After compounding, specimens to be used in dynamic mechanical analysis were manufactured in a resin transfer mold with a barrel temperature of 180°C and mold temperature of 110°C. The dwell time in the barrel was 10 min after which the plastic specimens were molded and removed immediately. The dimensions of the specimens were nominally 1.6 mm × 6 mm × 45 mm to fit the Rheometrics RSA II solids analyzer in dual cantilever mode. Specimens were tested at 0.1% strain as determined by a static strain sweep test at –50, 25, and 100°C to insure linearity throughout the test. The specimens followed a ramp from –50 to 100°C at 2°C increments with a 1-minute soak time and dynamic loading from 1 to 10 Hz.

Specimens to be used in differential scanning calorimetry (DSC) were ground in a laboratory Whiley Mill and placed in 40 μL hermetically sealed pans. The average sample size was kept at 7mg for the DSC analysis. DSC experiments followed the following regime: a ramp from 25 to 200°C at 20°C/min, soak for 10 min, cool at 20°C/min to the crystallization temperature, isothermal crystallization at that temperature cool to –20°C at 20°C/min ramp for –20 to 10°C to capture the glass transition, and then

heat through the melt from 10 to 200°C at 20°C/min. The melt temperature recorded was defined by the end of the melt endotherm at the intersection between the baseline and the trailing slope. The glass transition (T_g) was defined as the mid-point in the change of baselines.

4.6 Results and Discussion

4.6.1 Melt Behavior

The melt behavior of the binary blend lends insight into the morphology and the interaction between the lubricants, coupling agent, and PP. The presence of two melt peaks can be observed in Figure 4.1. The behavior is present in PP and all of its blends. The addition of the lubricants and coupling agent changes the relative magnitude of the peaks. This behavior is likely from the existence of two crystal species with varying degrees of perfection (Schmidtke et al. 1997, Supaphol et al. 2000, Zhou et al. 2000, Liu and Petermann 2001, Liu et al. 2001). The different crystal species have lamella of different thickness and different thermal stabilities. Differences the thermal stability of crystals can arise if from the presence of defects in the structure. This can occur when a crystalline polymer is miscible with an amorphous polymer or lower molecular weight polymer (Nishi and Wang 1976). Further, the use of nucleating agents can lead to thinner lamella with more defects (Wunderlich 1976). The spherulites that nucleated on a surface tend to melt at 5-6ºC prior to the melt of other spherulites (Harper 2003a). Nishi and Bussi (1991) hypothesized that densely nucleated crystals lead to thin, unstable

lamellas that display lower melting points than bulk-crystallized lamella. The melt of ZnSt and EBS blends displays a similar shift towards lower temperatures as described by this hypothesis. Although there is not the presence of a large surface to produce many closely packed lamella, the concept is similar for the melt. A nucleating surface will produce a thinner lamella surface by reducing the free energy needed nucleate growth. In contrast, OP behaves as a completely immiscible system in the melt. It does not behave as a good nucleating agent by reducing the free energy difference needed to nucleate growth, but creates localized shear zones at the phase boundaries increasing the perfection in the crystals. This leads to the sharper melting peak as compared to the other blends as observed in Figure 4.1.

The existence of isomorphic crystal structures in polymer blends is a rare occurrence (Utracki 1989). However, it has been demonstrated that isomorphic crystals exist in MAPP and PP blends (Duvall et al. 1994). Most recently, MAPP has been shown to exist within the spherulitic structure of PP spherulites (Harper 2003b). The incorporating is the result of interaction that is attributable to the PP backbone of the copolymer. The melting point of MAPP is lower than that observed for PP or its blends (Figure 4.2). The melt of blends of PP and MAPP displays very similar melting behavior as PP (Figure 4.2). An increase in MAPP content leads to further depression of T_m indicating miscibility of the MAPP in PP. A distinct increase in the melting endotherm between 140-150ºC over that of PP is not observed even at high MAPP percentages as would be expected when excluded from the crystal structure. This suggests that in fact there is isomorphic crystallization of MAPP and PP at the addition levels investigated. An

increase in the MA groups along the copolymer backbone would likely lead to further exclusion from the crystallites as seen by Duvall et al. (1994).

From the measure of the enthalpy (ΔH) during melting, there does not appear to be a dramatic change in the degree of crystallinity among the blends. The ΔH for a perfect crystal was taken to be 209.3 J/g (Wunderlich 1973). This translated into a crystallinity of 51% +/- 2% for all blends. A one-way ANOVA coupled with a Duncan test at α = 0.05 did not reveal any significant differences in crystallinity among blends used in the DSC analysis. Thus, it is not considered that the crystallinity of the blends was changed significantly, but that does not say that defects and other morphological changes were imparted on the crystals.

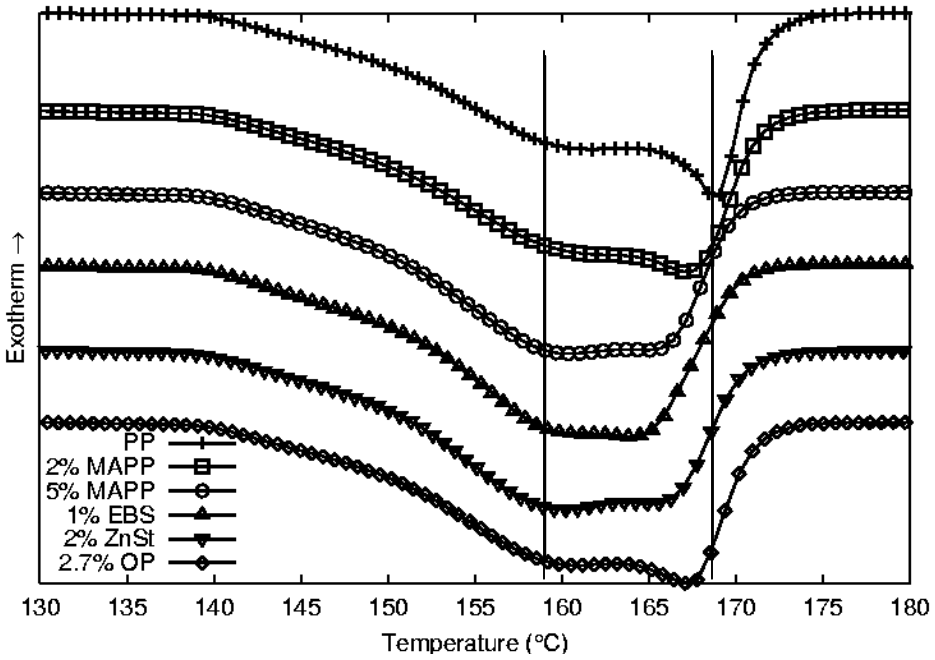

Figure 4.1: DSC melt curves for binary blends crystallized a 136ºC plotted every third point.

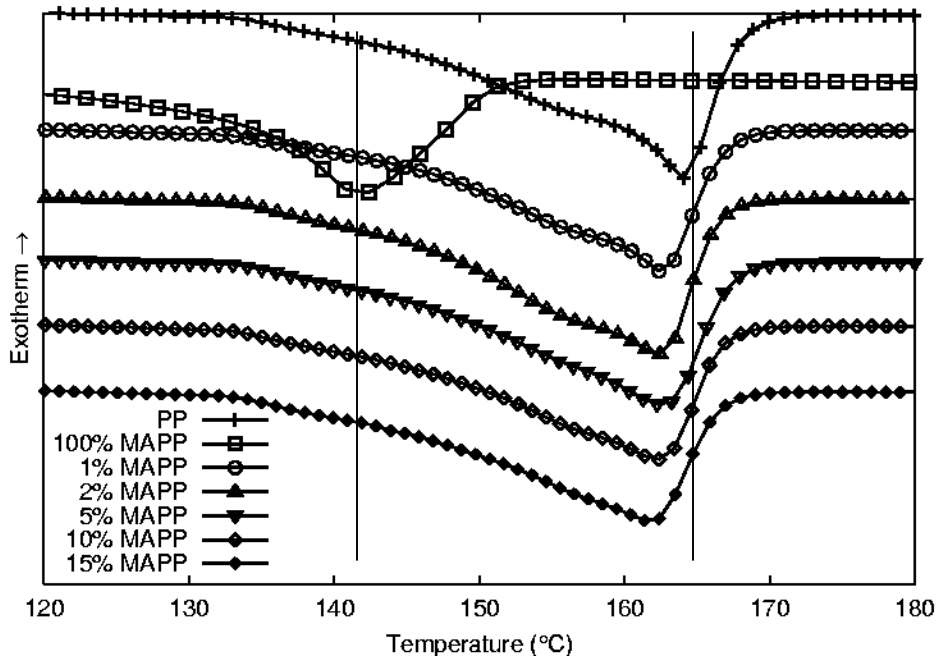

Figure 4.2: Comparison of DSC melt curves with varying amount of MAPP in a PP blend crystallized at 130ºC plotted every third point.

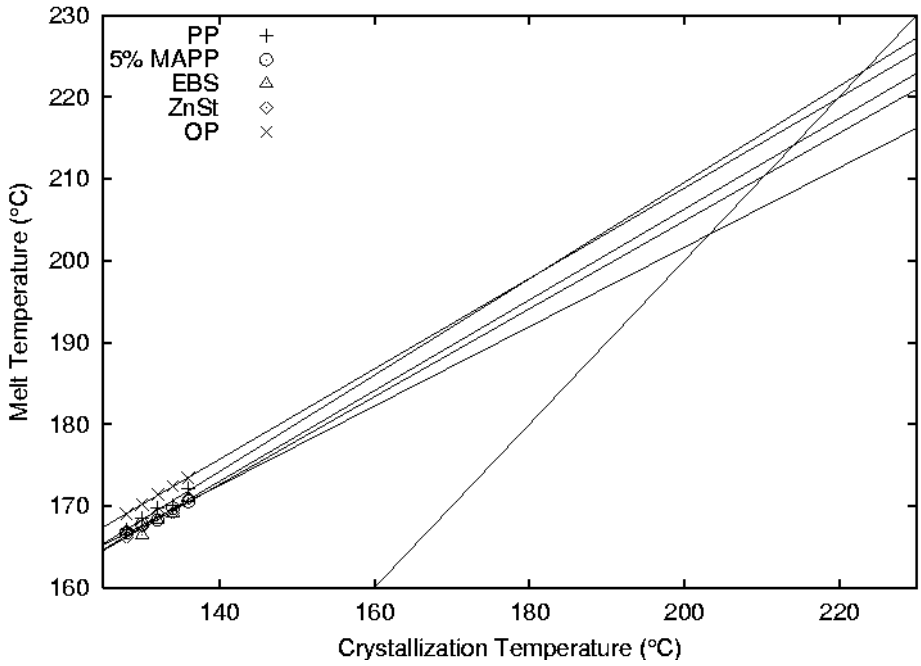

Figure 4.3: Hoffman-Weeks plot for binary lubricants, copolymer, and PP blends. T_m^o is the point where the extrapolated lines intersect the $T_c = T_m$ line with a minimum R^2 = 0.886. T_m^o was not determinable for the 2% MAPP data because of poor correlation.

4.6.2 Kinetics Results

The crystallization kinetics lends insight into the development of morphology in a polymer or blend. The Avrami exponent (n) has been empirically related to different crystallite morphologies (Wunderlich 1983). The changes in n are mainly the result of changes in nucleation mechanism. For example, heterogeneous nucleation (athermal) that produces round spherulitic shapes have an $n = 3$. More truncated shapes resulting from nucleating agents and secondary crystallization tend to possess lower n values.

The n for the PP, PP/OP, and PP/MAPP did not display any significant differences (Table 4.3). For these formulations, an Avrami exponent near $n = 3$ was obtained from the analysis. This observation is similar to that found Seo et al. (2000) when comparing MAPP kinetics to PP. The system moved from one that had homogeneous and

heterogeneous nucleation in the homopolymer to one that depended solely on heterogeneous nucleation in the copolymer. The shift in nucleation mechanisms seems to be the single largest difference among the blends. The ZnSt appears to act as nucleating agent that speeds up the crystallization process as is represented by its low *n*.

The growth kinetics of the polymer was examined using Lauritzen-Hoffman kinetics modified for thermal analysis. The assumption of $n = 3$ was immediately violated with the addition of ZnSt and EBS. However, little difference was observed in the K_g values between the formulations (Table 4.4). This is consistent with previous result that showed no change in growth rates for similar levels of MAPP and lubricant addition (Harper 2003a). The error estimated from the regression analysis may indicate little difference between the formulations (Figure 4.4). However, the error estimate is not indication of statistical significance, but an indication of a range of possible outcomes for the parameter in the regression analysis.

	Degrees of Freedom	***Sum of Squares***	***Mean Square***	***F Ratio***	***P***
Model	4	0.860275	0.215069	5.64443	0.00361806
Error	19	0.723955	0.0381029		
Total	23	1.58423			

Table 4.3: Oneway ANOVA table for *n* values from the Avrami kinetics for $\alpha = 0.05$. The Duncan groupings for the different blends were A = PP, 2.7% OP, and 5% MAPP and B = 1% EBS and 2% ZnSt.

Blend	n +/- 0.04	$T_m°$ (°C) +/- 1°C	K_g (K^2) +/- 0.6
PP	2.71	223	-21.0
2.7% OP	2.96	220	-22.1
5% MAPP	2.91	203	-22.5
1% EBS	2.58	210	-23.4
2% ZnSt	2.44	214	-22.2

Table 4.4: Kinetic parameters obtained from the Avrami analysis and Hoffman-Weeks plot for binary polymer and lubricant blends. The error was estimated from the maximum in the standard error from the regression analysis.

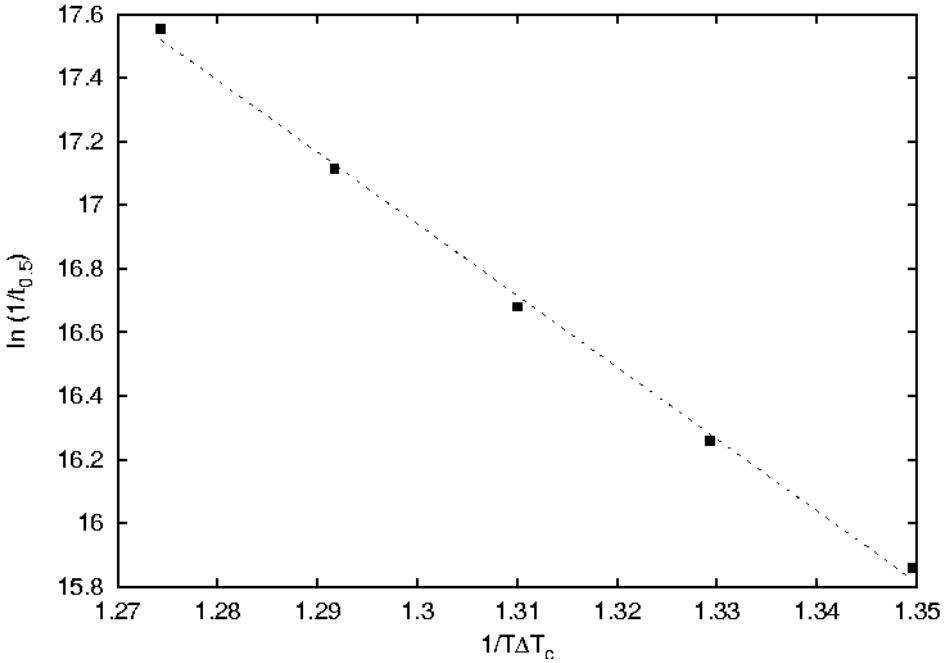

Figure 4.4: Plot for determining Lauritzen-Hoffman growth kinetic parameters for a 5% MAPP : 95% PP binary blend as derived from Avrami kinetics with a minimum R^2 = 0.963 for all.

There is likely an increase in chain interaction with the inclusion of MAPP in the blend. This is evident from the reduction in $T_m°$ as shown on the Hoffman-Weeks plot (Figure 4.3) (Table 4.3). Nishi-Wang (1976) demonstrated that binary blends of miscible polymers leads to melting point depression such as that observed. However, one must use caution when interpreting extrapolated data. Small fluctuations in the data can lead to large shifts in the predicted result. Therefore, these values do accurately depict a trend in the data, but the quantitative reliability of the prediction is questionable. Miscibility

may not be the only mechanism causing depression of the melting point with the addition of lubricants. The lubricant systems are acting as nucleating agents for the PP. Thus, the interfacial free energy difference needed to nucleate a crystal is reduced. Previously, it was observed that addition of ZnSt/EBS in PP has this effect (Harper 2003a). The result is thinner lamella that are not as thermally stable as those without lubricant addition.

4.6.3 Dynamic Mechanical Response

PP displays two rubbery transition in the temperature range tested in this paper. The low temperature is the β-transition that is often referred to as the glass transition. This transition is believed to be associated exclusively with the molecular relaxations of the amorphous phase (Boyd 1985). The higher temperature transition, α, is associated with the bound amorphous phase surrounding the crystals (Boyd 1985). In PP, the β transition occurs around 0ºC as can be observed by the large drop in storage modulus (*E′*) (Figures 4.5, 4.6). Another large drop in *E′* occurs at the α-transition between 40-60ºC. The PP/MAPP blends have a much higher *E′* than PP before both transitions. After the α-transition, all of the blends have about the same rubbery modulus (Figure 4.8). This is also true in the blends having more than two components (Figure 4.9). Interestingly, PP/MAPP/ZnSt/EBS has a high modulus prior to the glass transition, but drops to the levels of PP and the other formulations after the β process.

The polar functionality of MAPP is increasing interaction with the plastic. The addition of a miscible, lower molecular weight component into the system creates a broader distribution of relaxation times. In addition, the polar groups on the MAPP may retard

relaxation times by increasing interaction between molecules. This becomes less apparent with the addition of ZnSt because MAPP becomes hydrolyzed (Harper 2003a). The MAPP blends also exhibit a slightly lower amount of damping as compared to the other blends (Figure 4.6). A lower damping may be the result of a higher elastic modulus at the glass transition than the other blends. Among the binary blends, the peak in the tan δ plot does not move greatly for the β-transition. The location of the peak moves more dramatically when lubricants are incorporated in with MAPP (Figure 4.7). This behavior is especially pronounced in the β-transition region, but also there are changes in the α-transition. Unlike the β relaxation in PP that is in the amorphous phase, the α relaxation only occurs when a crystalline phase is present (Boyd 1985). The α-transition is highly dependent on the thickness of the lamella (Mathews et al. 1999) and not thermorheologically simple (Wortmann and Schulz 1995). Further, thermal treatment of the specimens would be needed to insure that the observed α-transition differences are independent of past thermal histories.

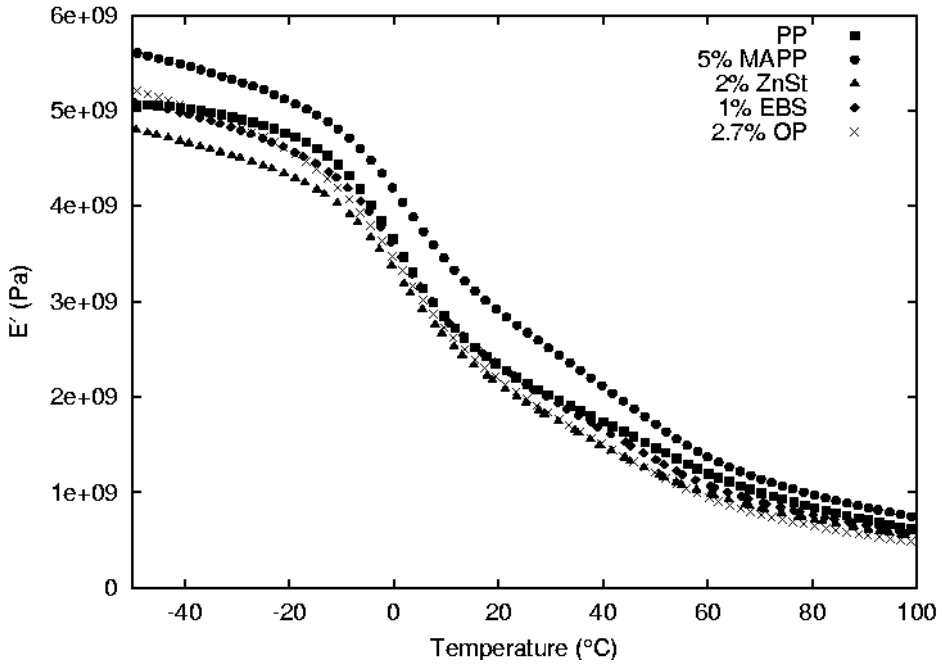

Figure 4.5: Comparison of E′ for binary polymer blends and straight PP at 1 Hz.

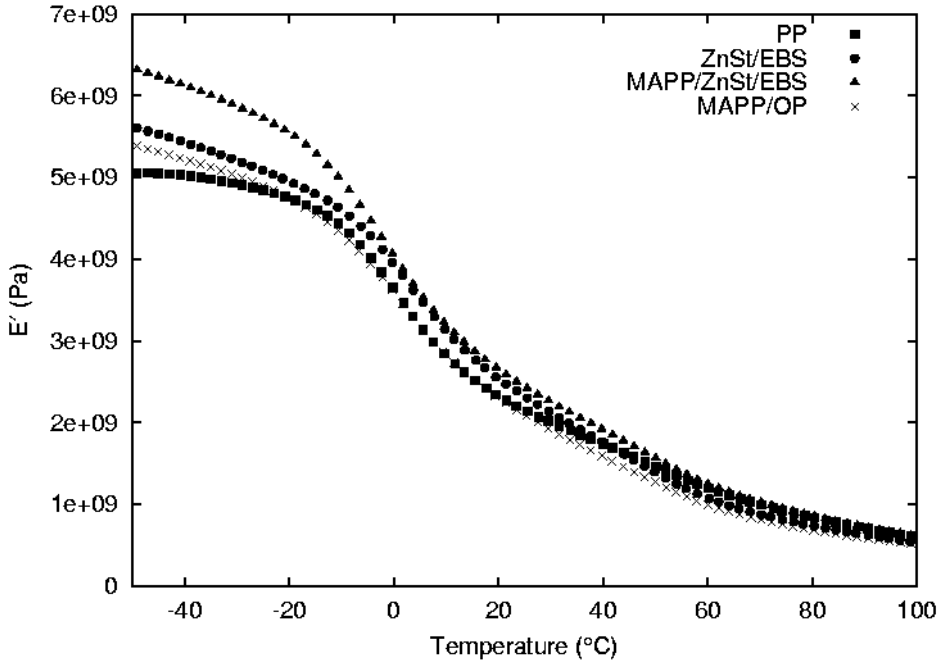

Figure 4.6: Comparison of E′ for lubricant and MAPP blends with PP at 1 Hz.

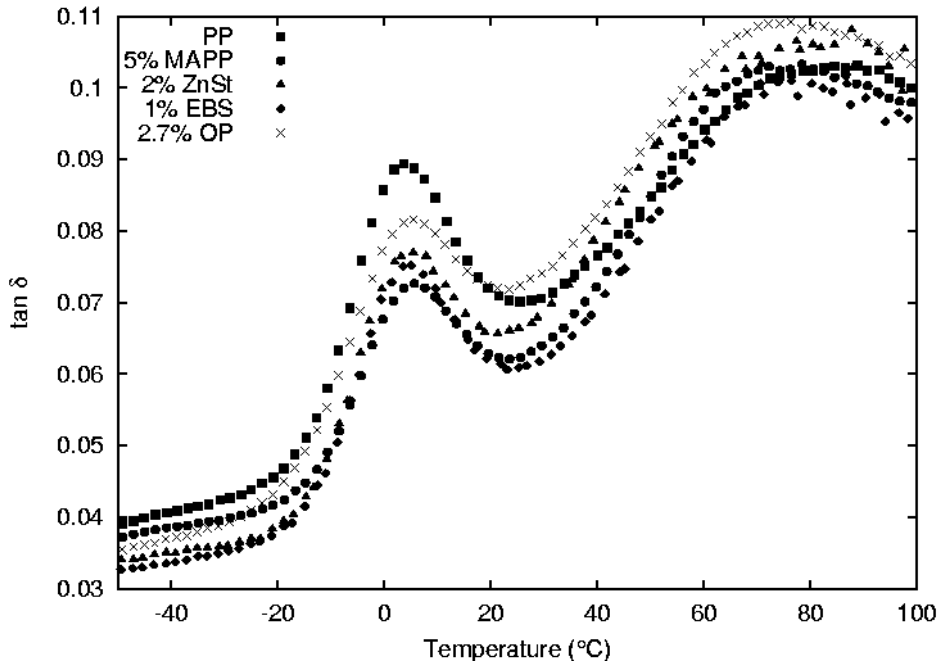

Figure 4.7: Comparison of the tan δ for binary blends tested at 1 Hz.

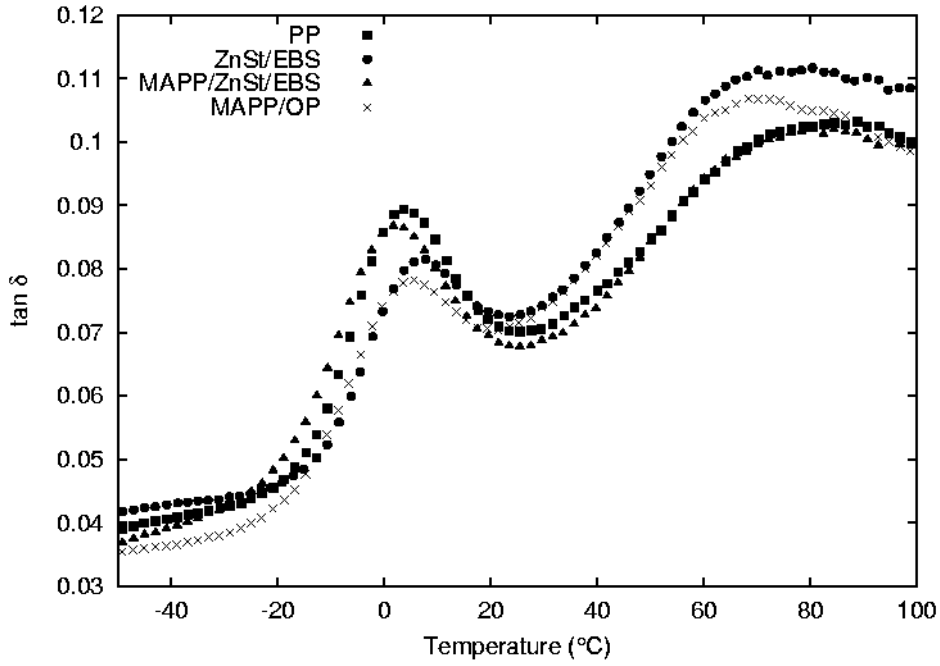

Figure 4.8: Comparison of the tan δ for lubricant and MAPP blends with PP tested at 1 Hz.

The mechanical relaxation of a semicrystalline polymer is generally accepted to follow the Struik model (1987). The crystalline phase of a material reduces the mobility of the amorphous segments that surround it. The mechanical consequence around the β-relaxation in PP is a broadening or increasing the distribution of glassy relaxations. This results from the bulk amorphous material relaxing at lower temperatures than that of the constrained amorphous fractions. When considering blends of a semicrystalline polymer, one may expect to find further broadening of the β-transition with increased interaction between when molecules are miscible. A degree of cooperative chain movement in the amorphous fraction has shown agreement between amorphous PP and isotactic PP when a normalized Arrhenius equation was used (Ngai and Roland 1993). From the principle of time-temperature superposition (TTSP) (Ferry 1980), the shift factor (a_T) may be substituted in to determine *m* when simple linear viscoelasticity is obeyed.

TTSP was performed on *E′* for all blends by using horizontal shifts only. The other viscoelastic properties shifted followed the same shift factors (Figures 4.9, 4.10). The blends behave simple viscoelasticity through the β-transition. However, the viscoelastic behavior of the blends becomes complex as it moves into the α-transition as was previously observed for semicrystalline polymer by Wortmann and Schulz (1995). The behaviors of the polymer blends appear to be Arrhenius in nature in the fragility plot as is expected for semicrystalline polymers around the β-transition (Figures 4.11). Considering Angell's model, the interaction of the molecules appears to be similar for all of the binary formulations (Table 4.5). Further, these values tend to be higher than with

those obtained by others for m = 137 for atactic PP (Plazek and Ngai 1991). However, Ngai and Roland (1993) have found that although the shape of the relaxation is different in atactic PP as opposed to PP, their normalized temperature dependence is equivalent by having similar m values. Ngai and Rolands observation suggests that the fragility for the blends studied in this work is dependent only on the molecular interactions in the amorphous fraction of the PP. This suggests that the crystallinity of the PP asserts very little influence on scaling about T_g.

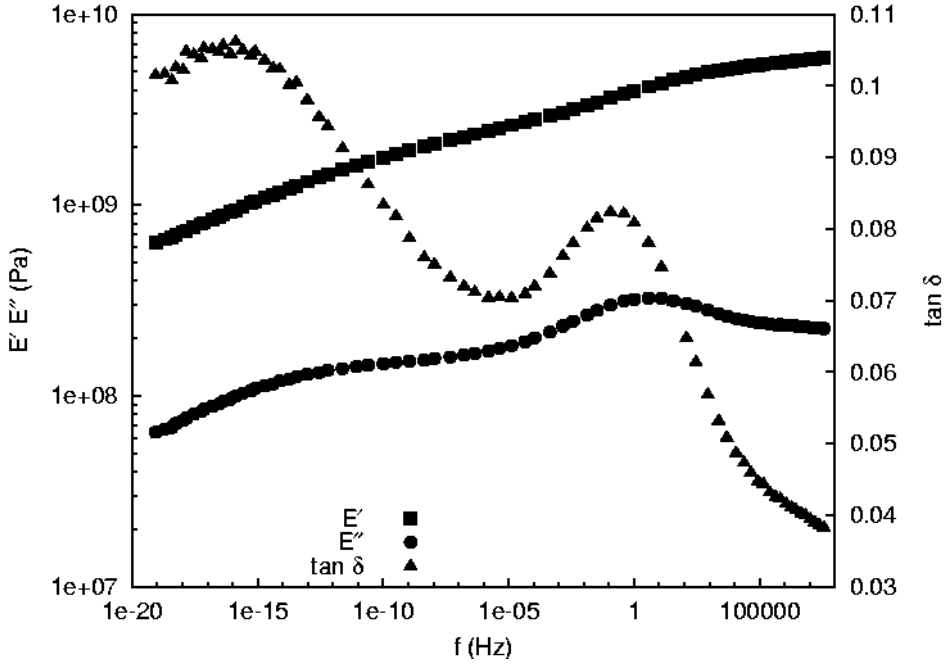

Figure 4.9: Master curve created from TTSP of E' for 1% OP blend plotted every six data points.

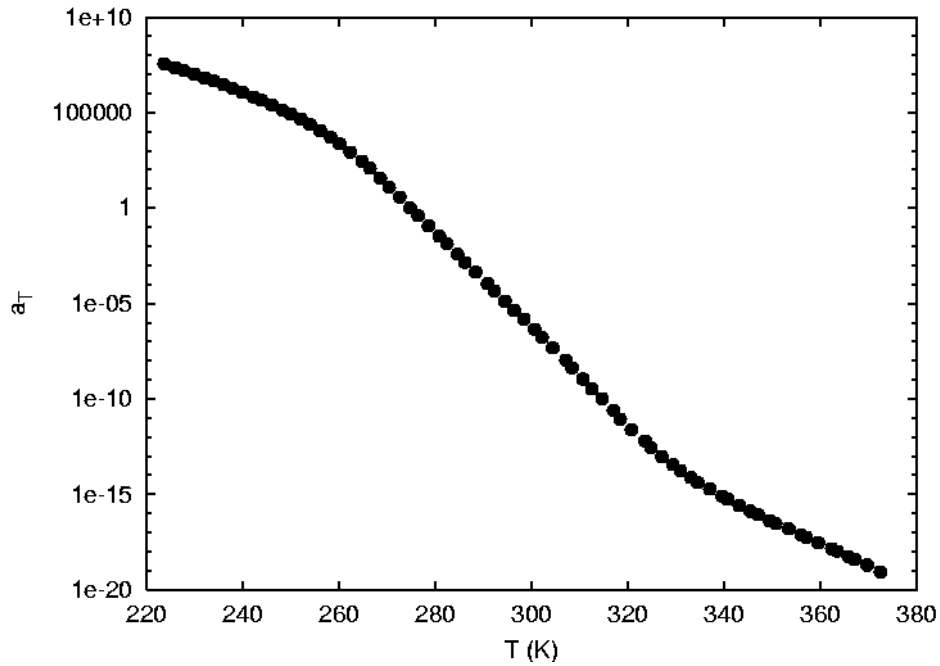

Figure 4.10: Shift factors determined for 1% OP blend to create the master curve in Figure 4.20.

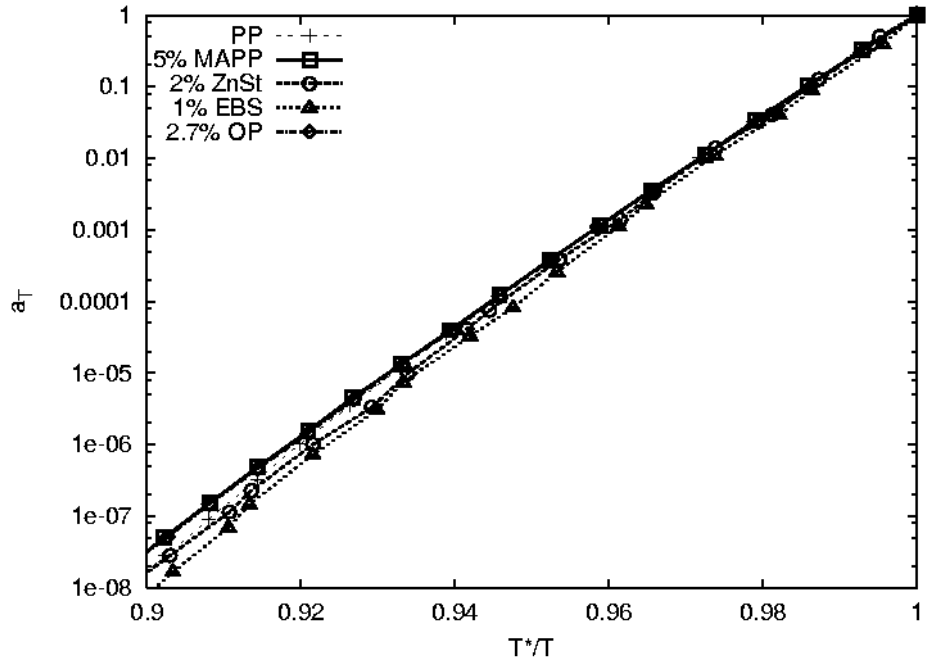

Figure 4.11: A cooperativity plot comparing represenative binary polymer blends that were normalized at *T**defined at T at the maximum in *E″*.

The glassy behavior of blends containing PP/ZnSt/EBS and PP/MAPP/OP yielded similar results as those previously observed in the binary blends (Figure 4.12). However, blends of PP/MAPP/ZnSt/EBS do reveal a deviation from the behavior observed in all the other blends. The increase in the *m* value may be related to a corresponding decrease in configurational entropy. The decrease in interaction undoubtedly stems from the hydration of the MAPP with the presence of ZnSt (Harper 2003b). This results in the possible formation of a carboxylic dimmer between adjacent MAPP copolymers. The formation of these groups is likely cause decreased interaction between the MAPP and PP in the blend.

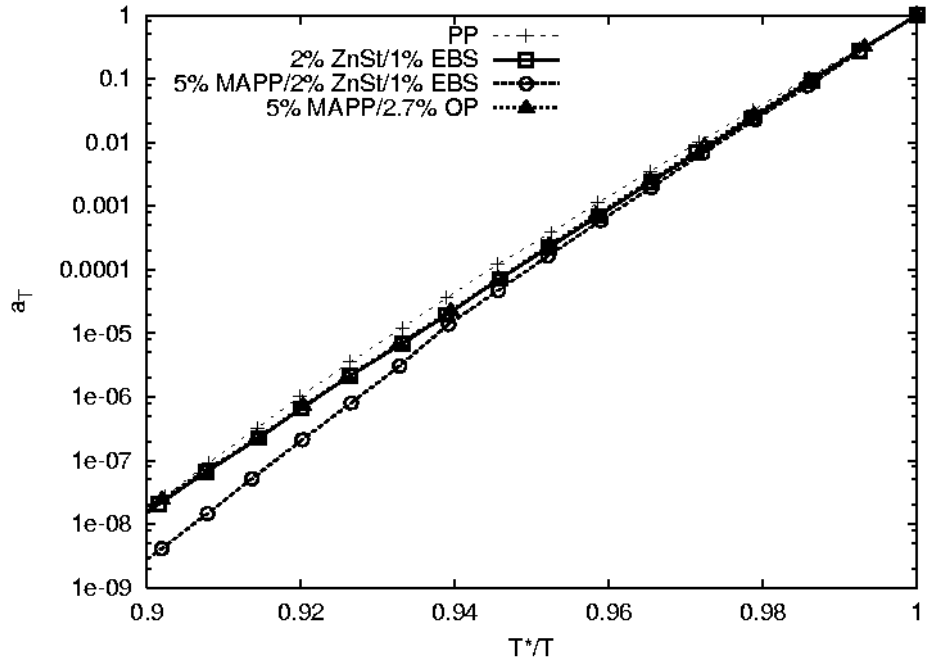

Figure 4.12: A cooperativity plot comparing representative lubricant and MAPP or PP blends that were normalized at *T**.

Blend	$E_{a,\beta}$ (kJ/mol) (+/- 7 kJ/mol)	*m* (+/- 4)	*T** (K) (+/- 2 K)
PP	371	175	277
5% MAPP	394	179	277
2% ZnSt	391	179	277
1% EBS	394	180	277
2.7% OP[†]	379	177	275
ZnSt/EBS	400	179	275
MAPP/ZnSt/EBS	351	191	275
MAPP/OP	372	178	275

Table 4.5: The activation energies for the b relaxation ($E_{a,\beta}$) calculated from the shift factors and the fragilities (*m*). The fragility was normalized with respect to *T**. [†]The error was estimated to be the largest standard error obtained from the regression analysis.

4.7 Conclusions

This paper has demonstrated that the inclusion of some common lubricant systems can change the morphology of PP and its mechanical response. ZnSt acts as a nucleating

agent that creates smaller spherulitic structures that reduce E' throughout the temperature range investigated. However, ZnSt does not appear to have any specific interaction with PP other than as a nucleating agent. The EBS, like ZnSt, appears to act as a nucleating agent as seen by the reduction in n. The mechanical spectroscopy results indicate that the behavior of the two lubricants is very similar in the system. The OP lubricant does not act as nucleating agent, but appears be immiscible with PP. The immiscibility of OP leads to phase separation and larger spherulites that possess fewer defects than observed in the other lubricant systems. As a result, it does not to have a detrimental impact intermolecular coupling.

The MAPP is miscible in the PP as observed by increasing melt point depression with increasing MAPP content. There is also a corresponding increase of defects as observed by shifts to lower crystal species in the DSC plots. The miscibility of the polymers does not impart any change on the location β-transition as observed in some systems. The addition of MAPP leads to increase E' in the rubbery state for the blend over PP. This increase over PP and the other blends carries until past the α-transition. However, the addition of ZnSt diminishes the gain in E' by MAPP addition after the β-transition. ZnSt previously was observed to take part in hydrolyzing the MAPP (Harper 2003b). This likely causes decreased interaction between molecular segments that lead to the increase in fragility of PP/MAPP/ZnSt/EBS blends. Thus, the mechanical consequence is a reduction in stiffness and an increase in damping ability in rubbery state over PP/MAPP blends.

4.8 References

Alfonso GC, Russell TP, Kinetics of crystallization in semicrystalline/amorphous polymer mixtures, Macromolecules, 19 (1986) 1143-1152.

Avrami M, Kinetics of phase change: I general theory, Journal of Chemical Physics (1939) 1103.

Böhmer R, Ngai KL, Angell CA, Plazek DJ, Nonexponential relaxations in strong and fragile glass fromers, Journal of Chemical Physics 99 (1993), 4201-4209.

Boyd RH, Relaxation processes in crystalline polymers: experimental behaviour – a review, Polymer, 26 (1985) 323-347.

Duvall J, Sellitti C, Myers C, Hiltner A, Baer E, Interfacial effects produced by crystallizatin of polypropylene with polypropylene-g-maleic anhydride compatibilizers, Journal of Appled Polymer Science, 52 (1994) 207-216.

Harper DP, A Thermodynamic, Spectroscopic, and Mechanical Characterization of the Wood-Polypropylene Interphase, Ch 2., Doctoral Dissertation, Washington State University, Pullman, WA, 2003.

Harper DP, Chemical Imaging of Wood-Polypropylene Composites, Ch 3., Doctoral Dissertation, Washington State University, Pullman, WA, 2003.

Hoffman JD, Davis GT, Lauritzen JI, The rate of crystallization of linear polymers with chain folding, Treatise on Solid State Chemistry, vol. 3: Crystalline and Noncrystalline Solids, ch. 7, pp. 497-614, Plenum Press, New York, 1976.

Hoffman JD, Weeks JJ, Rate of spherulitic crystallization with chain folds in polychlorotrifluoroethylene, Journal of Chemical Physics 37 (1963), 1723-1741.

Ishida I, Bussi P, Surface-induced crystallization in ultrahigh-modulus polyethylene fiber reinforced _olyethylene composites, Macromolecules 24 (1991) 3569-3577.

Ito H, Russell TP, Wingnall GD, Interactions in mixtures of poly(ethylene oxide) and poly(methyl methacrylate), Macromolecules, 20 (1987) 2213-2220.

Kumar SK, Yoon DY, Lattice model for interphases in binary semicrystalline/amorphous polymer blends. Macromolecules, 22 (1989) 4098-4101.

Liu T, Petermann J, He C, Liu Z, Chung TS, Transmission electron microscopy observations on lamellar melting of cold-crystallized isotactic polystyrene, Macromolecules, 34 (2001) 4305-4307.

Liu T, Petermann J, Multiple melting behavior in isothermally cold-crystallized isotactic polystyrene, Polymer, 42 (2001) 6453-6461.

Matthews RG, Ward IM, and Capaccio G, Structural heterogeneity and dynamic mechanical relaxations of ethylene α-olefin copolymers, Journal of Polymer Science : Part B: Polymer Phsics, 37 (1999) 51-60.

Ngai KL, Rendell RW, Plazek DJ, Couplings between the cooperatively rearranging regions of the Adam-Gibbs theory of relaxations in glass-forming liquids, Journal of Chemical Physics 94 (1991), 3018-3029.

Ngai KL, Roland CM, Intermolecular cooperativity and the temperature dependence of segmental relaxation in semicrystalline polymers, Macromolecules 26 (1993), 2688-2690.

Nishi T, Wang TT, Melting point depression and kinetic effects of cooling on crystallization in poly(vinylidene fluoride)-poly(methyl methacrylate), Macromolecules, 8 (1975) 909-915.

Parizel N, Laupretre F, Monnerie L, N.M.R and D.S.C. investigations of the miscibility of poly(methyl methacrylate)/poly(ethylene oxide) blends, Polymer, 15 (1997) 3719-3725.

Plazek D, Ngai KL, Correlation of polymer segmental chain dynamics with temperature-dependent time-scale shifts, Macromolecules, 24 (1991) 1222-1224.

Schmidtke J, Stobl G,Thurn-Albrecht T, A four-state scheme for treating polymer crystallization and melting suggested by calorimetric and small angle x-ray scattering experiments on syndiotactic polypropylene, Macromolecules, 30 (1997) 5804-5821.

Scott RL, The thermodynamics of high polymer solutions. V. phase equilibria in the ternary system: polymer 1-polymer 2-solvent, Journal of Chemical Physics 17 (1949), 279-284.

Seo Y, Kim J, Kim KU, Kim YC, Study of the crystallization behaviors of polypropylene and maleic anhydride grafted polypropylene, Polymer 41 (2000), 2639-2646.

Struik LCE, The mechanical and physical ageing of semicrystalline polymers: I, Polymer, 28 (1987)1521-1533.

Supaphol P, Spruiell JE, Thermal properties and isothermal crystallization of syndiotactic polypropylenes: differential scanning calorimetry and overall crystallization kinetics, Journal of Applied Polymer Science, 75 (2000), 44-59.

Utracki LA, Polymer Alloys and Blends: Thermodynamics and Rheology, Hanser Publishers, Munich, 1989.

Williams ML, Landel RF, Ferry JD. The temperature dependence of relaxation mechanisms in amorphous polymers and other glass-forming liquids. Journal of the American Chemical Society, 77 (1955) 3701-3707.

Wolcott MP, Chowdhury M, Harper DP, Li T, Heath R, Rials TG, Coupling agent/lubricant interactions in commercial woodfiber-plastic composite formulations, 6th International Conference on Woodfiber-Plastic Composites, Forest Products Society, May 2001, pp. 197-204.

Wortmann FJ, Schulz KV, Investigations on the thermorheological simplicity of polypropylene fibres in the α-transition range, Polymer 36 (1995), 1611-1615.

Wunderlich B, Macromolecular Physics: Vol. I. Crystal Structure, Morphology, Defects, Academic Press, New York, 1973.

Wunderlich B, The basis of thermal analysis. In. Turi E, editor. Thermal Characterization of Polymeric Material: Academic Press, 1981, p. 91-234.

Zawada JA, Ylitalo CM, Fuller GG, Colby RH, Long TE. Component relaxation dynamics in a miscible polymer blend: poly(ethylene oxide)/poly(methyl methacrylate), Macromolecules, 25 (1992)2896-2902.

Zhou W, Cheng SZD, Putthanarat S, Eby RK, Reneker DH, Lotz B, Magonov S, Hsieh ET, Geerts RG, Plackal SJ, Hawley GR, Welch MB, Crystallization, melting and morphology of syndiotactic polypropylene fractions. 4. *in situ* lamellar single crystal growth and melting in different sectors, Macromolecules, 33(2000) 6861-6868.

Chapter 5 Molecular Relaxations in Wood-Polypropylene Composites

5.1 Abstract

The extrusion of composite containing wood and PP usually requires the use of processing lubricants in order to produce a stable profile out of a die. In addition, a coupling agent is often added to promote adhesion between the wood and polymer matrix. However, there is little understanding of the mechanical implications on the composite with the addition of lubricants and couplents. The viscoelastic and mechanical performance of composites extruded with wood, polypropylene (PP), maleic anhydride polypropylene (MAPP), and lubricants were evaluated. Static bending was used to evaluate the mechanical properties of the extruded composites. In addition, dynamic mechanical analysis was performed on composites machined from the extruded material. Formulations that have previously displayed superior nucleating ability and the formation of a transcrystalline layer on the wood surface, displayed the greatest improvements in bending modulus of elasticity, modulus of rupture, and storage modulus. A ratio of the tan δ values for wood composite to that of the neat PP blend proved effective in predicting the formulations that have the greatest bending modulus of rupture. This result may indicate an increased adhesive interaction with the incorporation of MAPP. Surprisingly, wood-PP-MAPP composites without lubricants did not have the largest impact on activation energies for the PP β transition, but did increase relaxation times on both sides of the β transition more than other composite formulations. Because the

highest activation energy does not occur in the composite with the highest matrix-filler interaction, this is a strong indication that this interaction does not contribute directly to the β transition in PP composites. Rather, the broadening of the β transition was attributed to molecular interactions in the amorphous polymer phase.

5.2 Introduction

Over the past decade wood and agriculture fibers has been gaining interest and acceptance for use as reinforcement in thermoplastic matrix composites. The benefits of the renewable fiber source, including low cost, widespread availability, and high density to modulus ratio, have sparked interest in composites for building construction and automotive applications. However, the polarity of the agricultural fibers in a polyolefin matrix usually leads to poor interface development and poor dispersion (Johnson and Nearn 1972). The incorporation of polyolefin copolymers with polar functionality and lubricants during extrusion improves dispersion and mechanical properties (Takase and Shiraishi 1989, Lu et al. 2000). The most widely used copolymers consist of a grafted maleic anhydride group onto a polyolefin chain. The hypothesis is that anhydride will react with hydroxyl groups of the agricultural fiber producing a covalent ester bond with the matrix (Bledzki et al. 1996). Proof of ester bonds has been the subject of much research. To date, only composites with little to no lignin content have shown conclusive ability to covalently bond (Kazyawoko et al. 1997a, Kazyawoko et al. 1997b, Paunikallio et al. 2003). Other research has shown that little to no proof of bonding to an untreated fiber such as wood exists (Kazyawoko et al. 1997a, Kazyawoko et al. 1997b, Son et al. 2000, Lai et al. 2003, Li and Matuana 2003, Harper 2003).

The focus on the bond formation has distracted much attention away from the potential changes that the copolymer addition may impart on the matrix. Maleic anhydride polypropylene (MAPP) demonstrates the ability to co-crystallize with isotactic polypropylene (PP) in certain scenarios (Duvall et al. 1994, Harper 2003c). Consequently, the MAPP may change the morphology of the matrix and a composite composed of a whole wood component (Seo et al. 2000, Yin et al. 1999, Harper 2003a, Harper 2003b, Harper 2003c). The complex changes to the plastic morphology undoubtedly affect the mechanical properties of the composite. A recent study shows differences between the viscoelastic properties of the composite when nucleation density is changed in the matrix (Son et al. 2003). MAPP was used as a comparison in this study also, but the impact that it had on the morphology of the matrix and wood interface was neglected. Instead, the increase in activation energies in the composite was taken to be from bonding of MAPP and wood only; a bond that has not adequately been proven in the literature.

5.3 Objectives

The goal of this paper is to discern the mechanisms that contribute to the mechanical performance of wood-PP composites. Previous attempts at characterizing the mechanical properties of wood-PP composites did not differentiate between chemical interactions at the wood interface, changes in the amorphous polymer, or morphology changes with the addition of wood. The specific objectives of this paper are:

1. To determine how different lubricants affect the mechanical performance of the wood-PP composites with and without MAPP,

2. Characterize how wood impacts the molecular motions of PP at and near the interface.
3. Identify mechanisms that lead to differentiation in mechanical properties among composite formulations.

5.4 Materials and Methods

The materials used for this investigation consist of an isotactic polypropylene (iPP) homopolymer, a commercial maleic anhydride polypropylene (Honeywell A-C 950P) (MAPP) copolymer, two additives formulations, and a single wood species as a whole wood component (*Acer sp.*). The lubricant blends included 2 percent zinc stearate (Ferro) (ZnSt) with 1 percent ethylenebisstearamide (GE Specialty Chemicals) (EBS) system and 2.7 percent ester based lubricant (Honewell Optipac 100) (OP). Composites were formulated with 60 percent wood and 40 percent PP blend (Table 5.1). The formulations were initially dry blended and subsequently extruded using a 35 mm Cincinnati-Milacron conical twin-screw extruder to a density of 1.07-g/cm^3 +/- 0.02 g/cm^3 for all formulations. The sections were extruded through a 9.525 mm × 38.1 mm die and passed through a water-jet cooling tank.

Blend	***%PP***	***%MAPP***	***%OP***	***%ZnSt***	***%EBS***
PP	40	0	0	0	0
PP/ZnSt/EBS	38.8	0	0	0.8	0.4
PP/ OP	38.92	0	1.08	0	0
PP/MA	38	2	0	0	0
PP/MA/ZnSt/EBS	36.8	2	0	0.8	0.4
PP/MA/OP	36.92	2	1.08	0	0

Table 5.1: Blends extruded for mechanical and DMA analysis including blends of the copolymers and lubricants. The composites were extruded with 60% wood flour and 40% PP blends.

Mechanical evaluation was conducted on extruded material in third point bending according to ASTM D6109-97 (1998). Ten specimens were selected from each extruded formulation. The largest dimension was in the direction of extrusion. The test span was 152.4 mm with a crosshead speed of 0.0762 mm/s. The specimens were conditioned at 21ºC with 50 percent relative humidity for one week prior to testing. The bending specimens had nominal dimensions of 9.6 mm × 36.8 mm × 190.5 mm.

The extruded composites were then cut and machined to specimen dimensions that were nominally 1.6 mm × 6 mm × 45 mm to fit a Rheometrics RSA II solids analyzer operated in dual cantilever mode. The specimens were machined from the center left and right of the extruded section so that the length wise direction was in the direction of extrusion. The samples were rough cut from the section and then milled to the desired dimensions. Dynamic mechanical analysis (DMA) was conducted at 0.1% strain as determined by a static strain sweep test at –50, 25, and 100°C to insure linearity throughout the test. The specimens followed a ramp from –50 to 100°C at 2°C increments with a 1-minute soak time and dynamic loading from 1 to 10 Hz. The isothermal data were then shifted horizontally according to the principle of time temperature superposition (Ferry 1980). Shifting was performed on the storage modulus (E') data to find the horizontal shift factors (a_T). These shift factors were then used to shift all other viscoelastic properties. The reference temperature (T^*) for shifting was taken as the temperature at the maximum in the loss modulus (E''_{max}). The shift factors are considered the same for all viscoelastic properties.

5.5 Results and Discussion

5.5.1 Static Bending

Mechanical evaluation of the formulations reveals that different constituents have varying effects on the bending strength and stiffness of the composite. The bending modulus of a polymer is improved with the incorporation of a stiffer reinforcing fiber. Usually, the adhesion between the matrix and reinforcing fiber has little impact on the modulus of a composite (Nielsen and Landel 1994). The different lubricant formulations appear to have no substantial influence on the static bending modulus (Table 5.2). The MAPP on the other hand does increase the static bending modulus of the composite. This observation has been made in previous studies with PP and other polyolefins (Wolcott et al. 2001, Son et al. 2003). The increase in modulus from MAPP can be of its decreased bulk nucleation density leading to larger spherulites. It is unlikely a filler interaction because of the increase in MOE of the MAPP/ZnST/EBS composite. This is apparent because of its poor MOR in comparison with MAPP and MAPP/OP composites. Although material strength is dependent on many factors, it is in general a more reliable indicator of increased matrix filler interaction than modulus (Lipatov 1979). Efficient transfer of stress into a reinforcing filler of higher strength will increase the yield stress of the composite.

Formulation	*MOE (GPa)*	*MOE COV*	*MOR (MPa)*	*MOR COV*
PP	4.02	(3.87)	31.7	(13.9)
PP/OP	3.89	(6.50)	30.4	(5.38)
PP/ZnSt/EBS	4.03	(3.43)	31.4	(5.31)
MAPP	5.11	(4.99)	67.5	(1.70)
MAPP/OP	5.18	(3.67)	62.5	(1.94)
MAPP/ZnSt/EBS	5.07	(7.77)	48.2	(5.40)

Table 5.2: Static bending results for the extruded composites with 60% wood and 40% PP blend.

5.5.2 Storage Modulus

The addition of filler with a semicrystalline matrix changes the morphology of the plastic by inducing nucleation on the filler surface (Lipatov 1979). The PP-blends used in this study exhibit varying degrees of nucleating ability on wood (Harper 2003a). In particular, an interphase formed from a high nucleation density on the fiber increases the modulus of the composite in the fiber direction (Assoulini et al. 2001a). The lack of surface nucleation of a semicrystalline polymer can result in an amorphous phase around the filler. The amorphous may absorb onto the filler surface leading to good interaction, or its configuration may be interrupted and result in decreased mechanical properties (Lipatov 1979). The storage modulus (E') of the composite is highest among the blends that were earlier found to have the highest nucleation advantage on the wood surface (Figure 5.1). From previous research, PP, PP/MAPP, and PP/MAPP/OP had nucleating advantages of 1.40, 0.93, and 0.80 respectively (Harper 2003a). The nucleating advantage is a measure of the ability of the fiber to nucleate a crystal. When this advantage is 1 or greater, a strong nucleating surface leads to the formation of a transcrystalline layer around the filler (Ishida and Bussi 1991).

The transcrystalline layer aligns polymer chains in the direction of the fiber and twist to align with the bulk polymers (Assoulini et al. 2001b). The benefit to mechanical testing is aligning the crystals with the wood fibers that are primarily oriented in the direction of extrusion. Because of the anisotropy of the transcrystalline layer, this creates a polymer

that is much stiffer along the wood surface than in the transferse direction. The fibers generally align in the direction of extrusion and thus, the direction tested.

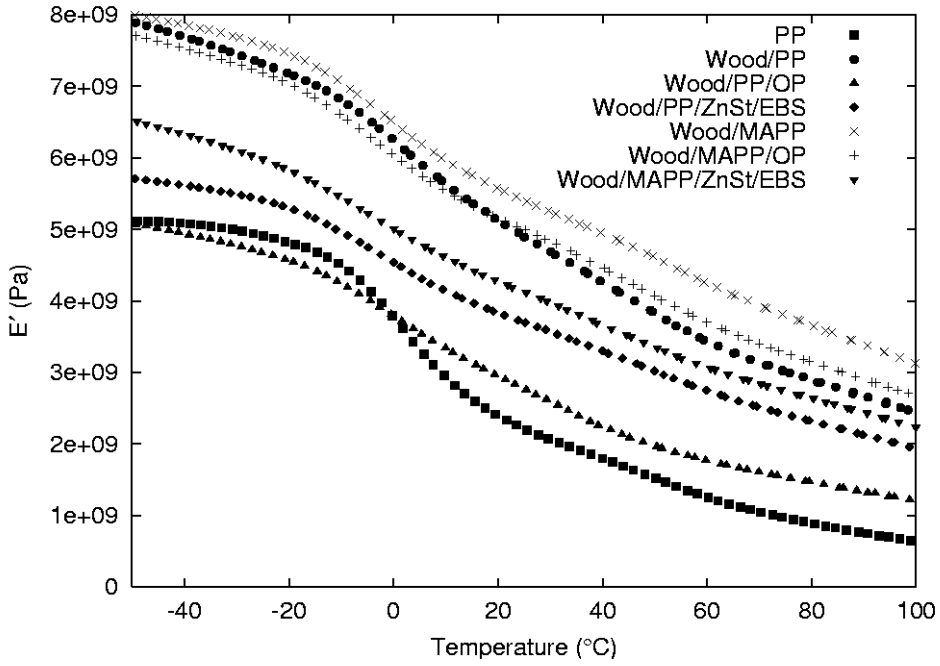

Figure 5.1: *E′* at 1 Hz for the extruded composites compared against a 100% PP specimen.

5.5.3 Loss Tangent

Below T_g, the polymer matrix contracts resulting in increased frictional forces on the reinforcing material, mimicking the effects of specific interactions. However, around the beta transition the molecules in the amorphous component of the matrix begin to relax (Boluk and Schrieber 1986). This transition is confined to the matrix component when the glass transition of the reinforcing material is much higher than that of the matrix; as is the case here.

The damping in the composite material should be directly proportional to the filler volume fraction (ϕ_f) as purposed by Nielson (1979),

$$\tan \delta_c = \tan \delta_p \left(1 - \phi_f\right), \qquad \text{Equation 5.1}$$

where, the subscripts *c*, *p*, and *f* refer to the composite, polymer, and filler respectively. The damping in the composite is decreased as predicted with the inclusion of wood into the PP blend (Figure 5.2). It is, also readily apparent that different formulations provide varying levels of damping and the temperature of the peak in tan δ changes. There are many possible causes for differences in the damping characteristic of the composite. Low crystallinity, loading direction, plastization of the matrix, and inefficient packing density in the amorphous phase around fillers are all possible causes for reduced tan δ (Lipatov 1979, Nielsen and Landel 1994). An increase in crystallinity of the matrix decreases the damping by decreasing the amount of polymer that can relax. Poor packing density of the amorphous phase and blends with plasticizers lead to increased damping. This is caused by increased molecular mobility of the amorphous and often lowers the T_g.

PP/ZnSt/EBS blends display an increase in T^* over the homopolymer when wood is not added (Table 5.3). However, adding wood lowers T^*. The ZnSt/EBS combination does not appear to plasticize the amorphous phase of the. However, previously ZnSt/EBS was found to have a negative impact on the nucleating ability of PP on wood surfaces (Harper 2003a). The nucleation of PP on the wood surface helps organize the molecules efficiently around the filler. The lack of nucleation may disrupt bulk crystallization and

lead to unstable amorphous polymer conformations around the wood. All of the lubricant and MAPP combinations displayed decreased T^* with wood addition.

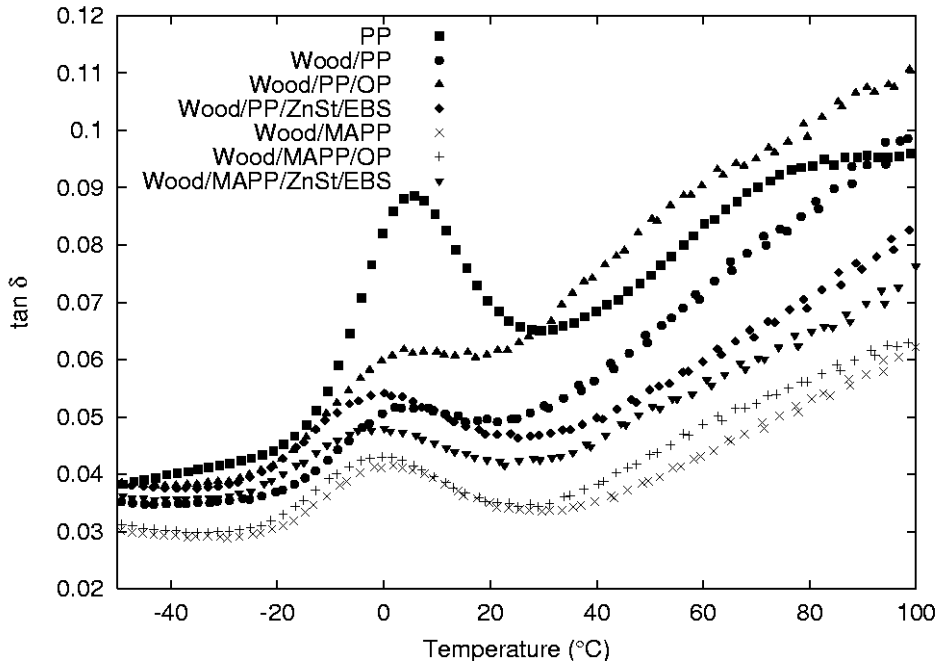

Figure 5.2: The loss tangent (tan δ) at 1 Hz for the extruded composites compared against a 100% PP specimen.

The perceived volume fraction of the filler can increase if the filler immobilizes a layer around it (Iisaka and Shibayama 1978). Wood-PP composites present a special problem when trying to estimate ϕ_f. Wood is a porous material with a cell wall density of ca. 1.5 g/cm^3 (Panshin and de Zeeaw 1980) compared to PP at 0.90 g/cm^3. PP can fill the wood cell lumens and pits in the cell wall during extrusion (Figure 5.3). The amount of infiltration of the plastic into the wood is very dependent on species because of wide differences in cell structures and there are certainly voids present. Therefore, the actual volume fraction of wood is a difficult quantity to estimate. However, because the wood

was added at a constant level for all composites and the densities were the same at 1.08+/-0.02 g/cm^3, an assumption of a constant fiber volume for all composites can be assumed. Thus, ϕ_f from Equation 5.1 can be thought of as an effective reinforcing volume fraction (ϕ_e) for the composite (Table 5.3). The order of the composites having the highest ϕ_e is the same as that for MOR: MAPP > MAPP/OP > MAPP/ZnSt/EBS > PP > PP/ZnSt/EBS > PP/OP. This is currently at best a qualitative tool for comparison, but it is a good indication that there is a specific adhesive interaction between the wood and MAPP. The adhesion is reduced with the inclusion of ZnSt in MAPP because of the hydrolysis of the anhydride group (Harper 2003b).

	PP-blend		***Composite***		
Formulation	***Tan δ***	***T* (°C)***	***tan δ***	***T* (°C)***	***Effective ϕ_e***
PP	0.0894	-0.80	0.0573	-4.6	0.360
PP/OP	0.0795	-1.0	0.0610	-3.4	0.233
PP/ZnSt/EBS	0.0741	1.7	0.0511	-7.7	0.311
MAPP	0.0754	2.3	0.0421	-4.0	0.441
MAPP/OP	0.0765	-1.2	0.0452	-6.1	0.409
MAPP/ZnSt/EBS	0.08013	-3.3	0.0486	-8.5	0.393

Table 5.3: This table shows the tan δ at the maximum in *E″* and the corresponding temperature *T**. ϕ_e is calculated from Equation 1.1. The blends are PP blends containing now wood where composite wood flour is added at 60% by mass. The mean of two samples was taken as the value.

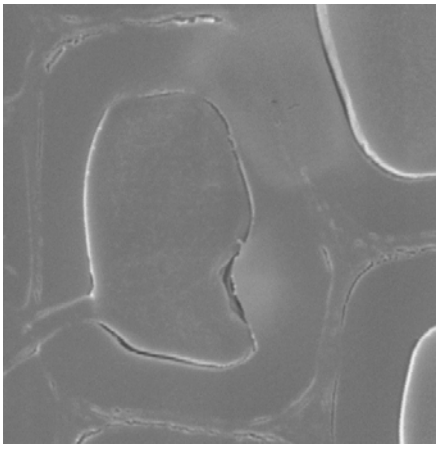

Figure 5.3: An SEM image showing that PP flows inside of a wood lumen and pit in an extruded PP-wood composite taken at 2500 magnification.

5.5.4 Molecular Interaction

The master curves for the composites created from TTSP follow simple behavior (Figure 5.3). However, moving into the α transition region the relaxation becomes quite complex at $T > 60$ºC. The long-range molecular interaction can be evaluated by the materials dynamic response. This is to say that the dynamic response of a polymer can depend solely on local unrestricted movements, or a polymer may need to impart large configurational changes to respond to an external stress. The viscoelastic response of cooperative movements of polymer chains manifests themselves differently than specific adhesive interactions. The result is a broadening of the β transition related to an increased distribution of relaxation times associated with group configurations. This broadening is common in semicrystalline polymers where rigid amorphous phase movements are restricted by neighboring crystals (Struik 1987). A normalized plot of the β transition displays a broadening with the inclusion of wood and further broadening when MAPP is included (Figure 5.4). Broadening is greatest in the MAPP/ZnSt/EBS as opposed MAPP, the narrowest peak seen in the formulations. Wood is restricting the

movement of some polymer molecules at the interface. This effect is greatest in the PP/MAPP blends since it displays the greatest specific interaction.

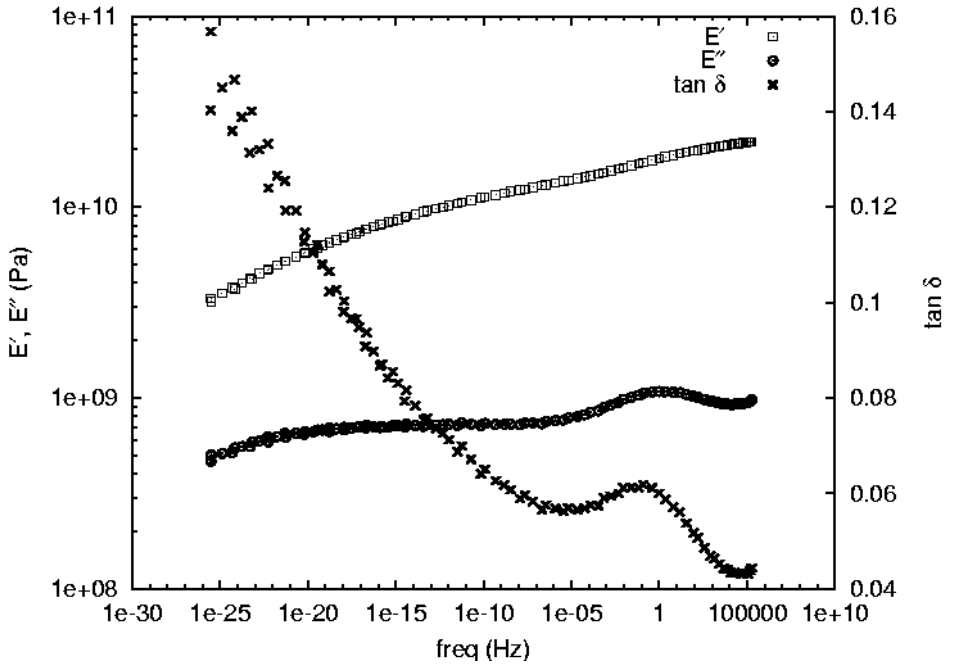

Figure 5.4: Master curve for PP/ZnSt/EBS composite generated from the DMA data by TTSP.

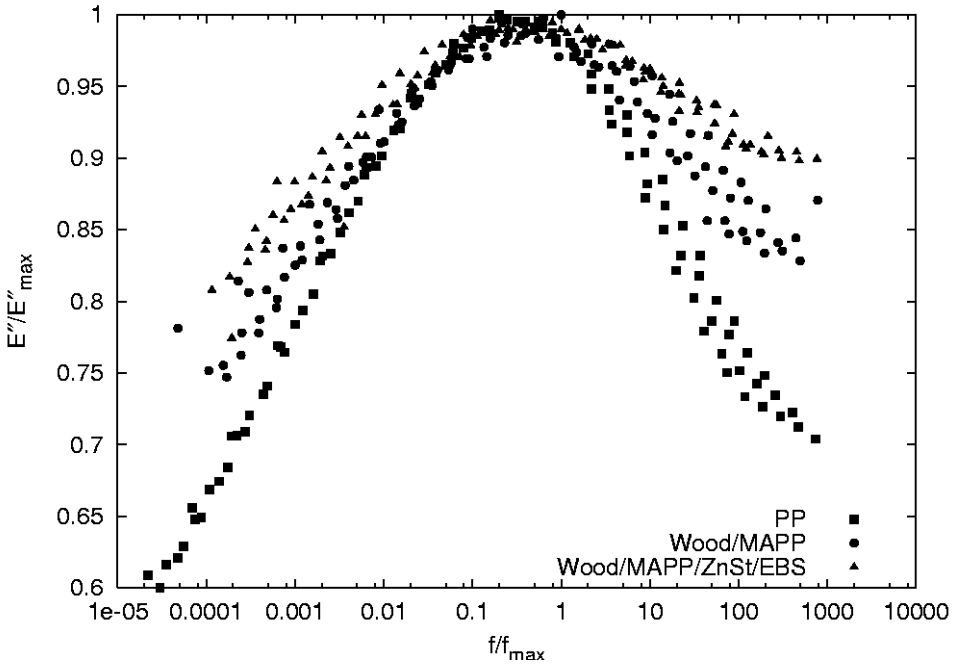

Figure 5.5: KWW plot displaying the broadening of relaxation times for the addition of wood. This plot was constructed from the master curves where E''_{max} is the maximum in E'' and f_{max} is the frequencies at E''_{max}. The Wood/MAPP and Wood/MAPP/ZnSt/EBS blends represent the two extremes of the composites where all others lie between them. PP was a 100% PP molded specimen.

The large configurational movements of polymer chains observed in the stretching are based on the thermodynamics explained in the Adams-Gibbs model (1965). Angel (1991) suggested a dynamic approach as a way to explain the nonArrhenius behavior of some supercooled liquids. A normalized Arrhenius equation was used to determine the steepness index (m) or otherwise known as fragility (Bohmer et al. 1993).

Equation 5.2

$$m = \left. \frac{d \log\langle \tau \rangle}{d\left(T_g / T \right)} \right|_{T=T_g},$$

where τ is the relaxation time. From the principle of time-temperature superposition (Ferry 1980), the shift factor (a_T) substitutes for τ in Equation 5.2 to determine m when

simple linear viscoelasticity is obeyed. Weak glass forming liquids tend to have weak unidirectional bonds and exhibit high *m* values. Whereas, strong glass formers possess strong intermolecular bonds possess a low steepness index. There is thought to be an elegant connection between the thermodynamics of the Adam-Gibbs model and the dynamics of fragility, but this has not been found (Bohmer et al. 1993, Ferrer 1999). A fundamental problem with the scaling about T_g exists since it does not relate to a universal material state, but is an easily experimentally attainable quantity. However, Ferrer et al.(1999) demonstrated that in spite of T_g's seemingly ambiguity, it does measure fragility accurately as long as $\tau(T_g) >> \tau(T_{cross})$, where the inequality represents the relaxation time at T_g and the relaxation time at the crossover point from a simple to a supercooled liquid.

The composite with MAPP and no lubricant was expected to be the strongest glass former from the interactions imposed by the polar groups (Figure 5.5). However, the PP and PP/OP composite displayed the highest values of *m* (Table 5.5). These composites are also the same formulations that display the highest degree of perfection in their crystal structures in an earlier study (Harper 2003a). Likewise, the MAPP/ZnSt/EBS composite previously showed the lowest degree of perfection and here display the lowest value of *m* for the materials tested. Athough the β transition involves only the amorphous component; the crystalline domains from the tie molecules that pass through the amorphous region to connect adjacent crystallites influence the rigid amorphous regions. Regardless, these results show that filler has no direct impact on the dynamics of the

system. The m and E_a are lowered in the composite because of the morphology resulting from the filler presence but not specifically by the adhesion.

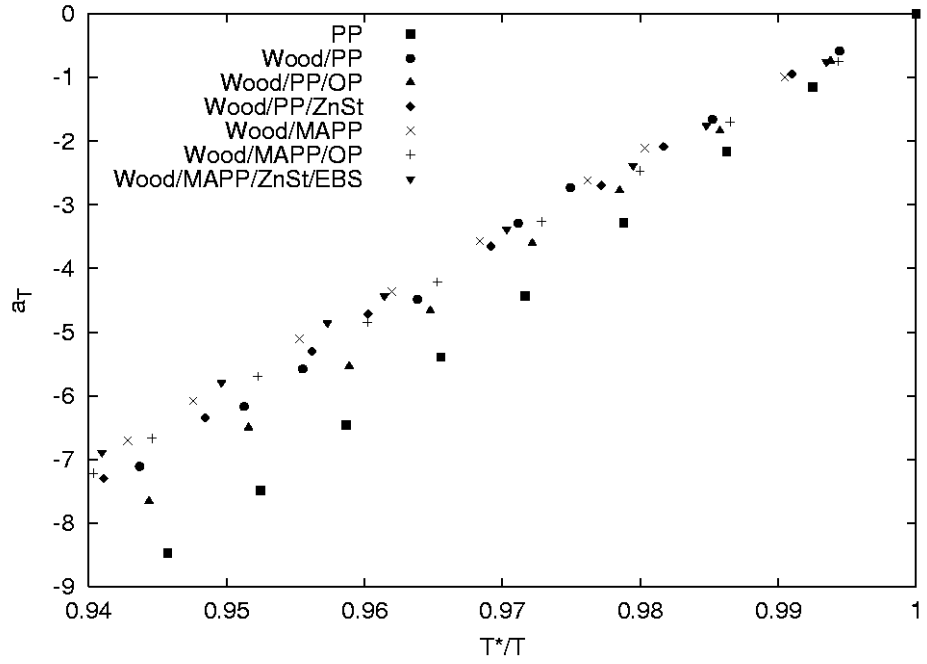

Figure 5.6: Fragility plots for extruded wood composites where T^* refers to the temperature at the maximum in E'' for the β transition. T^* is also taken as the reference temperature for TTSP.

Formulation	***E_a (kJ/mol)* (+/-7 *kJ/mol*)**	***m* (+/- 4)**
100% PP	371	166
Wood/PP	306	128
Wood/PP/OP	340	139
Wood/PP/ZnSt/EBS	273	124
Wood/MAPP	270	120
Wood/MAPP/OP	278	120
Wood/MAPP/ZnSt/EBS	275	116

Table 5.4: Comparison of activation energies (E_a) and the fragility (m) for the β transition of a 100% PP specimen and extruded composites.

5.6 Conclusions

The incorporation of MAPP into the polymer increases both the bending modulus and strength. The increase in bending modulus with MAPP may be two fold. First, there is improved interaction in the amorphous regions of the polymer as seen by a broadening in the β transion. Secondly, there is a possible reinforcing effect from improved alignment of the molecules in the fiber direction. This has been observed to improve tensile strength in other PP composites (Assouline et al. 2001). The composite formulations that produce the largest TCL also displayed the highest value for E'. This is a strong indication the TCL does have a substantial impact on composite modulus.

MOR is increased from specific adhesive interaction that allow efficient packing of the polymers around the wood fiber with the incorporation of MAPP. However, it is not clear that there is an actual covalent bond between the MAPP and the whole wood. The presence of some secondary interaction alone may contribute to the development of interfacial strength. The inclusion of MAPP also resulted in the largest depression of the loss tangent among the composites. This decrease is likely the result of improved adhesion with the matrix. The ZnSt in the composite acts a catalyst for the hydrolysis of MAPP, reducing adhesion (Harper 2003b). Consequently, an increase in the tan δ was observed. Further, the local movements of polymers containing MAPP are restricted by the adhesive interaction with the wood. This results in an increased reinforcement effect on the polymer.

The long-range molecular motions often play a role in the long term loading scenarios. An increased broadening of the β transition is observed with the incorporation of filler. The broadening is generally considered the direct result of the restricting of molecular mobility from interaction with the filler in a composite. The steepness index would suggest otherwise in these composites. At the high and low end of range of *m* values were the formulations with least possibility for wood adhesion. But, there is a connection with these formulations and nucleation. The lower nucleating formulations had lower *m* values while the high *m* coincided with the high nucleation advantage. This may put more amorphous polymer in contact with the wood surface increasing the distribution of relaxation. Thus, this is a result of morphological changes, not the result of increased adhesion. A degree of disorder is created in the amorphous phase around the filler that disrupts its packing density. These same composite formulations with poor nucleating ability also possess the largest drop in T^* and the highest damping. Therefore, there is a link to morphology of a semicrystalline polymer around the filler to its mechanical performance.

5.7 References

Angell CA, Relaxation in liquids, polymers and plastic crystals-strong/fragile patterns and problems. Journal of Noncrystalline Solids, 13 (1991) 131-133.

Assouline E, Grigull S, Marom G, Wachtel E, Wagner HD, Morphology of transcrystalline isotactic polypropylene under tensile stress studied with synchrotron microbeam x-ray diffraction, Journal of Polymer Science: Part B: Polymer Physics 39 (2001a), 2016-2021.

Assouline E, Wachtel E, Grigull S, Lustiger A, Wagner HD, Marom G, Lamellar twisting in isotactic polypropylene transcrystallinity investigated by synchrotron microbeam x-ray diffraction, Polymer 42 (2001b), 6231-6237.

Bledzki AK, Reihmane S, and Gassan, Properties and modification methods for vegetable fibers for natural fiber composites, Journal of Applied Polymer Science, 59 (1996), no. 8, 1329-1336.

Boluk MY, Schreiber HP, Interfacial interactions and the properties of filled polymers: I. Dynamic-mechanical responses, Polymer Composites, 7 (1986) 295-301.

D 6109-97: Standard test methods for flexural properties of unreinforced and reinforced plastic lumber, Annual Book of ASTM Standards, pg. 833-838, 1998.

Duvall J, Sellitti C, Myers C, Hiltner A, Baer E, Interfacial effects produced by crystallizatin of polypropylene with polypropylene-g-maleic anhydride compatibilizers, Journal of Appled Polymer Science, 52 (1994) 207-216.

Ferrer ML, Sakai H, Kivelson D, Alba-Simionesco C, Extension of the Angell Fragility Concept, Journal of Physical Chemistry B, 103 (1999) 4191-4196.

Ferry JD, Viscoelastic Properties of Polymers, 3rd ed., Wiley, New York 1980.

Harper DP, A Thermodynamic, Spectroscopic, and Mechanical Characterization of the Wood-Polypropylene Interphase, Ch 2, Doctoral Dissertation, Washington State University, Pullman, WA, 2003a.

Harper DP, A Thermodynamic, Spectroscopic, and Mechanical Characterization of the Wood-Polypropylene Interphase, Ch 3, Doctoral Dissertation, Washington State University, Pullman, WA, 2003b.

Harper DP, A Thermodynamic, Spectroscopic, and Mechanical Characterization of the Wood-Polypropylene Interphase, Ch 4, Doctoral Dissertation, Washington State University, Pullman, WA, 2003c.

Iisaka K, Shibayama K, Mechanical alpha-dispersion and interaction in filled polystyrene and polymethylmethacrylate, Journal of Applied Polymer Science, 22 (1978) 3135-3143.

Ishida I, Bussi P, Surface-induced crystallization in ultrahigh-modulus polyethylene fiber reinforced _olyethylene composites, Macromolecules 24 (1991) 3569-3577.

Johnson JA, Nearn WT, Theory and design of wood and fiber composite materials, ch. 15. Reinforcement of polymeric systems with Douglas-fir bark fibers, pp. 371-400, Syracuse University Press, 1972.

Kazayawoko M, Balantinecz JJ, Woodhams RT, Diffuse reflectance Fourier transform infrared spectra of wood fibers treated with maleated polypropylenes, Journal of Applied Polymer Science 66 (1997a), 1163-1173.

Kazayawoko M, Balatinecz JJ, Woodhams RT, Law S, Effect of ester linkages on the mechanical properties of wood fiber-polypropylene composites, Journal of Reinforced Plastics and Composites 16 (1997b), 1383-1406.

Lai SM, Yeh FC, Wang Y, Chan HC, Shen HF, Comparative study of maleate polyolefins as compatibilizers for polyethylene/wood flour composites, Journal of Applied Polymer Science, 87 (2003) 487-496.

Li Q, Matuana LM, Surface of cellosic materials modified with functionalized polyethylene coupling agents, Journal of Applied Polymer Science (2003) 278-286.

Lipatov SY, Physical chemistry of filled polymers, Rubber and Plastics Research Association of Great Britain, 1979.

Lu JZ, Wu Q, McNabb HS, Chemical coupling in wood fiber and polymer composites: a review of coupling agents and treatments, Wood and Fiber Science, 32 (2000) 88-104.

Ngai KL, Roland CM, Intermolecular cooperativity and the temperature dependence of segmental relaxation in semicrystalline polymers, Macromolecules 26 (1993), 2688-2690.

Nielsen LE, Dynamic mechanical properties of polymers filled with agglomerated particles, Journal of Polymer Science, Polymer Physics Edition, 17 (1979) 1897-1901.

Nielsen LE, Landel RF, Mechanical Properties of Polymers and Composites, second ed., Marcel Dekker, New York, 1994.

Panshin AJ, de Zeeaw C, Textbook of Wood Tchnology, 4th edition, McGraw-Hill, New York, 1980.

Paunikallio T, Kasanen J, Suvanto M, Pakkanen TT, Influence of maleated polypropylene on mechanical properties of composite made of viscose fiber and polypropylene, Journal of Applied Polymer Science, 87 (2003) 1895-1900.

Seo Y, Kim J, Kim KU, Kim YC, Study of the crystallization behaviors of polypropylene and maleic anhydride grafted polypropylene, Polymer 41 (2000), 2639-2646.

Son S, Lee Y, Im S, Transcrystalline morphology and mechanical properties in polypropylene composites containing cellulose treated with sodium hydroxide and cellulase, Journal of Materials Science 35 (2000), 5767-5778.

Struik LCE, The mechanical and physical ageing of semicrystalline polymers: I, Polymer, 28 (1987)1521-1533.

Takase S, Shiraishi N, Studies on composites from wood and polypropylene. II, Journal of Applied Polymer Science, 37 (1989) 645-659.

Yin S, Rials TG, Wolcott MP, Crystallization behavior of polypropylene and its effect on woodfiber composite properties, In The Fifth International Conference on Woodfiber-plastic Composites, pg. 139-146, 1999.

Chapter 6 Summary and Conclusions

Wood-plastic composites are gaining growing acceptance for structural applications. For these applications, extrusion is the preferred method of production. In order to extrude the most common types of polymers that are applicable at high filler levels, processing lubricants are often necessary. The addition of even small amounts of a foreign substance into a polymer can lead to dramatic changes in the properties. A good example is introducing polyethylene into isotactic polypropylene (PP), the two are chemically very similar, but are largely immiscible. This leads to very poor properties of the polymer blend. The introduction of a polar material into a PP can promote nucleation and change the morphology. This could also have a dramatic impact on structure. It was therefore a hypothesis of this study that different PP morphologies would be obtained with the addition of different lubricants, maleated polypropylene copolymer (MAPP), and wood. Further, these variations in morphology in the bulk polymer and at the wood-PP interface are the driving mechanism leading to differences in observed mechanical properties.

Much previous research has focused and assumed the existence of a covalent bond between wood and MAPP. However, this study did not follow that assumption. Fourier transform infrared spectroscopy was utilized in an attempt to discern the existence of a covalent bond. As many studies have found previously, there is no conclusive evidence to suggest its presence. However, MAPP was found in abundance in the interphase and at the wood-PP interface. This may suggest that there is the possible existence of adhesive interaction between the wood and the matrix. The improved nucleating ability at least suggest the improvement of the physical interaction between the wood and the PP

with MAPP. The incorporation of zinc stearate hydrolyzes MAPP and nullyfies most of its ability to interact with the wood surface. The shift in wave number from 1788 to 1712 cm^{-1} is present throughout the interphase and at the wood interface. This has an obvious detrimental effect on the packing efficiency of the molecules around the wood observed by the depression of the composite's T_g. The loose amorphous layer around the wood leads to increased damping observed in the tan δ. A ratio between the tan δ of composite and the polymer blend points to those formulations that have the best adhesive interaction between the matrix and wood. This ratio may be effective to use for comparisons of composite formulations. The ratio agreed closely with the MOR results in the static bending test. However, there is no theory at present linking bending strength to the packing density in a quantitative form, but the damping ratio may point out the presence of a mobile polymer layer around fills in composites.

One of the main things that appear to affect the packing density is the ability to nucleate off the wood's surface. This affects packing density and stiffness by creating an interphase that reinforces the composite in fiber direction. The wood helps to align the polymer molecules in along the wood before they twist to become compatible with the bulk matrix. This creates an anisotropic layer that has a modulus that is higher in the direction of the wood. The result is further reinforcement in bending and tension. The composite containing 5% MAPP and no lubricants had the second highest nucleating ability, highest bending stiffness, and highest E'. All of the composites that possessed a propensity to nucleate on the wood surface had the highest stiffness values.

There is a change in the nucleation mechanism with the addition of ZnSt and EBS. PP by

itself nucleates by homogeneous and heterogeneous nucleation. The homogeneous mechanism is more sensitive to temperature whereas heterogeneous nucleation depends upon a foreign substrate to reduce the free energy needed to nucleate. ZnSt acts as a nucleating agent for PP. This often speeds the overall nucleation process, but also creates many defects in the crystal structure. Also, there is still the homogeneous nucleating mechanism that is present in the ZnSt blends which leads to a great deal of secondary nucleation. The OP blend appears to shift everything to a heterogeneous nucleating mechanism although it is not a nucleating agent itself. OP, evident from FTIR mapping, is immiscible, and does not interfere with the perfectioning of PP crystals that lead to a high melting point.

Much data and many different experimental ideas were discussed in this dissertation. The main point discussed was the relationship of the morphology to composite properties when lubricants and coupling agents are added to a polymer. MAPP showed vast improvements to the mechanical properties of wood-PP composites. It has been previously proposed that the main mechanism for increased mechanical properties is a covalent ester bond between the MAPP and wood. Though there has been much scientific effort devoted to look for this bond, including this study, it has not been proven to exist in a composite utilizing a whole wood component. Instead, changes to the composite morphology were observed with the addition of MAPP. The MAPP produces a larger material wood interphase that helps reinforce the composite. This interphase is highly anisotropic and has its strong axis in the direction of the wood fiber. The interphase is formed by a combination of conditions for nucleation in the bulk matrix and

on the surface of the fiber. Nuclei form on the wood surface and impinge on each other. This forces the crystallites to then grow radially from the fiber surface until they impinge on spherulites in the bulk matrix. Therefore, the size of the interphase is more dependent on bulk nucleation than surface conditions. A high nucleation density on the fiber surface may prove detrimental to shear properties at the fiber surface. This may lower composite strength since shear is the primary mechanism for stress transfer between the matrix and wood.

There appears to be an optimal level of nucleation on the fiber surface and in the bulk matrix. The ideal would be an interface that reinforces the material and have good shear properties to deliver stress. This interphase would extend into the bulk material to provide a gradual transition in properties and mechanical interlocking. To accomplish the ideal, composite manufactures need to be aware of the consequences and the behavior of the lubricant systems. Further, composite manufactures need to determine what the optimal processing conditions are to facilitate interphase development. These conditions will be different depending on the properties of the constituent materials. In addition, as shown in this dissertation, the addition of certain additive may interact with coupling agents. This led dramatic differences in mechanical properties.

There appears to be room for optimization of the coupling agent also. A higher molecular weight coupling agent with ends grafted with anhydride may prove to be more effective. This type of molecule would produce a very miscible system that could crystallize, but still bond to a surface. A long molecular chain with large distances between bonding sites is believed to be ideal for entanglement in amorphous system.

Similar to that idea, crystals bound to a wood surface would nucleate other crystal growth. Thus, a crystallite would be chemically bound to the wood. It is possible that this is present in the system studied, but there was no proof. There need to be careful manipulation of molecular weight and grafting to investigate this further.

A Programs for Data Analysis

A.1. DSC Data Reduction and Convolution

The following program was written in Mathematica® to reduce isothermal crystallization data and to provide smoothing to reduce noise. It incorporates a convolution routine "ListConvolve" that performs a Gaussian convolution according to rules set in "kern". The area under the DSC curve was calculated by the trapezoidal method for the entire area and at time *t*. This then allowed for the determination of the relative crystallinity where $\chi = area(t)/area_{Total}$. The χ was then fit to the Avrami model for crystallization. The below example program is for PP crystallized at 137.5°C.

```
data = Import["/home/david/DSC-iso/pp-137,5-1.csv", "CSV"];
ListPlot[data[[All, 2]]]
kern = Table[Exp[-n^2/100]/Sqrt[2. Pi], {n, -10, 10}];
smoothdata = ListConvolve[kern, data[[All, 2]], {-1, 1}];
ListPlot[%]
minsmooth = Min[smoothdata]
maxsmooth = Max[smoothdata]
rangesmooth = maxsmooth - minsmooth
mindata = Min[data[[All, 2]]]
maxdata = Max[data[[All, 2]]]
rangedata = maxdata - mindata
scaledata = rangedata/rangesmooth*smoothdata;
smoothdata = scaledata - Min[scaledata];
plotsmooth = ListPlot[smoothdata]
n = Length[smoothdata]
a = 0
b = n*5 + a
h = b - a
t = Table[i*5 + 1, {i, n}];
area = Sum[
   h/3*(smoothdata[[i]] + 4*smoothdata[[i + 1]] + smoothdata[[i + 2]]), {i,
     1, (n - 2)}]
chi = Table[
     Evaluate[Sum[
        h/3*(smoothdata[[i]] + 4*smoothdata[[i + 1]] + smoothdata[[i + 2]])/
```

```
        area, {i, 1, j}]], {j, (n - 2)}];
Length[chi]
t = Table[i*5, {i, n - 100}];
chi2 = Take[chi, n - 100];
avrami = Array[a, {n - 100, 2}];
avrami[[All, 1]] = N[Log[t]];
avrami[[All, 2]] = Log[-1*Log[1 - chi2]];
cryst = Array[a, {n - 100, 2}];
cryst[[All, 1]] = t;
cryst[[All, 2]] = chi2;
ListPlot[chi]
ListPlot[avrami]
<< Statistics`LinearRegression`
Regress[avrami, {1, x}, x]
Export["/home/david/DSC-iso/avrami/avrami-pp-137,5-1.csv", avrami]
Export["/home/david/DSC-iso/cryst/chi-pp-137,5-1.csv", cryst]
```

A.2. Time Temperature Superposition

Time-temperature superposition was accomplished by utilizing a computer program written in Mathematica®. This program utilizes linear shifting of isothermal temperature scans to shift E' data linearly in the frequency domain. The amount of the linear shift is defined as a_T. The program accomplishes this by defining a reference value taken to be the maximum in E''. All values are referenced as line numbers in the program that coincide with the raw data from the DMA in tab delimited ASCII text. The header is dropped at the onset of the program. In addition, the data was acquired at the same frequencies always, and the program will not account for additional frequency data. The program is then split into two loops that are split at the reference. The loops fit an arbitrary interpolation function to the isothermal reference data. Then the E' value corresponding to the middle frequency of the next successive isotherm is used as input into the interpolation function to solve for its corresponding frequency. Then $a_T = f_{interpolation} / f_{data}$. The a_T are fit to the Arrhenius equation starting at the peak of the b

transition defined by E''_{max} continuing in the linear region. Further, the data is normalized to calculate fragility and the KWW plot.

```
"Packages";
<< Statistics`LinearRegression`
<< Statistics`NonlinearFit`
<< Graphics`Graphics`

"Variables";
Clear[dir, file, freq, data, f1, n, ff1, ref1, ref2, ref, a, aT, atmatrix,
   n];

"Directory";
dir = "/home/david/coop-1/";

"File";
file = "c-pp-1.txt";

"Raw data file in the form: freq,e',e",tan delta,Temp";
data = Import[dir <> file, "Table"];
data = Drop[data, 2];
"Number of frequencies";
freq = 6;

"Truncate the data to analyze on the relaxation transition of interest.  \
Otherwise, the shifting and interpolation in the analysis will be \
inaccurate.";

data = Drop[data, -6];
data = Drop[data, 6];
ref = 217;
MatrixForm[data];
atmatrix = {{data[[ref, 5]] + 273.15, 1}}
LogListPlot[data[[All, {5, 2}]]]

Do[{ClearAll[ref1, ref2, a, aT, p1, p2, z, x],
   ref1 = data[[{n, n + 1, n + 2, n + 3, n + 4, n + 5}, {2, 1}]],
   p = Interpolation[ref1],
   ref2 = data[[{n + 6, n + 7, n + 8, n + 9, n + 10, n + 11}, {1, 2}]],
   a1 = p[ref2[[5, 2]]], aT = a1/ref2[[5, 1]],
   ref2[[All, 1]] = aT ref2[[All, 1]],
   data[[{n + 6, n + 7, n + 8, n + 9, n + 10, n + 11}, {1, 2}]] = ref2,
   AppendTo[atmatrix, {data[[n + 9, 5]] + 273.15, aT}]}, {n, ref,
```

```
   Length[data] - 6, 6}]
MatrixForm[data];
MatrixForm[atmatrix];

Do[{ClearAll[ref1, ref2, a, aT, p1, p2, z, x],
    ref1 = data[[{ref - n, ref - n + 1, ref - n + 2, ref - n + 3,
          ref - n + 4, ref - n + 5}, {2, 1}]], p = Interpolation[ref1],
    ref2 = data[[{ref - n - 6, ref - n - 5, ref - n - 4, ref - n - 3,
          ref - n - 2, ref - n - 1}, {1, 2}]], a1 = p[ref2[[2, 2]]],
    aT = a1/ref2[[2, 1]], ref2[[All, 1]] = aT ref2[[All, 1]],
    data[[{ref - n - 6, ref - n - 5, ref - n - 4, ref - n - 3, ref - n - 2,
          ref - n - 1}, {1, 2}]] = ref2,
    PrependTo[atmatrix, {data[[ref - n - 4, 5]] + 273.15, aT}]}, {n, 0,
    ref - 7, 6}];
MatrixForm[data];
MatrixForm[atmatrix]


c = data[[All, {1, 2}]];
d = data[[All, {1, 3}]];
e = data[[All, {1, 4}]];
Show[LogLogListPlot[data[[All, {1, 2}]]],
  LogLogListPlot[data[[All, {1, 3}]], PlotStyle -> {Hue[0]}],
  LogLogListPlot[data[[All, {1, 4}]], PlotStyle -> {Hue[.1]}]]
LogListPlot[atmatrix]

"arrhenius"

arrhenius = atmatrix;
arrhenius[[All, 1]] = 1/atmatrix[[All, 1]];
arrhenius[[All, 2]] = N[Log[atmatrix[[All, 2]]]];
Regress[arrhenius, {1, x}, x]
arrhenfit[x_] = Fit[Take[arrhenius, {24, 33}], {1, x}, x]
DisplayTogether[ListPlot[arrhenius], Plot[arrhenfit[x], {x, .0032, .004}]]

"Activation Energy"
eactive = (arrhenfit[1] - arrhenfit[0])*8.31451

Solve[arrhenfit[x] == Log[100], x];
invtg = x /. %;
invtg = invtg.{1};
"Tg"
tg = 1/invtg
"Fragility"
m = (arrhenfit[1] - arrhenfit[0])*invtg
```

```
Export[dir <> "full-" <> file, data, "Table"]
Export[dir <> "aT-full-" <> file, atmatrix, "Table"]

"KWW"

kww = data[[All, {1, 3}]];
kww[[All, 1]] = data[[All, 1]]/Max[data[[All, 1]]];
kww[[All, 2]] = data[[All, 3]]/Max[data[[All, 3]]];
b = 1/kww[[Position[kww[[All, 2]], Max[kww[[All, 2]]]].{1}.{1}, 1]];
kww[[All, 1]] = data[[All, 1]]/Max[data[[All, 1]]]*b;
LogLogListPlot[kww, Frame -> True, FrameLabel -> {"f/fmax", "E/Emax"},
  RotateLabel -> True]
Export[dir <> "kww-" <> file, N[kww], "Table"]
```

A.3. β Transition Peak Fit

The following program was written to fit a sixth order polynomial to the *E″* data around the β transition. The program solves for the maximum in the polynomial by taking the derivative and setting it equal to zero. The solve function within Mathematic® is then invoked to obtain the value at the maximum.

```
"Variables";
Clear[dir, file, freq, data, f1, n, ff1];

"Directory";
dir = "/home/david/coop-1/"

"File";
file = "c-pp-1.txt"

"Raw data file in the form: freq,e',e",tan delta,Temp";
data = Import[dir <> file, "Table"];
data = Drop[data, 2];

"Number of frequencies"
freq = 6;

"Truncate the data to analyze on the the relaxation transition of interest.  \
Otherwise the shifting and interpollation in the analysis will be \
inaccurate."
data = Drop[data, -228];
data = Drop[data, 156];
```

```
MatrixForm[data];

"Separate the data by frequencies";
length = Length[data];
f1 = {{0, 0, 0, 0, 0}};
Do[{AppendTo[f1, data[[n, All]]]}, {n, 1, length - 5, freq}];
f1 = Drop[f1, 1];

f2 = {{0, 0, 0, 0, 0}};
Do[{AppendTo[f2, data[[n, All]]]}, {n, 2, length - 4, freq}];
f2 = Drop[f2, 1];

f3 = {{0, 0, 0, 0, 0}};
Do[{AppendTo[f3, data[[n, All]]]}, {n, 3, length - 3, freq}];
f3 = Drop[f3, 1];

f4 = {{0, 0, 0, 0, 0}};
Do[{AppendTo[f4, data[[n, All]]]}, {n, 4, length - 2, freq}];
f4 = Drop[f4, 1];

f5 = {{0, 0, 0, 0, 0}};
Do[{AppendTo[f5, data[[n, All]]]}, {n, 5, length - 1, freq}];
f5 = Drop[f5, 1];

f6 = {{0, 0, 0, 0, 0}};
Do[{AppendTo[f6, data[[n, All]]]}, {n, 6, length, freq}];
f6 = Drop[f6, 1];

"Fit an interpolation function to the individual frequencies to find the \
maximum in the loss spectra at the given freqency";
ff1[x_] = Fit[f1[[All, {5, 3}]], {1, x, x^2, x^3, x^4, x^5, x^6}, x]
Solve[ff1'[x] == 0, x]
Plot[ff1[x], {x, -20, 20}]
ListPlot[f1[[All, {5, 3}]]]
Show[%, %%]

ff2[x_] = Fit[f2[[All, {5, 3}]], {1, x, x^2, x^3, x^4, x^5, x^6}, x]
Solve[ff2'[x] == 0, x]
Plot[ff2[x], {x, -20, 20}]
ListPlot[f2[[All, {5, 3}]]]
Show[%, %%]

ff3[x_] = Fit[f3[[All, {5, 3}]], {1, x, x^2, x^3, x^4, x^5, x^6}, x]
Solve[ff3'[x] == 0, x]
Plot[ff3[x], {x, -20, 20}]
ListPlot[f3[[All, {5, 3}]]]
```

```
Show[%, %%]

ff4[x_] = Fit[f4[[All, {5, 3}]], {1, x, x^2, x^3, x^4, x^5, x^6}, x]
Solve[ff4'[x] == 0, x]
Plot[ff4[x], {x, -20, 20}]
ListPlot[f4[[All, {5, 3}]]]
Show[%, %%]

ff5[x_] = Fit[f5[[All, {5, 3}]], {1, x, x^2, x^3, x^4, x^5, x^6}, x]
Solve[ff5'[x] == 0, x]
Plot[ff5[x], {x, -20, 20}]
ListPlot[f5[[All, {5, 3}]]]
Show[%, %%]

ff6[x_] = Fit[f6[[All, {5, 3}]], {1, x, x^2, x^3, x^4, x^5, x^6}, x]
Solve[ff6'[x] == 0, x]
Plot[ff6[x], {x, -20, 20}]
ListPlot[f6[[All, {5, 3}]]]
Show[%, %%]
```

B Statistical Analysis of Static Bending

B.1. Summary of Bending Results

Coupling Agent	*Lubricant*	*Number of observations*	*Variable*	*Mean*	*COV*
MAPP	None	10	Density (g/cm^3)	1.06	1.29
			MOE (GPa)	5.11	4.99
			MOR (MPa)	67.2	1.70
			Strnbrk	0.0251	8.13
	OP	10	Density (g/cm^3)	1.08	0.939
			MOE (GPa)	5.18	3.67
			MOR (MPa)	62.5	1.94
			Strnbrk	0.0218	7.31
	ZnSt/EBS	10	Density (g/cm^3)	1.10	2.27
			MOE (GPa)	5.07	7.77
			MOR (MPa)	48.2	5.40
			Strnbrk	0.0162	18.7
None	None	10	Density (g/cm^3)	1.064	3.11
			MOE (GPa)	4.02	3.87
			MOR (MPa)	31.7	13.9
			Strnbrk	0.0219	21.6
	OP	10	Density (g/cm^3)	1.07	0.312
			MOE (GPa)	3.89	6.50
			MOR (MPa)	30.4	5.38
			Strnbrk	0.0241	6.16
	ZnSt/EBS	10	Density (g/cm^3)	1.08	1.15

			MOE (GPa)	4.03	3.43
			MOR (MPa)	31.4	5.31
			Strnbrk	0.0221	13.8

Table B.6.1: Table showing the bending properties of the extruded composites.

B.2. ANOVA for Bending MOE and MOR

Source	DF	Sum of Squares	Mean Square	F	Pr > F
Model	6	430518681284	71753113547	74.17	<.0001
Error	53	51275785662	967467654		
Corrected Total	59	481794466945			

R-Square	Coeff Var	Root MSE	*MOE* Mean
0.893573	4.712682	31104.14	660009

Source	DF	Type I Sum of Squares	Mean Squares	F	Pr > F
Coupling Agent	1	409198604524	409198604524	422.96	<.0001
Lubricant	2	119238984	59619492	0.06	0.9403
Coupling * Lubricant	2	3652878713	1826439357	1.89	0.1614
Density	1	17547959062	17547959062	18.14	<.0001

Source	DF	Type III Sum of Squares	Mean Squares	F	Pr > F
Coupling Agent	1	368356702785	368356702785	380.74	<.0001
Lubricant	2	3829441178	1914720589	1.98	0.1483
Coupling * Lubricant	2	4759941163	2379970582	2.46	0.0951
Density	1	17547959062	17547959062	18.14	<.0001

Table B.6.2: ANOVA table calculated for the MOE with the lubricants, coupling agents, density, and interactions used as sources of variability. Type I error was set for $\alpha = 0.05$. This analysis was conducted using units of psi for MOE.

Source	DF	Sum of Squares	Mean Square	F	Pr > F
Model	6	292298444	48716407	555.85	<.0001
Error	53	4645333.5	87647.8		
Corrected Total	59	296943778			
	R-Square	Coeff Var	Root MSE	*MOE* Mean	
	0.984356	4.512903	296.0537	6560.161	
Source	DF	Type I Sum of Squares	Mean Squares	F	Pr > F
Coupling Agent	1	249001448	249001448	2841	<.0001
Lubricant	2	206229934	10314967	117.7	<.0001
Coupling * Lubricant	2	20807025	1043512.7	118.7	<.0001
Density	1	1860037.7	1860037.7	21.22	<.0001
Source	DF	Type III Sum of Squares	Mean Squares	F	Pr > F
Coupling Agent	1	248902312.8	248902312.8	2839.8	<.0001
Lubricant	2	12748955.6	6371177.8	72.73	<.0001
Coupling * Lubricant	2	18596483.4	9298241.7	106.09	<.0001
Density	1	1860037.7	1860037.7	21.22	<.0001

Table B.6.3: ANOVA table calculated for the MOR with the lubricants, coupling agents, density, and interactions used as sources of variability. Type I error was set for $\alpha = 0.05$. This analysis was conducted using units of psi for MOR.

B.3. Duncan's Multiple Range Test for MOR

Alpha = 0.05
Error Degrees of Freedom = 53
Error Mean Square = 87647.3

Duncan Group	***Mean (psi)***	***N***	***Lub***
A	7171.28	20	None
B	6740.04	20	OP
C	5769.16	20	ZnSt/EBS

Table B.6.4: The Duncan's groupings for the Duncan's Multiple Range test used for comparing the differences among means of lubricants in the MOR data.

C DSC Melt Curves for Binary Blends

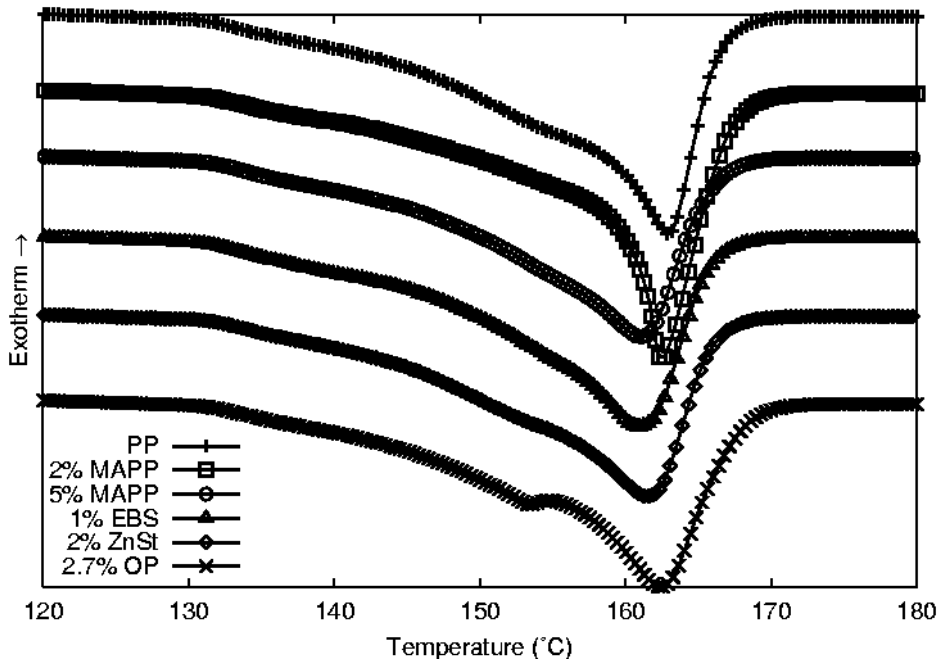

Figure C.6.1: DSC melt curves for binary blends crystallized at 128°C.

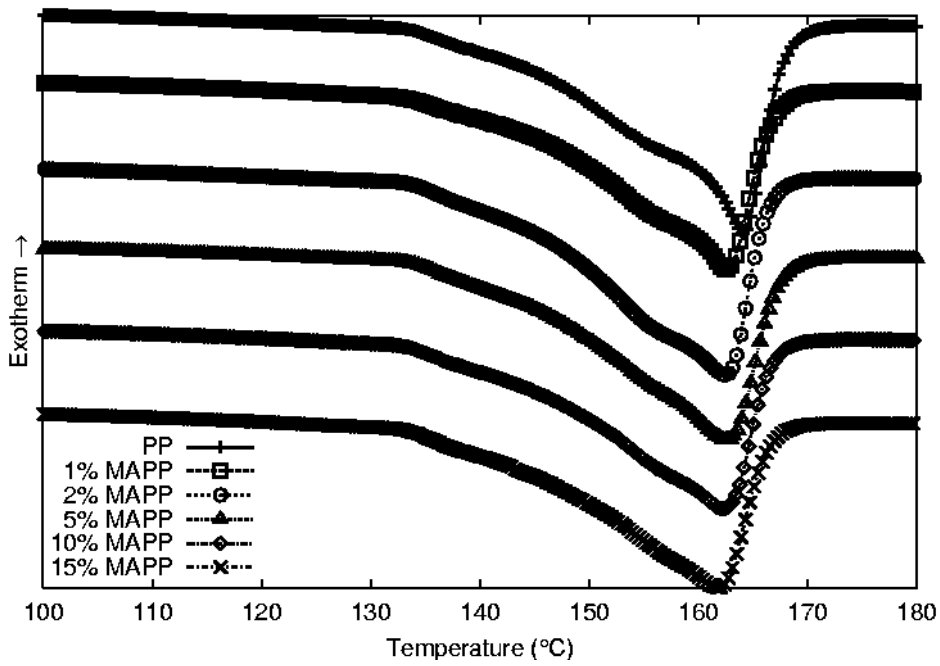

Figure C.6.2: DSC melt curves for binary blends crystallized at 130°C.

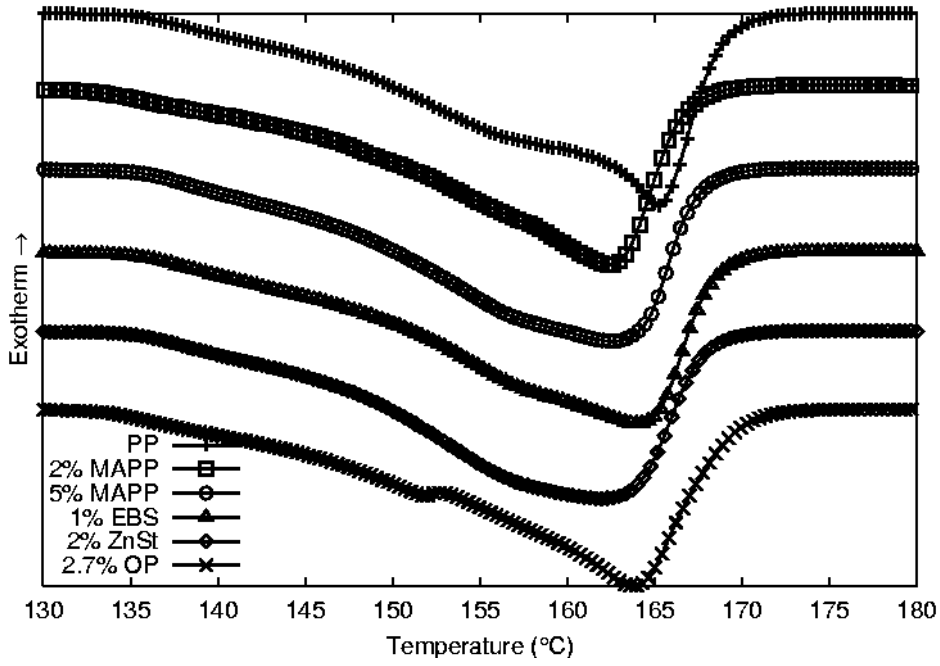

Figure C.6.3: DSC melt curves for binary blends crystallized at 132°C.

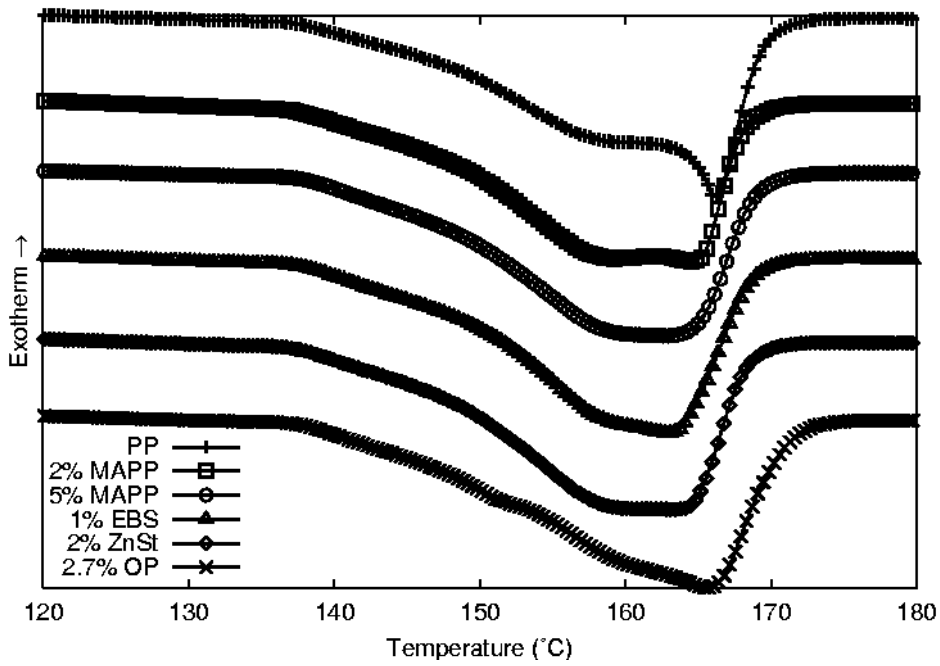

Figure C.6.4: DSC melt curves for binary blends crystallized at 134°C.

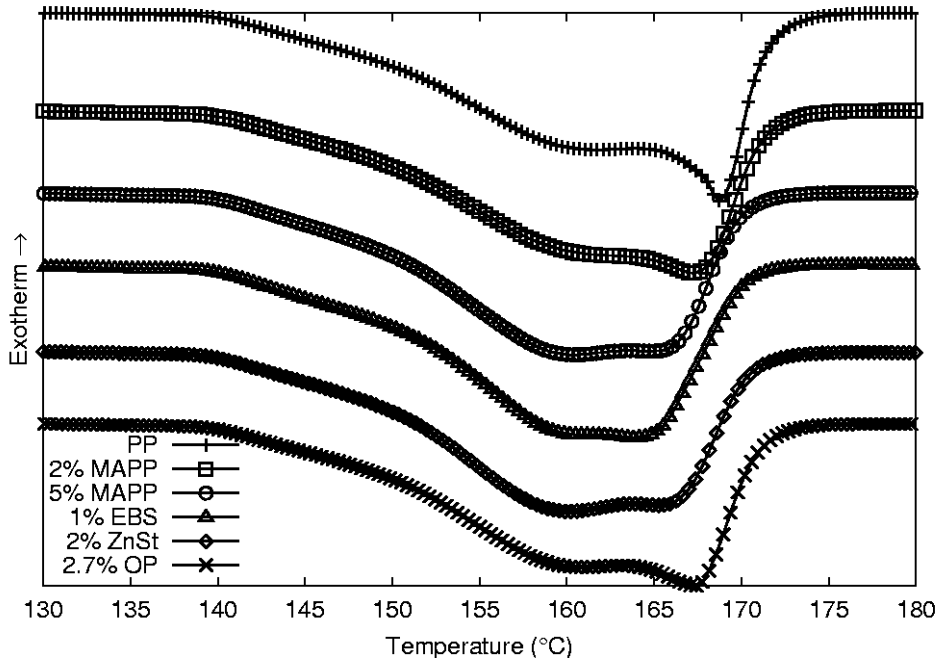

Figure C.6.5: DSC melt curves for binary blends crystallized at 136°C.